Tesis Doctoral

HEAT TRANSFER AND THERMAL STORAGE IN FIXED AND FLUIDIZED BEDS OF PHASE CHANGE MATERIAL

Autora
María Asunción Izquierdo Barrientos

Director
Jose Antonio Almendros Ibáñez
Co-directora
Celia Sobrino Fernández

DEPARTAMENTO DE INGENIERÍA TÉRMICA Y DE FLUIDOS

Leganés (Madrid), noviembre 2014

Tesis doctoral

HEAT TRANSFER AND THERMAL STORAGE IN FIXED AND FLUIDIZED BEDS OF PHASE CHANGE MATERIAL

Autora: María Asunción Izquierdo Barrientos

Director de Tesis: Jose Antonio Almendros Ibáñez
Co-directora de Tesis: Celia Sobrino Fernández

Firma del Tribunal Calificador:

Firma

Presidente: D. Bo Leckner, Chalmers University of Technology

Secretario: D. Sergio Sánchez Delgado, Universidad Carlos III de Madrid

Vocal: Dña. Luisa F. Cabeza Fabra, Universitat de Lleida

Calificación:

Leganés (Madrid), 14 de noviembre de 2014

A mis padres

Agradecimientos

Me siento afortunada. Afortunada porque haya llegado este momento y pueda concluir una etapa que hace tiempo parecía muy lejana. Una cosa que te enseñan los años de doctorado es que ser organizado y estructurado nunca está de más. Así que, por partes, mis agradecimientos.

No son suficientes las palabras de gratitud hacia mis directores de tesis, Jose y Celia. Ellos han hecho posible que esta tesis vea la luz con todo el esfuerzo que también han dedicado a ella. Son un ejemplo a seguir, no sólo en el plano académico.

La ventaja de trabajar entre dos universidades ha sido tener la oportunidad de compartir estos años con mucha gente excepcional. El inconveniente, que le faltan dígitos al cuentakilómetros. Quién me iba a decir que salir un día a correr por el parque podría llegar a marcar mis próximos años. Por eso agradezco a Antonio impulsarme a tomar esta decisión y estar siempre pendiente de cada paso. A mis compañeros del Instituto de Energías Renovables por los ratos compartidos y especialmente a Juanfran por el derroche de optimismo que contagia.

Mi agradecimiento también a los doctores del grupo ISE, que marcan camino y prestan su colaboración siempre que se necesita. A mis compañeros de despacho (T08, despacho patera, Luismi y Luis) por su compañía y anécdotas. Esos momentos de relax son los que te ayudan a recargar fuerzas y hacen la jornada más llevadera. A Mariano, por su paciencia y su voluntad para echar siempre una mano. A Cristina, por tener su puerta abierta.

I would like to acknowledge my supervisors Naoko Ellis, Xiatao Bi and Norman Epstein for their interest in this work and their time spent on our meetings during my stay at UBC. I deeply appreciate their valuable comments. My gratitude to my colleague Paula Reyes who hosted me and made me feel at home.

Estos años no habrían sido lo mismo sin actividades deportivas. Por ello, mi agradecimiento a "Carlos Corre", por ser más que un grupo que queda para correr y donde la palabra compañerismo adquiere su máximo significado.

Por supuesto, a mis padres y a mi hermana, son pilares fundamentales en mi vida, y su apoyo incondicional es el que me ayuda a confiar en mí misma y seguir alcanzando metas, esta tesis es una de ellas.

Finalmente, a Benja, por mantener la ilusión del primer día y ayudarme en todo lo que está en su mano.

Abstract

Thermal energy storage is a key technology for energy conservation since many energy sources are intermittent in nature. Latent heat storage is considered one of the most efficient ways of storing thermal energy because, unlike sensible heat storage, it provides a high-energy storage density with a small temperature swing. There are available many storage techniques, including sensible and latent heat storage or a combination of both. Fixed and fluidized beds may be feasible technologies when the storing materials may be encapsulated in cans, spheres or microencapsulated in highly porous structures with protecting envelopes.

This PhD thesis deals with thermal storage and heat transfer in fixed and fluidized beds with phase change materials (PCMs). The behavior of a bed with granular PCM as a thermal storage system is studied. Charging and discharging experiments are carried out and models for the transient response of the bed are developed for fixed and fluidized bed configurations. Moreover, a model for the heat transfer coefficient between the bed of PCM and an immersed surface is presented and validated with experimental measurements.

The experimental studies are conducted in a cylindrical bed filled with granular PCM and with air as the working fluid. The bed has an internal diameter of 200 mm. The granular PCMs used consist of paraffin, which is the material that changes its phase, bounded within a secondary supporting structure of SiO_2, which ensures that the paraffin does not leak from the granulate when in its liquid form. The material is commercialized by Rubitherm® and is available in two sizes involving particle diameters of 1-3 mm and 0.2-0.6 mm. The finer grade is used in fluidized bed because the particle size is appropriate for obtaining a bubbling fluidization, whereas the coarser grade is employed in the fixed bed conditions to achieve high gas velocities without exceeding the minimum fluidization velocity.

The study of the storage behavior of a fluidized bed filled with PCM includes the comparison of its performance to that of well-known storage methods such as fluidized beds with sand and packed beds with sand and PCM. To accomplish this, heating and cooling experiments are conducted in the cylindrical bed mentioned before. For the fluidized bed with PCM the bed height and flow rate are varied to study their influence on the storage and recovery efficiencies. In

addition, the stability of the PCM during several charging-discharging cycles is examined.

The transient response of a packed and fluidized bed with PCM is modeled taking into account the progressive evolution of the enthalpy with the temperature during the phase change and the energy stored in the wall of the bed. The equations presented for each model are non-dimensionalized, which result in the same differential equation system regardless of whether a granular PCM or a conventional material is used. The models are positively verified against experimental data for the granular PCM and the conventional storage material, sand.

The experimental determination of the heat transfer coefficient between a heated surface immersed in a fixed or fluidized bed and granular PCM is performed employing a heat transfer probe which consists of a cylindrical variable resistance of small diameter, 6 mm. The flow rate is varied to quantify its influence on the heat transfer coefficient. The results obtained for the granular PCM are compared with the heat transfer coefficients measured for the sand. The heat transfer coefficient for the particles when they undergo a phase change process is twice the heat transfer coefficient when there is no phase change of the PCM.

These experimental data are used to validate a model proposed to calculate the heat transfer coefficient between an immersed surface and fixed and bubbling fluidized beds of granular PCM. The model consists of a two-region model with two different voidages, where a steady conduction problem is solved for the fixed bed case and a transient one for the fluidized bed case.

Resumen

El almacenamiento térmico es una tecnología clave para la conservación de energía ya que muchas fuentes energéticas son por naturaleza intermitentes en el tiempo. El almacenamiento de calor latente se considera una de las formas más efectivas de almacenar energía térmica ya que proporciona una alta densidad de almacenamiento energético con pequeñas variaciones en la temperatura, a diferencia del almacenamiento mediante calor sensible.

Existen diversas tecnologías para almacenar calor sensible, latente o la combinación de ambos. Entre ellas, los lechos fijos y fluidizados son una opción válida cuando los materiales están encapsulados o microencapsulados en estructuras porosas protegidas por algún tipo de carcasa.

Esta tesis doctoral estudia el almacenamiento térmico y la transferencia de calor en lechos fijos y fluidizados con materiales de cambio de fase (MCF). Con el fin de analizar el comportamiento de estos lechos con MCF como sistema de almacenamiento térmico, se han realizado ciclos de carga y descarga y se ha modelado la respuesta transitoria del lecho en condiciones de lecho fijo y de lecho fluidizado. Además, se incluye un modelo para el cálculo del coeficiente de transferencia de calor entre el lecho con MCF (ya sea fijo o fluidizado) y una superficie sumergida en el mismo. Tanto los modelos de almacenamiento de calor en el lecho como el del coeficiente de transferencia han sido validados con medidas experimentales.

Los ensayos experimentales se han realizado en un lecho cilíndrico con MCF y aire como fluido de trabajo. El MCF granular utilizado consiste en una parafina, que es el material que cambia de fase, inmersa en una estructura secundaria de sílice que la soporta. Este tipo de recubrimiento asegura que no haya pérdidas de parafina cuando ésta esté en estado líquido. Este material lo comercializa la empresa Rubitherm® y está disponible en dos tamaños de partícula: 1-3 mm y 0.2-0.6 mm. Las partículas más finas se utilizan en el lecho fluidizado ya que su menor tamaño permite conseguir un lecho burbujeante sin necesidad de altos caudales de aire, en cambio las partículas más gruesas se usan en el lecho fijo para poder aumentar el caudal sin llegar a sobrepasar la velocidad de mínima fluidización del material.

El estudio del comportamiento de un lecho fluidizado con MCF incluye la comparación de su rendimiento con el de otros métodos de almacenamiento

conocidos como son los lechos fluidizados con arena y los lechos fijos con arena y MCF. Con esta finalidad se han realizado ensayos de calentamiento en el lecho cilíndrico descrito anteriormente. Para el caso del lecho fluidizado con MCF también se ha estudiado la influencia que tiene la altura del lecho y el caudal utilizado en el almacenamiento y rendimiento de recuperación de energía. Además, se ha comprobado la estabilidad del MCF tras varios ciclos de carga y descarga.

Para los modelos de respuesta transitoria de un lecho fijo y fluidizado con MCF se ha tenido en cuenta la variación de la entalpía con la temperatura durante el cambio de fase así como la energía almacenada en la pared del lecho. Las ecuaciones se presentan en forma adimensional y son válidas para cualquier tipo de material granular, indistintamente de si contiene MCF en su interior o no. Los modelos se han validado con los datos experimentales tanto del MCF como de la arena.

La determinación experimental del coeficiente de transferencia de calor entre una superficie sumergida en un lecho fijo o fluidizado y el MCF granular se ha realizado utilizando un sensor de transferencia de calor que consiste en una resistencia cilíndrica de potencia variable de 6 mm de diámetro. El flujo de aire se ha modificado para cuantificar su influencia en el coeficiente de transferencia de calor. Los resultados experimentales obtenidos para el MCF se han comparado con los de la arena para los dos tipos de tecnología, lecho fijo o fluidizado. Estos datos experimentales se han usado para validar un modelo que calcula el coeficiente de transferencia de calor entre una superficie y un lecho fijo o fluidizado de MCF granular. El modelo diferencia entre dos regiones del lecho con distintas propiedades, una region cercana a la superficie de intercambio de calor y otra alejada de ésta. El modelo es apto para lecho fijo y fluidizado aunque para el primer caso se resuelve un problema de conducción estacionaria y para el segundo uno de conducción transitoria.

Contents

List of Figures

List of Tables

CHAPTER
ONE

Introduction

1.1 Thermal energy storage

Power demands, in general, are not steady. Moreover, some thermal and electrical energy sources, such as solar energy, are not steady in supply. In those cases where either supply or demand is highly variable, reliable power availability requires energy conversion systems large enough to supply the peak-demand requirements. The results are high and partially inefficient capital investments, since the systems operate at partial load much of the time.

The success of any intermittent energy source in meeting demand depends critically on energy storage. The use of energy storage often results in benefits as reduction of energy consumptions, capital investments and energy costs, and an increase in flexibility of operations. Furthermore, smaller power-generating systems can be used.

Thermal energy storage (TES) appears to be an important solution to correct the imbalance between the supply and demand of energy. A good thermal energy storage should minimize thermal losses and permit the highest possible extraction efficiency of the stored thermal energy (Dincer & Rosen, 2002).

The TES systems can be sensible or latent heat storage, or a combination of both. For each storage medium, there is a wide variety of choices depending on the temperature range and application. In sensible heat storage, the material increases or decreases its temperature when the energy is stored or released. Its effectiveness depends on the specific heat of the storage material and, if volume is important, on its density. Sensible storage systems commonly use rocks or water as the storage medium. The heat transfer fluid commonly used is water, due to its high heat capacity. An alternative heat transfer fluid is the air, which has a smaller heat capacity but is inexpensive and usually simplifies the set-ups.

In latent heat storage the material undergoes a phase change. The thermal

energy is stored when the material changes its phase, usually from solid to liquid. The enthalpy of solidification/fusion or vaporization and the temperature at which the phase change occurs are of design importance. The storage capacity of the material depends on its latent heat during the phase change process. Thus, it is desirable a storage medium with a high latent heat value. Latent heat storage may be classified on the basis of the phase change process as solid-solid, solid-liquid, solid-gas and liquid-gas. Solid-gas and liquid-gas transformations are generally not employed for energy storage in spite of their highest latent heats, since gases occupy large volumes. Large changes in volume make the system large, complex and impractical. In solid-solid transitions, heat is stored as the material is transformed from one crystalline form to another. These transitions generally have small latent heats making such materials less desirable (Regin *et al.*, 2008).

Figure 1.1 shows the increase of internal energy when energy in the form of heat is added to a substance. The consequence is an increase in temperature (sensible heating) or change of phase (latent heating).

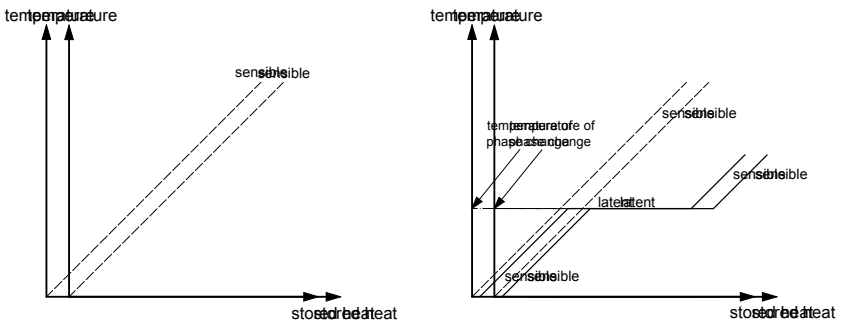

(a) Sensible energy storage (b) Latent energy storage

Figure 1.1: Temperature diagrams for (a) sensible and (b) latent heat storage.

1.2 Phase Change Materials (PCMs)

Latent heat storage by solid-liquid phase transition is a particularly attractive technique, since it provides a high energy storage density and has the capacity to store energy as latent heat of fusion at a constant temperature corresponding to the phase transition temperature of the phase change materials (PCMs)

Thermal properties
Phase change temperature suitable to the operating range
High latent heat per unit mass
High specific heat
High thermal conductivity in both solid and liquid phase
Physical properties
High density
Low density variation during phase change
Little or no supercooling during freezing
Non-poisonous, non-inflammable and non-explosive
Low volume change during phase transition
Chemical properties
Chemical stability
No chemical decomposition
Compatibility with container materials
Non-poisonous, non-inflammable and non-explosive
Economic factors
Available in large quantities
Inexpensive
Long term reliability

Table 1.1: Desirable characteristics of PCMs.

(Husnain, 1998; Dincer & Rosen, 2002). As the temperature increases, the material changes phase from solid to liquid. The reaction being endothermic, the PCM absorbs heat. Similarly, when the temperature decreases, the material changes phase from liquid to solid. This reaction is exothermic and therefore, the PCM desorbs heat (Kuznik *et al.*, 2011). No material has all the optimal characteristics required for a PCM. The selection of a PCM for a given application requires careful consideration of the properties of various substances. Table 1.1 summarizes the main characteristics required to PCMs.

The solidification of a PCM begins with a nucleation effect. The nucleation is the formation of initial crystals, called nucleus. The nucleation rate of a material is its capability to produce nucleus when the temperature decreases

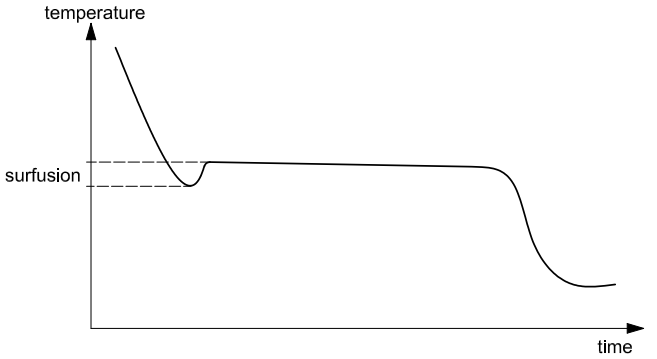

Figure 1.2: Supercooling effect.

below the fusion temperature. If the nucleation rate of a material is too low, it can remain in the liquid phase when its temperature decreases below the fusion temperature. The solidification starts later: the material temperature rises again suddenly to the phase change temperature (see Figure 1.2) (Kuznik *et al.*, 2011). This effect is called supercooling and nucleating additives should be added to minimize it. Another typical problem is the segregation of the PCM due to incongruent melting. This could be overcome by adding thickening agents. Also the low thermal conductivity of some PCMs could be improved by adding conductor materials. One of the most efficient conducting material is ex-foliated graphite. Zhang *et al.* (2006) and Cabeza *et al.* (2002) have deeply studied these additives.

Among the most extensive references related with PCMs, it can be cited Zalba *et al.* (2003); Farid *et al.* (2004); Dincer & Rosen (2002); Mehling & Cabeza (2008) and Regin *et al.* (2008). These contain a complete review of the type of materials that have been used, their classification, characteristics, advantages and disadvantages and the various experimental techniques used to determine the behavior of these materials in melting and solidification.

1.2.1 Types of PCMs

PCMs can be grouped into organic and inorganic materials. The organic PCMs are paraffins, fatty acids and the polyethylene glycol (PEG). The inorganic PCMs are typically hydrated salts. Some of the common advantages and disadvantages of organic and inorganic PCMs are compiled in Table 1.2 and 1.3 respectively.

Organic PCM	
Advantages	Disadvantages
Availability in a large temperature range	Flammable
Ability to melt congruently	Low thermal conductivity
Self-nucleating properties	High cost
No segregation	Low density
Recyclable	Low volumetric heat capacity
High heat of fusion	
Freeze without much supercooling	
Safe and non-reactive	
Non-corrosive	

Table 1.2: Advantages and disadvantages of organic PCMs.

Inorganic PCM	
Advantages	Disadvantages
High latent heat her per unit weight	Supercooling
Sharp phase change	Segregation
High thermal conductivity (0.5 W/m·K)	Degradation
Non-flammable	
High volumetric latent heat storage capacity	
Low cost	

Table 1.3: Advantages and disadvantages of inorganic PCMs.

The enthalpy of solidification/fusion or vaporization and the temperature at which the phase change occurs are essential for an optimum design. Figure 1.3 (taken from Mehling & Cabeza (2008)) shows the melting and phase change enthalpy of existing PCMs.

In addition, Table 1.4 presents the experimental thermophysical properties of both the liquid and solid states for several PCMs reported by Lane (1980).

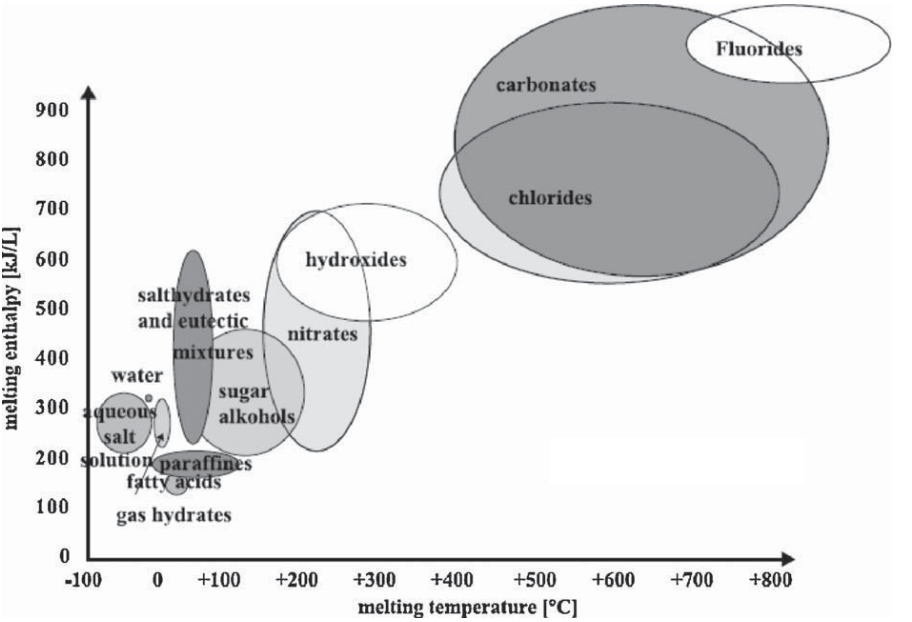

Figure 1.3: Melting temperature and phase change enthalpy for existing PCMs (Mehling & Cabeza, 2008).

Compound	Melting Temp.[°C]	Heat of fusion [kJ/kg]	Thermal conductivity [W/m·K]		Density [kg/m^3]	
Inorganics						
$MgCl_2{\cdot}6H_2O$	117	168.6	0.570	Liquid, 120°C	1450	Liquid, 120°C
			0.694	Solid, 90°C	1569	Solid, 20°C
$Mg(NO_3)_2{\cdot}6H_2O$	89	162.8	0.490	Liquid, 95°C	1550	Liquid, 94°C
			0.611	Solid, 37°C	1636	Solid, 25°C
$Ba(OH)_2{\cdot}8H_2O$	48	265.7	0.653	Liquid, 85.7°C	1937	Liquid, 84°C
			1.225	Solid, 23°C	2070	Solid, 24°C
Organics						
Paraffin wax	64	173.6	0.167	Liquid, 63.5°C	790	Liquid, 65°C
			0.346	Solid, 33.6°C	916	Solid, 24°C
Polyglycol E600	22	127.2	0.189	Liquid, 38.6°C	1126	Liquid, 25°C
			-		1232	Solid, 4°C
Fatty acids						
Palmitic acid	64	185.4	0.162	Liquid, 68.4°C	850	Liquid, 65°C
			-		989	Solid, 24°C
Capric acid	32	152.7	0.153	Liquid, 38.5°C	878	Liquid, 45°C
			-		1004	Solid, 24°C
Caprylic acid	16	148.5	0.149	Liquid, 38.6°C	901	Liquid, 30°C
			-		981	Solid, 13°C
Aromatics						
Naphthalene	80	147.7	0.132	Liquid, 83.8°C	976	Liquid, 84°C
			0.341	Solid, 49.9°C	1145	Solid, 20°C

Table 1.4: Measured thermophysical data of some PCMs (Lane, 1980).

The successful utilization of PCM depends on developing means of containment. The PCM encapsulation with different geometries of capsules has its own advantages and disadvantages. The most common type of PCM containment is macroencapsulation in which a significant quantity of PCM is encapsulated in a discrete unit. The advantage of the macroencapsulation is its applicability to both liquid and air as heat transfer fluids and easier to ship and handle. The PCM is packaged in tubes, pouches, spheres, paneles or other receptacles.

Microencapsulated PCMs present many advantages such as increasing heat transfer area, reducing PCMs reactivity towards the outside environment and controlling the changes in the storage material volume as phase change occurs (Farid *et al.*, 2004). Microencapsulation refers to techniques in which a large number of small PCM particles are contained within a sealed, continuous matrix. Unless the matrix encapsulating the PCM has high thermal conductivity, the microencapsulation system suffers from low heat transfer rate. The rigidity of the matrix prevents convective currents and forces all heat transfer to occur by conduction. Physical processes used in microencapsulation are spray drying, centrifugal and fluidized bed processes, or coating processes (Mehling & Cabeza, 2008).

1.2.2 Applications

The application of energy storage with phase change is not just limited to solar energy heating and cooling. Some of the possible applications of PCMs are gathered in Table 1.5. Specially in buildings, the use of wallboards containing PCM has received much attention. The effect of the PCMs in the building envelope is to reduce the indoor temperature fluctuations and to delay the air temperature extremum.

1.3 Packed and fluidized beds

Fixed and fluidized bed concepts have been widely studied for sensible energy storage.

Packed beds represent a suitable storage option for air-based systems. A packed bed storage system consists of loosely packed solid material through which the heat transport fluid is circulated. Heated fluid (usually air) flows into a bed of graded particles in which thermal energy is transferred during the charging phase.

PCM-TES Applications
Thermal storage of solar energy
Space and water heating
Integration in building walls
Passive storage in bioclimatic buildings
Cooling: use of off-peak rates and reduction of installed power
Heating and sanitary hot water
Thermal protection of food
Thermal protection of electronic devices
Medical applications
Satellite power testing

Table 1.5: Possible applications of PCMs.

Sensible heat storage is the most common method of thermal energy storage in packed beds, although research on advanced materials for latent thermal storage has increased recently because the density of stored energy is greater for latent thermal storage than for sensible heat storage. Packed beds for latent TES have been studied previously, mainly in beds of macro-encapsulated spheres of PCM with diameters of a few centimeters and water as the heat transfer fluid (Xia *et al.*, 2010). On the other hand, the utilization of encapsulated PCMs with a small particle diameter is advantageous in terms of heat transfer rates. Regin *et al.* (2009) observed that the charging and discharging rates were significantly higher for capsules of smaller radius than for those of larger radius particles. Because the inlet fluid temperature typically varies, the heat transfer transient response of packed beds has also been the subject of many theoretical and experimental investigations.

In gas-solid systems, when increasing the flow rate of the fluid that passes through the bed, a point is reached where all the particles are just suspended by the upward-flowing gas. At this point the frictional force between particle and fluid just counterbalances the weight of the particles, the vertical component of the compressive force between adjacent particles disappears, and the pressure drop through any section of the bed about equals the weight of fluid and particles in that section (Kunii & Levenspiel, 1991). The bed is considered to be just fluidized and the pressure drop does not vary with the gas flow. The pressure drop through any section of the bed equals the weight of fluid and particles in that section. With an increase in flow rate beyond the minimum

fluidization velocity, large instabilities with bubbling are observed, this regimen is called, bubbling or fluidization.

Fluidized beds of solid particles provide an attractive means of storing energy. One of the remarkable features of fluidized beds is its temperature uniformity. This uniformity exists in both radial and axial directions. The same temperature is quickly established throughout the system because general agitation of the particles disperse local regions of cold or hot. The good mixing of solids gives rise to good heat transfer and high rate of heat transfer to a solid object placed in the bed, therefore, high transfer coefficients are obtained.

The knowledge of the heat transfer coefficient between surface and fluid or between fluid and particles in fluidized beds is important for the design of industrial equipment. Numerous experimental studies and correlations for the heat transfer coefficient have been reported in the literature, most limited to a narrow range of conditions. Because of the complex nature of fluidized contacting, these correlations are far from universal. On the contrary, the unsteady state behavior of fluidized bed thermal storage systems has been modeled in a limited number of studies in the literature, and only for sensible heat. Furthermore, only Sozen *et al.* (1988) and Brown *et al.* (1998) focused their studies on fluidized beds with PCM besides the potential of these materials. Sozen *et al.* (1988) overcame the segregation problem of Glauber's salt by encapsulating the PCM in 25-mm-diameter hollow spheres and agitating in a liquid fluidized bed of diameter 0.34 m. They demonstrated improvements over fixed bed TES systems of about 60% and enhancements on the performance of the system by increasing the superficial water velocity. Brown *et al.* (1998) studied several types of microencapsulated products as heat transfer media in a fluidized bed including shells of polymethylene-urea, cross-linked nylon, and gelatin and cores of octadecane and paraffin. Microcapsules with shells of gelatin and cores of octadecane were the most useful in their study. They observed heat transfer enhancements of 30% although enhancements of at least 85% were expected based on the effective specific heat of the microcapsules.

1.4 Scope of the thesis

This PhD thesis presents a study about the heat transfer and thermal energy storage in fixed and fluidized beds of PCMs. The study includes experimental and numerical analysis of the performance, heat storage and heat transfer from the bed to immersed surfaces of two thermal storage technologies, fixed and

fluidized beds, when they are filled with a granular material that changes its phase. Some of the experimental results are used as inputs for the numerical analysis.

This dissertation is organized in 7 more chapters.

Chapter 2 collects an overall explanation of the experimental set up, a description of the materials used and the different tests carried out for their characterization.

From Chapter 3 to Chapter 7 (both of them included) every unit has been written as an independent article. Thus, each one has its own abstract, introduction, notation and bibliography.

In **Chapter 3** the performance of an air-fluidized bed of a microencapsulated PCM as storage system is evaluated. The charging and discharging efficiencies are calculated and the stability of the system under continuous operation is studied.

Chapter 4 presents a numerical and experimental study of the transient response of a packed bed filled with granular PCM. Numerical and experimental results are compared. The proposed numerical model accounts for the progressive evolution of the enthalpy with temperature during the phase change and includes the energy stored in the wall.

Chapter 5 covers the description and validation of a model for the transient response of a fluidized bed containing PCM. The heat accumulated in the vessel and in the plate distributor is included in the simulations.

Chapter 6 and **Chapter 7** respectively concern the measurement and model of the heat transfer coefficient from a surface to particles in a fixed and fluidized bed filled with a granular PCM.

Finally, in **Chapter 8** the main conclusions of the thesis are summarized and briefly discussed.

References

Brown, R.C., Rasberry, J.D. & Overmann, S.P. 1998 Microencapsulated phase-change materials as heat transfer media in gas fluidized beds. *Powder Technology* 98, 217–222.

Cabeza, L.F., Mehling, H., Hiebler, S. & Ziegler, F. 2002 Heat transfer enhancement in water when used as pcm in thermal energy storage. applied thermal engineering. *Applied Thermal Engineering* 22, 1141–1151.

Dincer, I. & Rosen, M. 2002 *Thermal energy storage*. John Wiley & Sons.

Farid, M.M., Khudhair, A.M., Razack, S.A.K. & Al-Hallaj, S. 2004 A review on phase change energy storage: materials and applications. *Energy Conversion and Management* 45, 1597–1615.

Husnain, S.M. 1998 Review on sustainable thermal energy storage technologies, part i: heat storage materials and techniques. *Energy Conversion and Management* 39, 1127–38.

Kunii, D. & Levenspiel, O. 1991 *Fluidization Engineering*. Butterworth-Heinemann.

Kuznik, F., David, D., Johannes, K. & Roux, J.J. 2011 A review on phase change materials integrated in building walls. *Renewable and Sustainable Energy Reviews* 15, 379–391.

Lane, G.A. 1980 Low temperature heat storage with phase change materials. *International Journal of Energy Research* 5, 155–160.

Mehling, H. & Cabeza, L.F. 2008 *Heat and cold storage with PCM*. Springer.

Regin, A.F., Solanki, S.C. & Saini, J.S. 2008 Heat transfer characteristics of thermal energy storage system using pcm capsules: A review. *Renewable and Sustainable Energy Reviews* 12, 2438–2458.

Regin, A.F., Solanki, S.C. & Saini, J.S 2009 An analysis of a packed bed latent heat thermal energy storage system using pcm capsules: Numerical investigation. *Renewable Energy* 34, 1765–1773.

Sozen, Z.Z., Grace, J.R. & Pinder, K.L. 1988 Thermal energy storage by agitated capsules of phase change material: pilot scale experiments. *Industrial and Engineering Chemistry Research* 27, 679–684.

Xia, L., Zhang, P. & Wang, R.Z. 2010 Numerical heat transfer analysis of the packed bed latent heat storage system based on an effective packed bed model. *Energy* 35, 2022–2032.

Zalba, B., Marín, J.M., Cabeza, L.F. & Mehling, H. 2003 Review on thermal energy storage with phase change: materials, heat transfer analysis and applications. *Applied Thermal Engineering* 23, 251 – 283.

Zhang, Y., Ding, J., Wang, X., Yang, R. & Lin, K. 2006 Influence of additives on thermal conductivity of shape-stabilized phase change material. *Solar Energy Materials & Solar Cells* 90, 1692–1702.

CHAPTER

TWO

Experimental set-up and materials

This chapter presents the set-up and materials used for the different experimental studies carried out in this thesis. Some characterization experiments for the materials are also explained. Nevertheless, a brief description of the experimental set-up and the methods is included in each chapter.

2.1 Set-up

Heating and cooling experiments are conducted in the experimental apparatus illustrated in Figure 2.1. The bed consists of a cylindrical tube of stainless steel with walls 2 mm thick and filled with particles. A fine mesh screen is mounted at the bottom of the distributor plate to prevent the solid particles from entering the plenum chamber. The air enters the plenum of the column and then flows into the bed through a distribution plate with a thickness of 1.5 mm containing 300 perforations with a diameter of 2 mm, which results in a 3% open area. In this way, the air is uniformly distributed in the bed. The instrumentally monitored section of the test apparatus has a height of 500 mm and an internal diameter of 200 mm, and it is insulated with 2-cm-thick glass wool. Additionally, the piping is insulated with a thermal insulator with a thickness of 1 cm. To ensure the homogeneous velocity distribution of air at the exit from the test section and to reduce the elutriation and entrainment of particles from the bed the freeboard of the column is divided into two parts. The first part is a cylinder with an internal diameter of 200 mm, and the second part another cylinder with an internal diameter of 300 mm.

The air flow is produced by a blower with variable mass flow rate, and heated by electrical heaters that are regulated by a PID controller before flowing into the column. Type K thermocouples are used to measure the temperature at specific locations inside the test section and in the plenum chamber. At

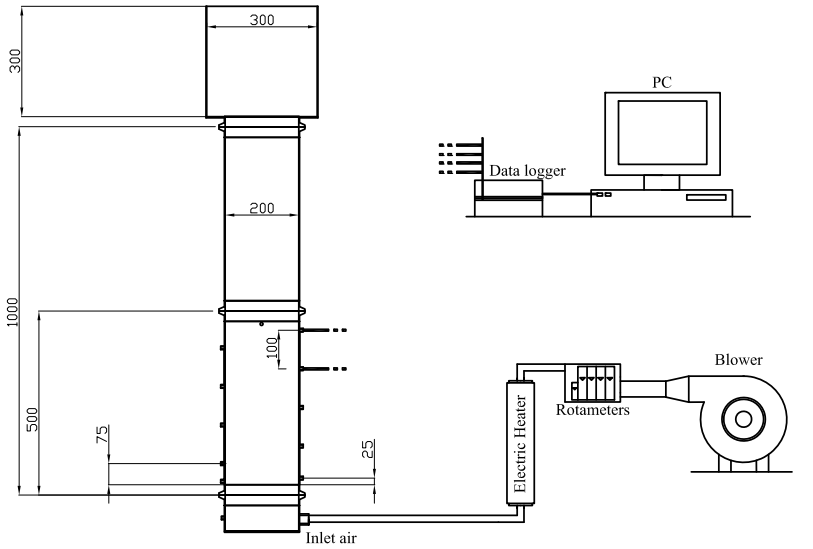

Figure 2.1: Schematic representation of the experimental apparatus. Dimensions in mm.

these locations, pressure variations can be measured using pressure sensors with two different ranges: 100 mbar and 1 bar. Also, in the same locations, a heat transfer probe of small diameter can be introduced. The heat transfer sensor used consists of a cylindrical variable resistance of 200 W with three thermocouples distributed around its surface. The thermocouples, pressure sensors and heat transfer probe are connected to a data acquisition system for continuous monitoring and recording of the data.

2.2 Materials

This work focuses on the study of phase change materials (PCMs) as thermal storage material. The granular materials used are GR42, GR50 and GR80 which are commercialized by Rubitherm®. The number that names the materials correspond, according to the manufacturer, to their approximate phase change temperature T_{pc}, then, $T_{pc\,GR42} \approx 42°C$, $T_{pc\,GR50} \approx 50°C$ and $T_{pc\,GR80} \approx 80°C$. The material that changes its phase is paraffin, and it is bound within a secondary supporting structure of SiO_2. These granular PCMs are available in two sizes with particle diameters between 1-3 mm and 0.2-0.6 mm.

The behavior of the PCMs has been compared to a common material used for sensible heat storage, silica sand. The sand used in the different experiments presents small differences in the particle size distribution.

In this section different experiments to characterize the sand and the PCMs are presented.

2.2.1 Density

An helium pycnometer has been used to obtain the density of the materials. Pycnometers are devices for measuring volume, and density is calculated as the ratio of mass to volume; mass being invariably measured on a discrete device. Table 2.1 shows the density values for the PCMs used and their standard deviation. The density of the sand is 2632.3 kg/m^3 with a standard deviation of 1.2 kg/m^3.

These measurements were carried out by the Department of Materials of Carlos III University of Madrid.

2.2.2 Specific heat

The specific heat is the amount of heat per unit mass required to raise the temperature by one degree Celsius. The relationship between the apparent specific heat and the temperature for the sand is shown in Figure 2.2 and for the granular PCMs in Figure 2.3. These data were obtained by differential scanning calorimetry (DSC) with a slow heating rate of 0.5°C/min. This slow heating rate ensures the thermal equilibrium in the sample during the DSC measurements. The apparent specific heat for the granular PCM is obtained from the enthalpy-temperature relation as $c_p = \partial i / \partial T$. Figure 2.3 also shows the enthalpy-temperature curves for the finer PCMs and the coarser PCMs, respectively.

	Finer grade		**Coarser grade**	
	ρ [kg/m^3]	σ_ρ [kg/m^3]	ρ [kg/m^3]	σ_ρ [kg/m^3]
GR42	1531.7	0.7	1563.1	0.4
GR50	1550.5	1.0	1512.8	1.6
GR80	1594.7	1.6	1618.0	0.3

Table 2.1: Density values for the PCMs.

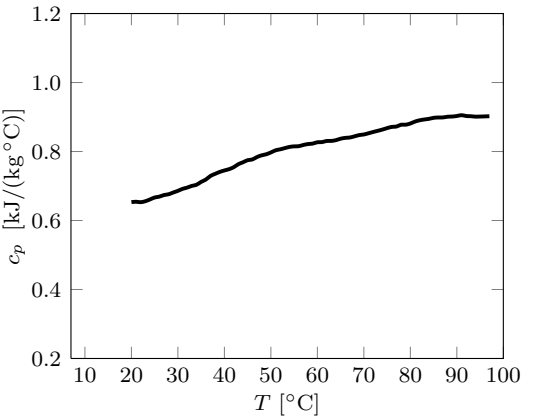

Figure 2.2: Variation of the specific heat with temperature for the sand.

The mean specific heat for the sand, for the temperature range used in this work, is 0.776 kJ/(kg °C).

The phase changes of the PCMs, GR42, GR50 and GR80, are clearly distinguished at approximately 42°C, 50°C and 80°C, respectively.

The GITSE research group from University of Zaragoza carried out the DSC measurements. The equipment used was the DSC200F3-Maia from Netzsch.

2.2.3 Particle size distribution

The particle size distribution (PSD) of the materials has been measured with the vibratory sieve shaker AS200-Control from Retsch. The cummulative size distribution for the sand are plotted in Figure 2.4 and in Figure 2.5 for the finer and coarser PCMs.

Table 2.2 summarizes the mean particle diameters for the different materials used.

Mean particle diameter[mm]					
	Sand		**Finer PCM**		**Coarser PCM**
Sand 1	0.755 ± 0.069	GR42	0.368 ± 0.066	GR42	1.382 ± 0.202
Sand 2	0.911 ± 0.125	GR50	0.541 ± 0.082	GR50	1.642 ± 0.196
Sand 3	0.566 ± 0.070	GR80	0.334 ± 0.069	GR80	1.586 ± 0.202

Table 2.2: Mean particle diameter for the materials studied.

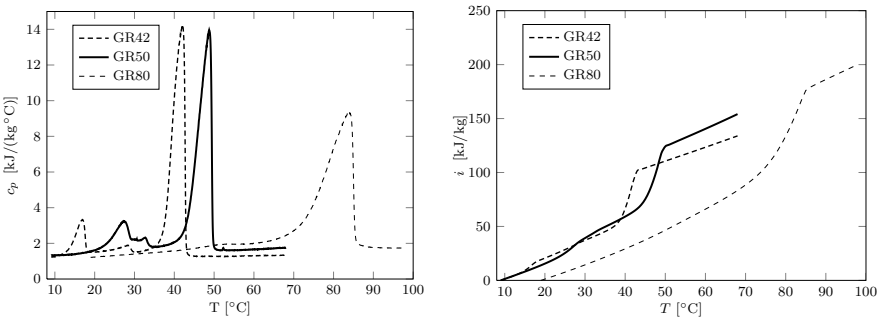

(a) Finer grade

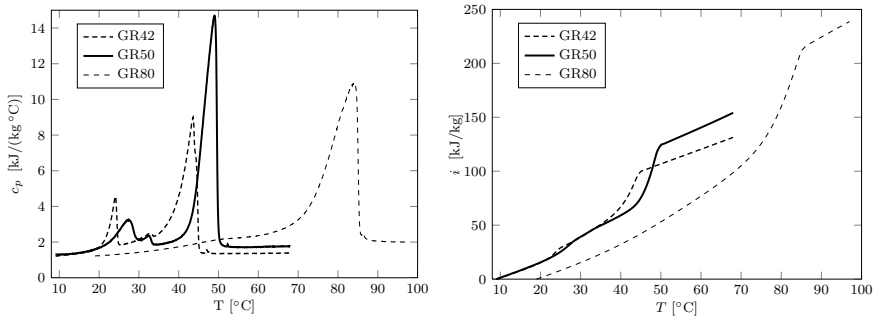

(b) Coarser grade

Figure 2.3: Variation of the apparent specific heat and the enthalpy with temperature for (a) the finer grade PCMs and (b) the coarser grade PCMs.

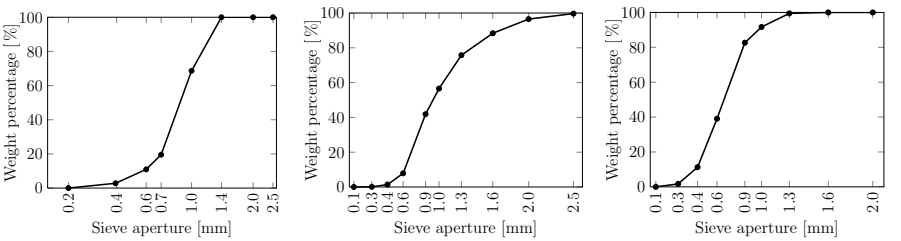

(a) Sand 1 (b) Sand 2 (c) Sand 3

Figure 2.4: PSD for the sand.

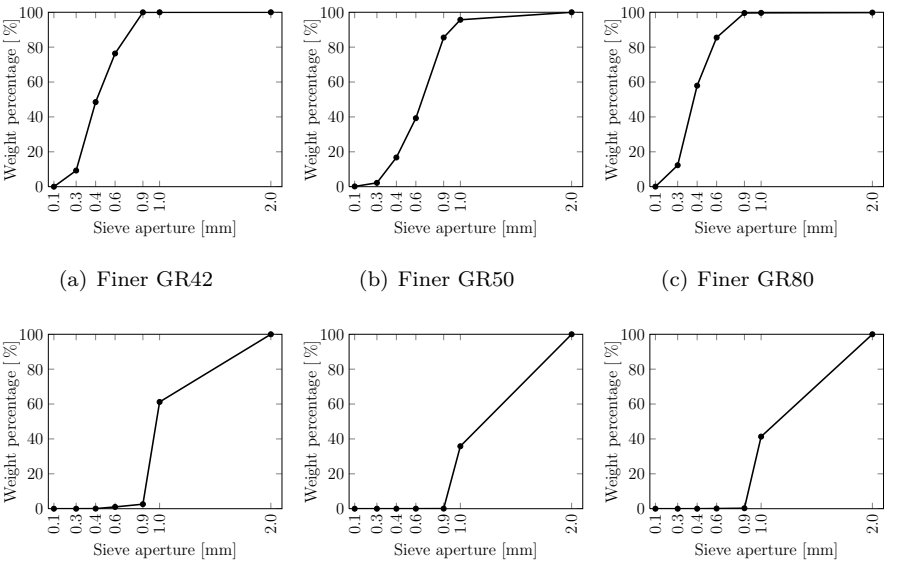

(a) Finer GR42 (b) Finer GR50 (c) Finer GR80

(d) Coarser GR42 (e) Coarser GR50 (f) Coarser GR80

Figure 2.5: PSD for the finer PCMs (a,b,c) and the coarser PCMs (d,e,f).

2.3 Agglomeration problems

A preliminary study (Izquierdo-Barrientos *et al.*, 2013) of the finer PCMs, GR42, GR50 and GR80 in terms of fluidization showed that the finer PCMs GR42 and GR80 do not properly fluidize when the bed temperature is over the T_{pc} of the material. These two materials seem to be agglomerated because the thermocouples placed in the bed do not show a temperature uniformity during charging experiment. On the other hand, the finer PCM GR50 fluidized well, with vigorous bubbling and presenting uniform temperature.

Figure 2.6 shows different pictures of the GR42 and GR80 PCMs agglomerated when emptying the bed. Figure 2.7 shows the distributor covered by the PCM agglomerated.

Heating experiments were carried out in a 2D fluidized bed showing good fluidization when the bed temperature was below their T_{pc} (see Figure 2.8(a)) but agglomeration when above their T_{pc} (see Figure 2.8(b) and 2.8(c)). These experiments were carried out in the Chemical and Biological Department of the University of British Columbia.

A further analysis of the flowability and wear resistance for the PCMs was

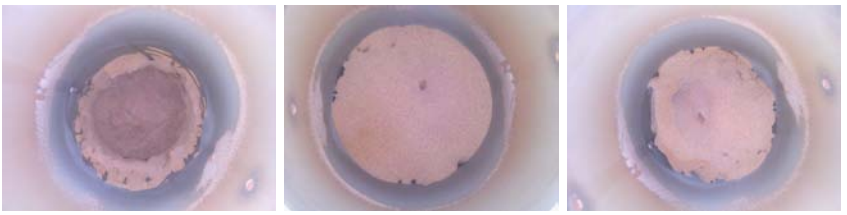

Figure 2.6: Pictures of the bed agglomerated with PCM GR42 and GR80.

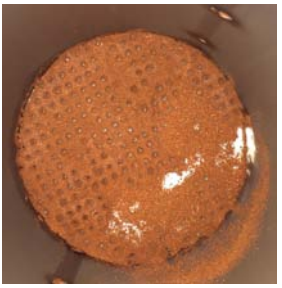

Figure 2.7: Distributor with PCM agglomerated.

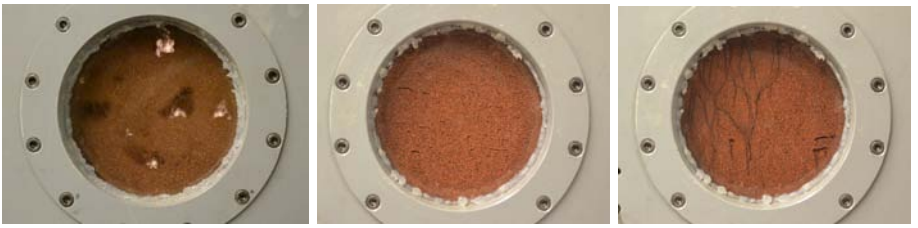

(a) Good fluidization (b) Agglomeration (c) Channeling

Figure 2.8: Pictures of a 2D bed filled with PCM when there is (a) good fluidization and (b,c) agglomeration.

carried out by measuring the angle of repose and attrition. Moreover, SEM pictures were taken before and after fluidization process to observe any change in the materials' microstructure.

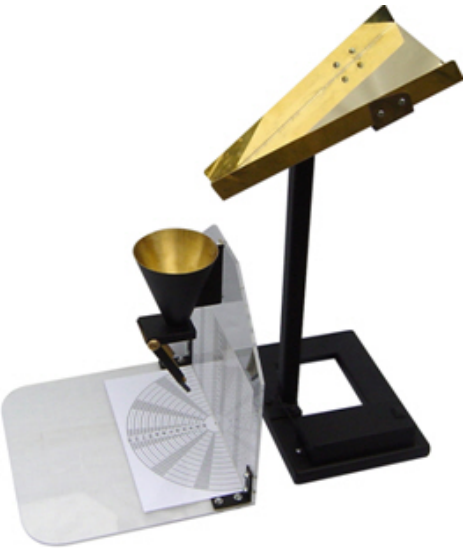

Figure 2.9: Schematic of the device used to measure the AOR (Geldart *et al.*, 2006).

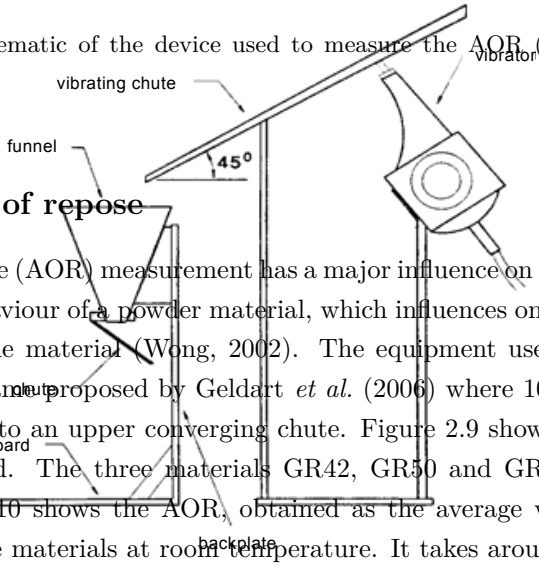

Fig. 2. Mark 4 Powder Research Ltd. AOR tester.

2.3.1 Angle of repose

The angle of repose (AOR) measurement has a major influence on the flowability and dynamic behaviour of a powder material, which influences on the fluidizing performance of the material (Wong, 2002). The equipment used to measure the AOR is the same proposed by Geldart *et al.* (2006) where 100 g sample is poured slowly on to an upper converging chute. Figure 2.9 shows a schematic of the device used. The three materials GR42, GR50 and GR80 have been tested. Figure 2.10 shows the AOR, obtained as the average value of seven runs, for the three materials at room temperature. It takes around 25 seconds to pour the entire sample. No noticeable differences appear between the three materials. Due to the large error bars, it is not possible to delineate a clear trend with AOR. This is because the AOR measurement inherently has human errors associated. Nevertheless, the Chauvenet's criterion, with a 90% of confidence, has been applied to assess whether one piece of experimental data from the set of observations is likely to be spurious.

As GR42 and GR80 become difficult to fluidize when heated close to their T_{pc}, further analysis of the AOR against temperature is presented in Figure 2.11. No significant conclusions can be drawn as no remarkable changes appear

Another commonly used simple method for characterising powders that are cohesive or semi-cohesive should be mentioned, the Hausner Ratio (Grey & Beddow, 1969) in which the tapped and aerated bulk densities are measured and the former is divided by the latter. It turns out that there is a good correlation between AOR and HR as shown later.

3. Materials Used

Two types of powders have been used in some of our recent work: spherical and porous Fluid Cracking Catalyst (FCC) (Fig. 3), and angular and non-porous aluminum

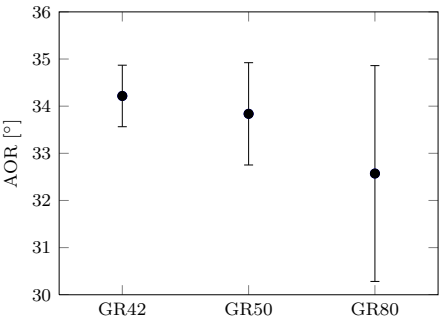

Figure 2.10: AOR at room temperature for GR42, GR50 and GR80.

in the AOR when heated beyond T_{pc}. The AOR does not seem to be influenced by the temperature of the material.

However, when the materials are heated (specially beyond T_{pc}), their flowability retards and present signs of cohesiveness. The pouring time is decreased to 12 seconds because the materials do not flow continuously, but in clumps. Some of these qualitative characteristics are illustrated in Figure 2.12.

2.3.2 Attrition

In order to further analyze the fluidizing characteristics of the materials and explain the possible causes of agglomeration found in the finer materials GR42 and GR80, attrition tests have been performed. The attrition testing apparatus follows the ASTM D5757-00 standard (ASTM, 2006), with the four main stainless steel components: the three orifice (0.397 mm) distributor plate, the attrition column (710 mm in height, 35 mm), the conically divergent/convergent freeboard settling chamber (630 mm in height), and the fines collector containing a ceramic filter (0.1 mm pore size). The unit is loaded with 50 g of the particulate sample, and operated at 10 l/min of air at room temperature and pressure for a run period of 5 hours.

The PSDs before and after the attrition tests for the three materials and their corresponding mean particle diameter with their standard deviation are presented in Figure 2.13. The distributions are Gaussian and have similar width. Although the mean particle diameter is slightly higher for the GR50, the shape of the distribution has been shown to have a higher influence than the mean particle size on the defluidization of a fluidized bed (Lin *et al.*, 2011).

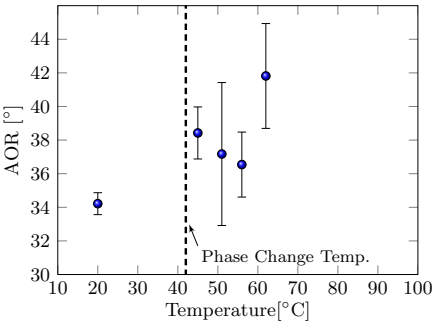

(a) GR42

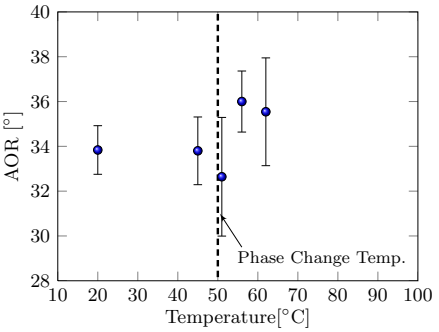

(b) GR50

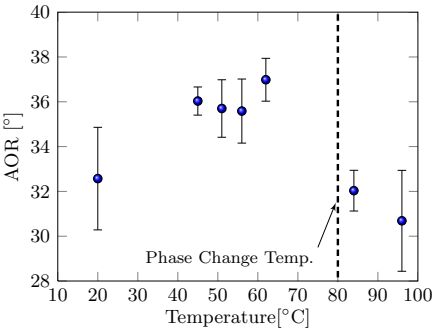

(c) GR80

Figure 2.11: Evolution of the AOR with temperature for (a) GR42, (b) GR50 and (c) GR80.

The PSDs after the attrition tests indicate that the bed particles are just slightly smaller than the original ones. It has been proved that attrition in-

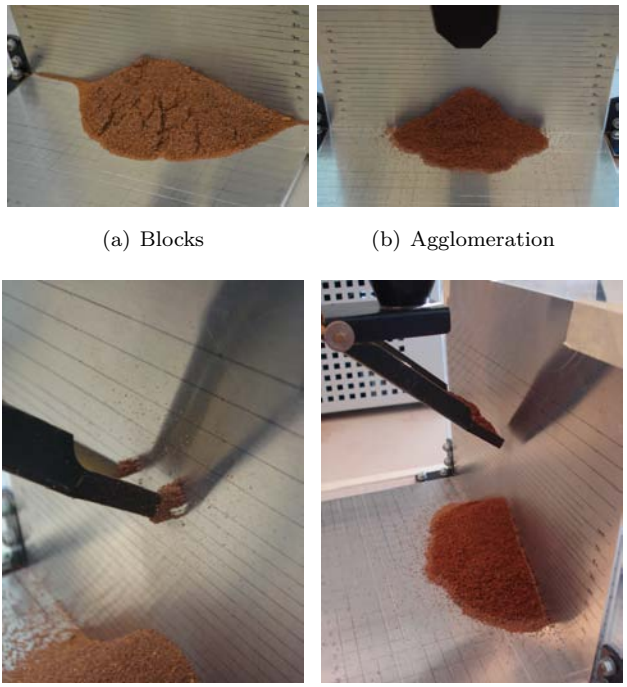

(a) Blocks (b) Agglomeration

(c) Electrostatics (d) Material stuck

Figure 2.12: Different problems observed during AOR measurements.

creases the number of particles and decreases their size (the mean diameters are smaller than before the attrition tests). As a consequence, the PSDs are modified, being the degree of variation of the PSD after the attrition test very similar for the three materials. Fines, of a size smaller than 50 μm, are only detected for the finer GR80 with a fraction of 0.33% of the total mass, which is not very significant. Nevertheless, because of the abrasion of the material, some leakages of the PCM might happen and influence on the agglomeration of the material.

2.3.3 SEM

One more test has been carried out to study the PCM structure before and after fluidization. The microstructure of the three finer PCMs was examined by Scanning Electron Microscopy (SEM) performed on a Jeol 6490 LV electron microscope equipped with an EDS detector (Oxford INCA Energy) and detec-

tors for secondary and backscattered electrons. This test was carried out by the Section of Fuel Cells in the Renewable Energy Research Institute of Albacete. Figure 2.14 presents several SEM pictures for the materials GR42, GR50 and GR80 with a resolution of 2500 μm.

The contrast of light is related to the conductivity of the material where the white beams represent low conductivity. No significant differences are appreciated between the initial and after fluidization pictures. Only the appearance of the post-fluidization pictures, specially for the GR42 and GR80, seems softer than the initial ones which could mean that part of the paraffin has leaked through the secondary structure.

References

ASTM 2006 Standard test method for determination of attrition and abrasion of powdered catalysts by air jets. *Tech. Rep.* D5757-00.

Geldart, D., Abdullah, E.C., Hassanpour, A., Nwoke, L.C. & Wouters, I. 2006 Characterization of powder flowability using measurement of angle of repose. *China Particuology* 4, 104–107.

Izquierdo-Barrientos, M.A., Sobrino, C., Almendros-Ibáñez, J.A., Ellis, N., Bi, X.T. & Epstein, N. 2013 Experimental studies of phase change materials in a bubbling fluidized bed. In *Fluidization XIV From fundamentals to products*. Noordwijkerhout, Holland.

Lin, C.L., Peng, T.H. & Wang, W.J. 2011 Effect of particle size distribution on agglomeration/defluidization during fluidized bed combustion. *Powder Technology* 207, 290–295.

Wong, A. Chi-Ying 2002 Use of angle of repose and bulk densities for powder characterization and the prediction of minimum fluidization and minimum bubbling velocities. *Chemical Engineering Science* 57, 2635–2640.

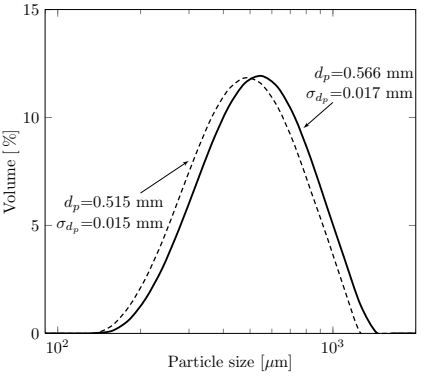

(a) GR42

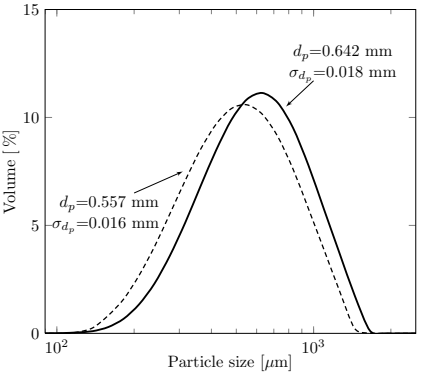

(b) GR50

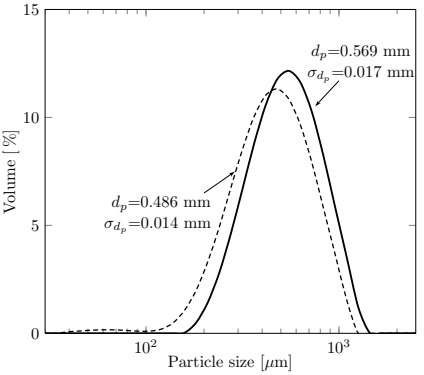

(c) GR80

Figure 2.13: PSD for (a) GR42, (b) GR50 and (c) GR80 before (continuous line) and after (dashed line) the attrition tests.

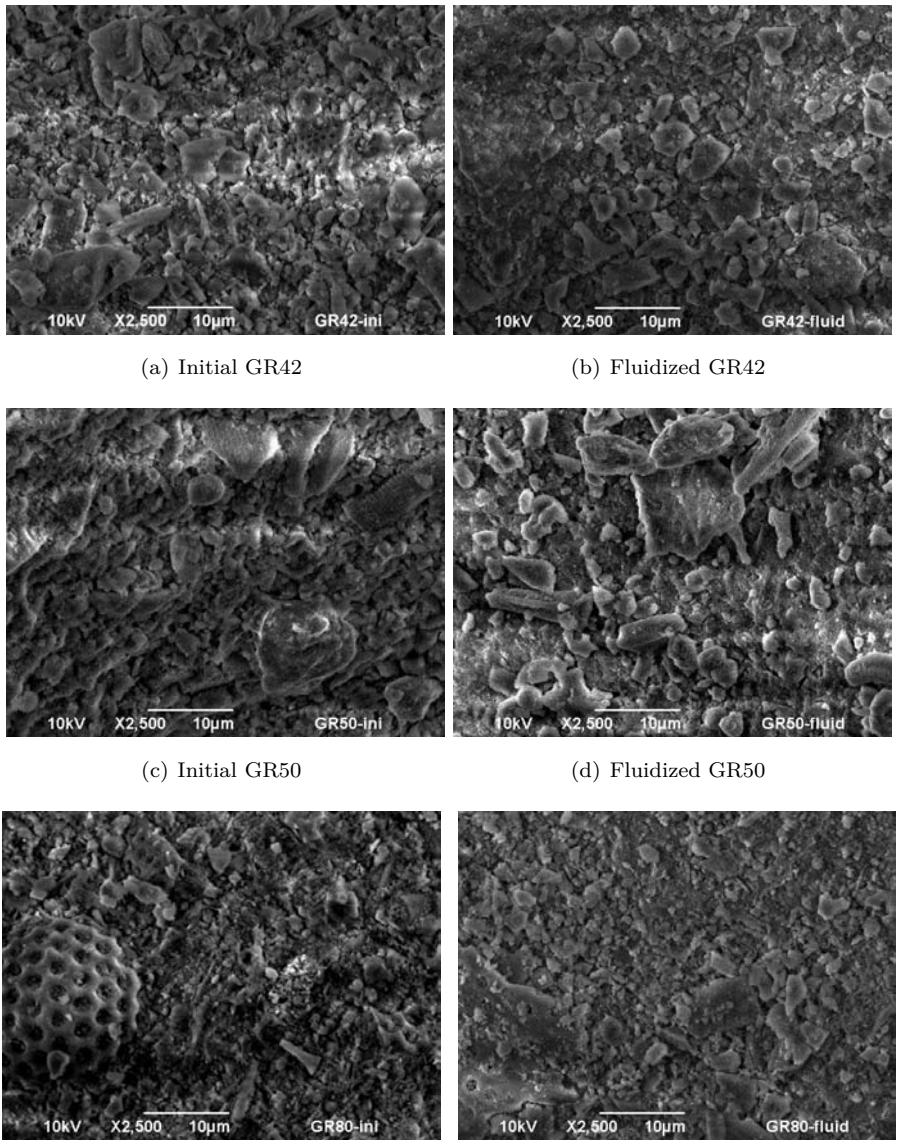

(a) Initial GR42

(b) Fluidized GR42

(c) Initial GR50

(d) Fluidized GR50

(e) Initial GR80

(f) Fluidized GR80

Figure 2.14: SEM pictures before and after fluidization for the materials (a,b) GR42, (c,d) GR50 and (e,f) GR80.

CHAPTER

THREE

Thermal energy storage in a fluidized bed of PCM

The objective of the present work is to research the storage behavior of a fluidized bed filled with a granular phase change material (PCM) with a small particle diameter, $\overline{d}_p = 0.54$ mm. The performance of the fluidized bed is compared to that of well-known storage methods such as fluidized beds with sand and packed beds based of sand and PCM. For this purpose, heating experiments are conducted in a cylindrical bed with air as the working fluid.

The influence of the bed height and flow rate on the storage and recovery efficiencies of the fluidized bed of PCM is analyzed. Additionally, the stability of the PCM during various charging-discharging cycles is studied.

The results indicate that this PCM is an alternative material that can be used in fluidized bed systems to increase the efficiency of storing thermal energy in the form of latent heat. Under the experimental conditions tested in this study, higher charging efficiencies are observed for fixed and fluidized beds based on PCM than those of sand. High gas velocity and low bed height shorten the charging time but also reduce the charging efficiency. The cycling test shows that the PCM is stable under bubbling conditions up to 15 cycles, which corresponds to approximately 75 hours of continuous operation.

3.1 Introduction

Energy storage is needed in many applications when the availability and demand for energy do not coincide. Sensible heat storage is the most common method of thermal energy storage, although research on advanced materials and systems for latent thermal storage has increased recently because the density of stored energy is greater for latent thermal storage than for sensible heat storage. Additional information about PCMs, their classification and applications

in thermal storage can be found in different reviews (Zalba *et al.*, 2003; Cabeza *et al.*, 2011; Regin *et al.*, 2008).

Packed beds are a suitable option when air is used as the heat transfer fluid. Moreover, micro-encapsulation of PCMs has been proposed as a heat transfer enhancement technique for latent heat thermal storage because it increases the heat transfer area. Similar to packed beds, fluidized beds can be utilized for thermal energy storage and have some properties, such as a uniform temperature in the bed or a high rate of heat transfer to a solid object within the bed, which can be advantageous in several applications.

In most cases where published numerical studies have been verified experimentally, the experimental results for packed bed sensible heat storage have been limited to beds of spheres or cylinders with large characteristic diameters on the order of 1 cm (Beasley & Clark, 1984). An experimentally validated heat transfer model for energy storage fixed bed systems (Hänchen *et al.*, 2011) shows higher storage efficiencies for smaller particle sizes.

The application of fluidized beds to sensible heat storage has been studied in the past, and it has been shown that a fluidized bed behaves similarly to a well-mixed tank with negligible variations in the temperature along the bed (Elsayed *et al.*, 1988). Wagialla *et al.* (1991) modeled the behavior of a fluidized bed and showed that the optimum performance of the fluidized bed, when it was used as an energy storage device, was achieved by employing a superficial air velocity similar to the minimum fluidization velocity. Moreover, there is an optimum bed height that maximizes the efficiency of energy recovery because the bed height has opposite effects on the residence time and the heat transfer coefficient.

Packed beds for latent thermal energy storage have been studied previously, mainly in beds of macro-encapsulated spheres of PCM with diameters of a few centimeters and water as the heat transfer fluid (Xia *et al.*, 2010). The behavior of a packed bed of spherical capsules with a radius of 20-60 mm and filled with a PCM, suitable for use with a solar water heating system, was simulated by Regin *et al.* (2009), who observed that the charging and discharging rates were significantly higher for capsules of smaller radius than those of larger radius. The transient response of a cylindrical packed bed of PCM encapsulated in 31.8-mm-spheres with air as the working fluid was investigated by Benmansour *et al.* (2006), who conducted two-dimensional numerical calculations for the separate phases that were verified by measurement of the temperature of the fluid and the PCM.

In recent years, granular phase changing composites with a small particle diameter (1-3 mm) have been tested in latent heat thermal storage packed bed systems. The utilization of encapsulated PCMs with a small particle diameter is advantageous in terms of heat transfer rates and pumping requirements when 1) storage systems of small characteristic length are applicable (Rady, 2009*a*), and 2) the time required for the phase change is inversely proportional to the superficial gas velocity and depends on the air supply temperature (Nagano *et al.*, 2004). A PCM encapsulated in spheres with a diameter of 25 mm and agitated in a liquid-fluidized bed was tested by Sozen *et al.* (1988), who demonstrated improvements over fixed bed thermal energy storage systems and enhanced the performance of the system by increasing the superficial water velocity. Merry & Rubinsky (1989) studied the heat transfer coefficients for a surface immersed in a two-dimensional fluidized bed of solid-to-solid phase transition material particles with a mean diameter of 0.4 mm that were fluidized with air. Heat transfer coefficients were also studied by Brown *et al.* (1998) in a cylindrical gas-fluidized bed containing several types of micro-encapsulated PCMs undergoing solid-liquid transitions, with nominal diameters ranging from 140 to 655 μm.

The aim of this study is to evaluate the performance of an air-fluidized bed of micro-encapsulated PCM with a mean diameter of 0.54 mm as a storage system in terms of its charging and discharging efficiencies and stability under continuous operation. The behaviors of a fixed bed of sand, a fluidized bed of sand and a fixed bed of PCM are also studied and compared.

3.2 Experimental apparatus and materials

In the present study, heating experiments are conducted with sand and PCM in a packed bed and in a fluidized bed. A schematic diagram of the experimental apparatus is illustrated in Figure 3.1. The bed consists of a cylindrical tube of stainless steel with walls 2 mm thick and filled with particles. The air enters the plenum of the column and then flows into the bed through a distribution plate with a thickness of 1.5 mm containing 300 perforations with a diameter of 2 mm, which results in a 3% open area. In this way, the air is uniformly distributed in the bed. A fine mesh screen is mounted at the bottom of the distributor plate to prevent the solid particles from entering the plenum chamber. The instrumentally monitored section of the test apparatus has a height of 500 mm and an internal diameter of d_i =200 mm, and it is insulated with glass wool

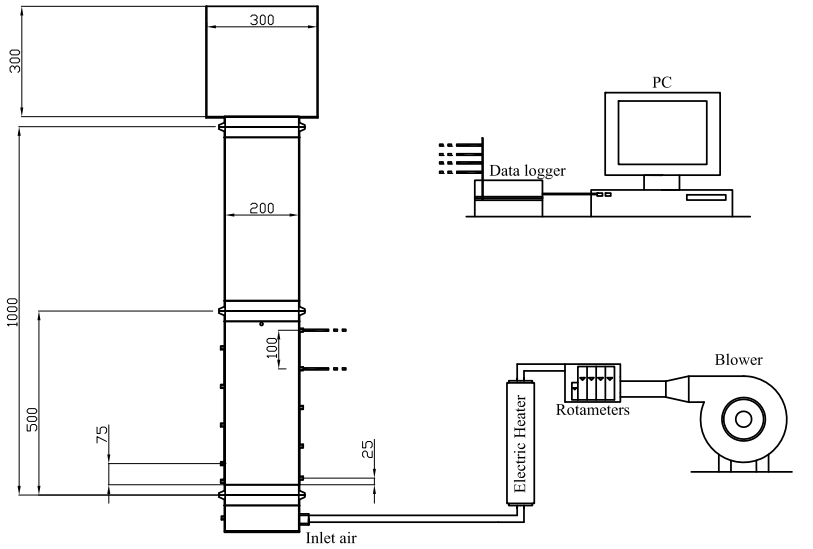

Figure 3.1: Schematic representation of the experimental apparatus in mm.

with a thickness of 2 cm. Additionally, the piping is insulated with a thermal insulator with a thickness of 1 cm. The freeboard of the column is divided into two parts: 1) a cylinder with an internal diameter of 200 mm, and 2) another cylinder with an internal diameter of 300 mm. The purpose of these two parts is to assure the homogeneous velocity distribution of air at the exit from the test section and to reduce the elutriation and entrainment of particles from the bed.

The air flow is produced by a blower with variable mass flow rate, and heated by electrical heaters before flowing into the column. Type K thermocouples are used to measure the temperature at specific locations inside the test section and in the plenum chamber. At these locations, pressure variations can be measured using pressure sensors with two different ranges: 100 mbar and 1 bar. Air temperatures are also measured at the inlet and outlet of the test section. The thermocouples and pressure sensors are connected to a data acquisition system for continuous monitoring and recording of the data.

The materials used for the experiments are sand, which is a typical material used in fixed and fluidized beds, and a granular phase changing composite GR50 from Rubitherm®. The material that changes its phase is paraffin, and it is bound within a secondary supporting structure of SiO_2. This composite

material is commercially available in two sizes: a coarser grade with a particle size between 1 and 3 mm, which is suitable for use in a fixed bed (Rady, 2009*a*,*b*), and a finer grade with a particle size between 0.2 and 0.6 mm. The sand and the finer GR50 material correspond to group B according to Geldart's classification (Geldart, 1973), which means that the sand and the finer GR50 composite fluidize easily with vigorous bubbling action and that bubbles grow large (Kunii & Levenspiel, 1991). In addition, the use of two different PCM particle sizes permits the use of the same gas flow rate (450 l/min) in the fixed bed configuration for the sand and the coarser PCM, and also a similar excess gas velocity over minimum fluidization conditions $U/U_{mf} \approx 1.7$ in the fluidized bed for the sand and the finer PCM.

Some properties of the sand and PCM such as density ρ, effective thermal conductivity k_e and mean diameter of the particles $\overline{d}_p$ (with its standard deviation , σ_{dp}) are shown in Table 3.1. In addition, the variation of the specific heat with temperature is presented for each material in Figure 3.2. For the GR50 composite, the variation of specific heat with temperature is nearly the same for the two grades, and, therefore, only one case is shown. For the PCM, the curve of the specific heat versus temperature shows a clear peak between 42 and 50°C where the phase change process occurs. In solid form there is small variation of the specific heat around 30°C, which corresponds with a solid-solid transition. Under 20°C the specific heat is approximately constant around 1.45 kJ/(kg·K). In contrast, the curve for sand is approximately linear, varying between 0.6 kJ/(kg·K) for 20°C and 0.8 kJ/(kg·K) for 95°C.

Differential scanning calorimetry (DSC) is the technique used to study the specific heat variation for the sand and the PCM. The tests were carried out using a sapphire standard. For the coarser PCM one granule was placed in the DSC sample pan while for the finer PCM and the sand a handful of granules was used. A heating rate of 0.5 °C/min was selected. According to Rady (2009*b*),

Material	ρ [kg/m^3][1]	k_e [W/m·K][2]	$\overline{d}_p$ [mm][1]	σ_{dp} [mm][1]
Sand*	2632.3	4.2	0.76	0.069
Finer GR50	1550.5	4.0	0.54	0.082
Coarser GR50	1512.8	4.0	1.64	0.196

Table 3.1: Properties of the materials used in these experiments. [1]Measured at room temperature. [2]Data from the manufacturer.*This sand corresponds to Sand 1 from Table 2.2.

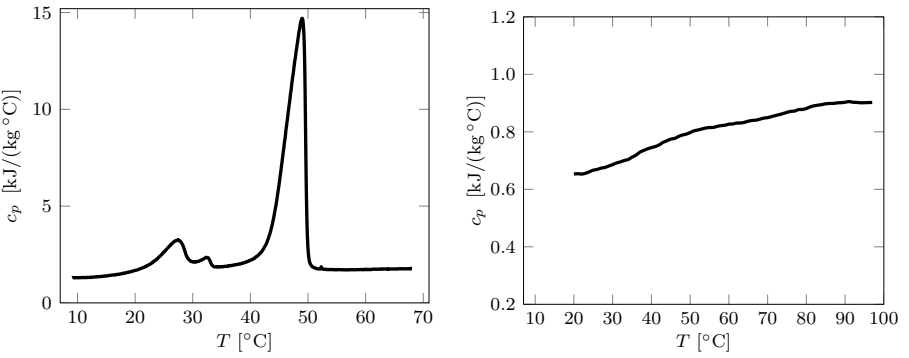

(a) GR50 (b) Sand

Figure 3.2: Variation of the specific heat with temperature for (a) the GR50 and (b) the sand.

who studied in detail the same granular PCM used in our work, this heating rate is slow enough to guarantee that the onset of crystallization occurs at the same temperature as the termination of the melting process. This DSC method has also been used to study the phase changing behavior of the granular GR50. The characterization results are shown in Table 3.2. These DSC results include the specific heats of the solid and liquid phases $c_{p,s}, c_{p,l}$, the latent heat of phase change h_{ls} and the characteristic temperatures of the phase change: onset temperature T_{on}, end temperature T_{end}, extrapolated starting temperature T_s, extrapolated ending temperature T_e and peak temperature T_p (Rady, 2009*b*).

For the comparison between fixed and fluidized beds of sand and PCM, a static bed height of $H = 200$ mm is defined for all of the experiments in order

Material	$c_{p,s}$ [J/kg·K]	$c_{p,l}$ [J/kg·K]	h_{ls} [J/kg]	T_{on} [°C]
Finer GR50	1458.3	1668.7	52049.8	39.4
Coarser GR50	1448.6	1735.7	54379.0	38.6

Material	T_s[° C]	T_e[°C]	T_{end}[°C]	T_p[°C]
Finer GR50	45.3	51.6	54.3	49.8
Coarser GR50	45.3	51.8	56.2	50.0

Table 3.2: Characterization of the PCM using DSC.

to have the same storage volume in all cases. The column is filled with 5 kg of PCM or 9 kg of sand. When we analyze the influence of flow rate on the operation of the fluidized bed of PCM, the height of the bed is fixed at 200 mm and the flow rate is varied. For the study of the influence of the bed height on the performance of the bed, the flow rate remains constant while the bed height is augmented and the mass of solids in the bed varies accordingly.

The bed temperature is uniform and equal to the ambient temperature at the beginning of every experiment. An experiment starts by blowing air at the desired rate into the column and switching on the electric heaters with the required power. The air is heated from room temperature up to 65°C by regulating the electrical resistance power using a PID controller with the control thermocouple placed at the plenum chamber. The PID controller has been selected to provide the same supply temperature pattern for all of the experiments.

When the temperature along the bed is stabilized, the blowing air is no longer heated. Then, the inlet temperature of the air and the bed temperature both start to decrease. Temperatures are measured on the bed axis at different heights from the distributor: 25, 75, 125, 175 and 425 mm, where the last location (425 mm) is above the bed surface.

3.2.1 Hydrodynamics of the fluidized bed

Figure 3.3 shows the distributor pressure drop Δp_{dist} for different superficial gas velocities, U (m/s). These data can be properly fit to a parabola shape.

The pressure drop across the bed of particles, Δp_{bed}, is defined as the distributor pressure drop subtracted from the pressure drop of the system when it is filled with particles (Kathuria & Saxena, 1987). Thus,

$$\Delta p_{bed} = \Delta p_{system} - \Delta p_{dist}. \tag{3.1}$$

The pressure drop of the system, Δp_{system}, is the pressure difference between the plenum chamber and the ambient pressure measured when the bed is filled (to a height equal to the bed diameter) with sand and the finer grade of GR50. Figure 3.4 shows the pressure across the bed as function of the superficial gas velocity for the sand and for the finer grade of GR50. These measurements are used to determine the minimum fluidization velocity of each material, U_{mf}. The minimum fluidization velocity is usually defined as the intersection of the horizontal fluidized bed line and the sloping packed bed line (Geldart, 1986),

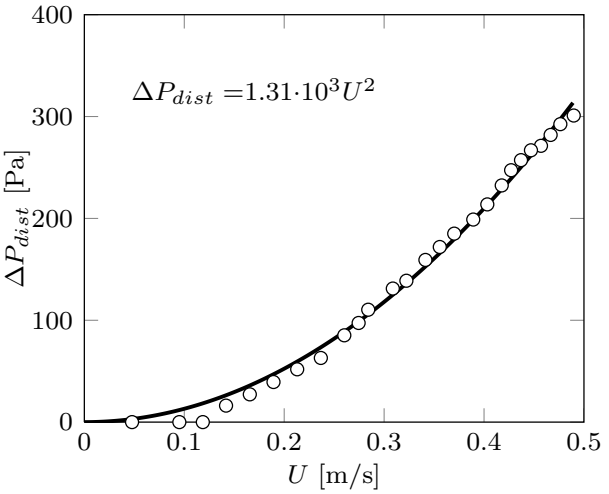

Figure 3.3: Pressure drop across the distributor plate.

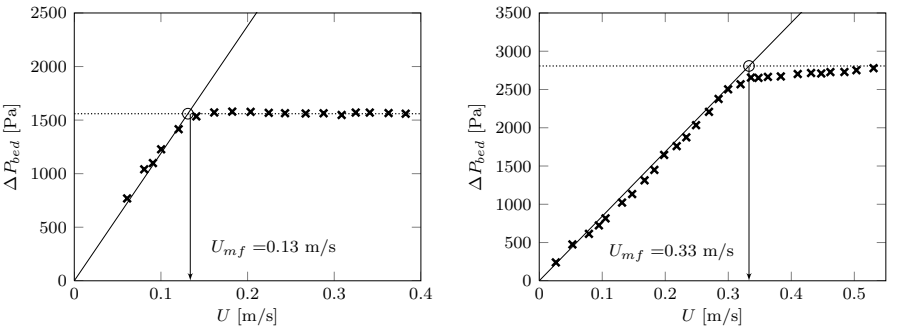

(a) GR50 (b) Sand

Figure 3.4: Pressure across the bed at different superficial gas velocities for the sand and the finer GR50.

which results in $U_{mf} = 0.33$ m/s for the sand and $U_{mf} = 0.13$ m/s for the finer GR50 grade.

The flow rates for the fluidization experiments are chosen to provide the same excess air, U/U_{mf}, conditions for the different experiments. Therefore, the flow rates are 450 l/min for both fixed beds, and 450 l/min and 1000 l/min for the fluidized beds of the PCM material and the sand, respectively (because

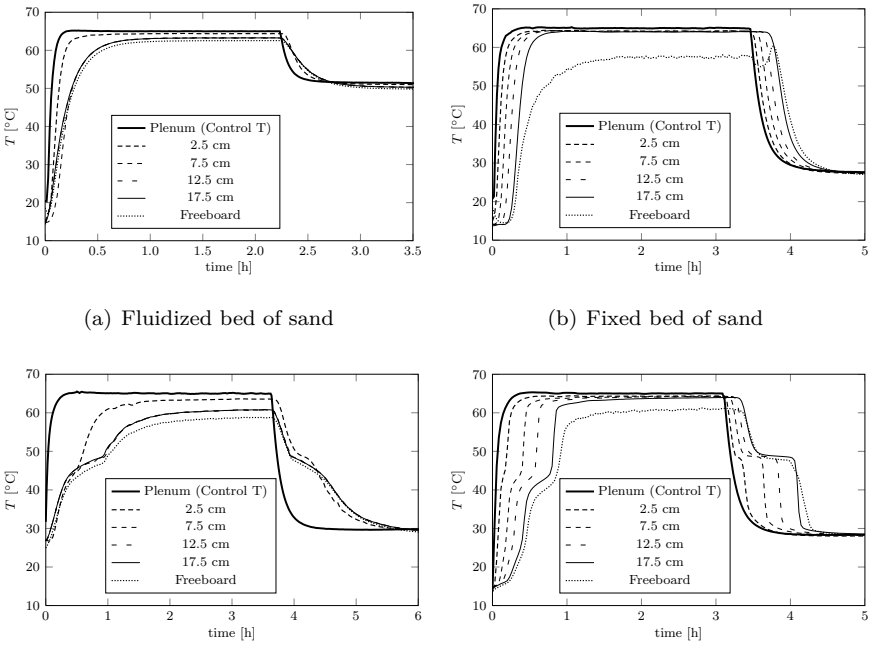

(a) Fluidized bed of sand

(b) Fixed bed of sand

(c) Fluidized bed of GR50 0.54 mm

(d) Fixed bed of GR50 1.64 mm

Figure 3.5: Temperature profiles for the sand and the GR50 PCM in fixed and fluidized beds.

the PCM and sand have different minimum fluidization velocities). At these flow rates, both fluidized materials are working with an excess of air velocity over the minimum fluidization conditions, U/U_{mf}, of approximately 1.7. The fixed bed height is the same in the two cases so both fluidization experiments are comparable because they are under similar bubbling conditions.

3.3 Results and discussion

Four experiments are performed to compare the behavior of a bed filled with PCM and that of a bed filled with sand. Figure 3.5 shows the temperatures that are measured at different heights during the charging and discharging processes for the four different configurations.

Under fluidization conditions, the temperature along the bed is uniform regardless of the fluidized material (either sand or PCM) because the system

behaves similarly to a well mixed tank (Kunii & Levenspiel, 1991). Three of the four thermocouples inside the bed (the thermocouples located at 7.5, 12.5 and 17.5 cm above the distributor) measure the same temperature during the charging process. The first thermocouple, located only 2.5 cm over the distributor, shows a higher temperature than the other thermocouples during almost the whole process. These results could be attributed to the influence of the air jets from the distributor perforations (Rees *et al.*, 2006). These jets could be long enough to modify the temperature measured by the first thermocouple. The temperature measured at 2.5 cm is thus an average of the air temperature coming from the plenum chamber through the distributor and the bed temperature.

For fixed bed conditions, the behavior is different. The bed behaves similarly to a plug flow system. The regions of the bed closer to the distributor are heated before those regions located farther away from the distributor. In the tests with GR50, this composite material takes longer than sand to reach the set temperature because of the latent heat that is stored while the phase change is taking place around 50°C.

For the fixed bed experiments, the phase change takes place at different times at different heights because of the temperature stratification, in accordance with results presented by Rady (2009*a*). In contrast, in the fluidized bed, the phase change of the material takes place uniformly throughout the whole bed.

To analyze the experiments, two parameters are studied: the storage efficiency during the charging process, η_C, and the recovery efficiency of the discharging process, η_R (Elsayed *et al.*, 1988; Dhifaoui *et al.*, 2007).

The storage efficiency is defined as

$$\eta_C = \frac{E_s}{E_{in}} = \frac{\rho_s(1-\varepsilon)A_t \displaystyle\int_{x=0}^{x=H} (i_{b_x} - i_0)\,\mathrm{d}x}{\displaystyle\int_{t=0}^{t} \dot{m}_{air}\, c_{p,air}\, (T_{air} - T_0)\,\mathrm{d}t}, \tag{3.2}$$

where ρ_s is the solid density (sand or PCM), ε the voidage of the bed, $A_t = (\pi/4)\, {d_i}^2$ the cross section of the bed, $\dot{m}_{air}$ is the mass flow rate of air to the bed, $c_{p,air}$ is the specific heat of the air as a function of the inlet air temperature T_{air}, T_0 is the initial bed temperature and $i_{b_x} - i_0$ is the specific energy stored in the bed defined in the expression

$$i_{b_x} - i_0 = \int_{T_0}^{T_{b_x}} c_p\,\mathrm{d}T, \tag{3.3}$$

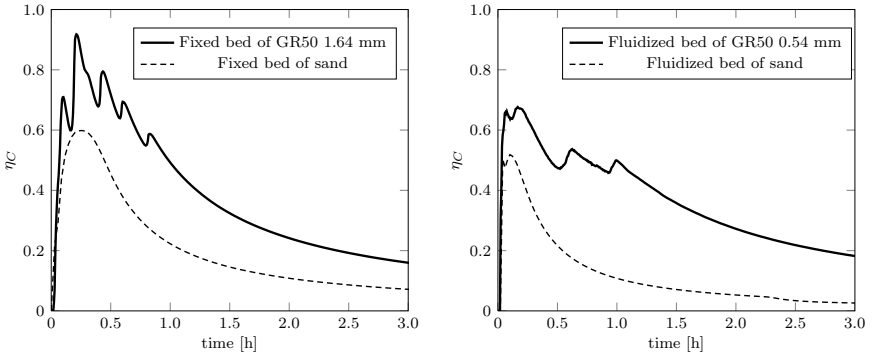

Figure 3.6: Evolution of efficiency with time for the sand and the GR50 PCM in fixed and fluidized beds during the charging process.

where c_p is the apparent specific heat of the material in the bed as a function of T_{b_x} (the bed temperature at height x and time t).

According to Equation (3.2) η_C relates the energy stored, E_s, in the bed at time t and the total thermal energy supplied by the air at the inlet of the bed, E_{in}, (relative to the initial temperature of the bed T_0) up to the same time, t. The value of the energy stored in the bed at a given time has been calculated by dividing the bed into four elements because there are four thermocouples in the bed (at heights x = 2.5, 7.5, 12.5 and 17.5 cm).

The variation of η_C with time for the sand and the GR50 PCM in the fixed bed is presented in Figure 3.6(a) and that for the same materials under fluidized conditions is presented in Figure 3.6(b). The efficiency is higher with the GR50 material than with the sand for both types of beds. This is due to the inherent characteristics of both materials. One of the main advantages of the PCM is its high capacity of storing energy per unit volume. In this case, the energy storage capacity of the GR50 is approximately double of the energy capacity of the sand in the same volume. Therefore, when the temperature reaches the maximum and steady temperature (after approximately two hours) the maximum efficiency of the GR50 for the fixed bed is twice the maximum efficiency of the sand (see Figure 3.6(a)). Another advantage of the GR50 over the sand is its lower density and minor particle size, which permits to fluidize the GR50 PCM with a lower air flow rate. In the experiments compared in Figure 3.6(b) the air flow rate in the GR50 PCM is approximately half of the flow rate used with the sand. As a consequence, the maximum efficiency of

the GR50 is approximately four times higher than the maximum efficiency of the sand when the temperature of the bed reaches the maximum and steady temperature.

The first minutes of each experiment should not be taken into account as they correspond to the stabilization of the system. After this stabilization period, the efficiency increases with the bed temperature because the inlet air is also being heated during the charging process. When the inlet air temperature reaches its maximum achievable value, the efficiency starts to decrease. The variation of the efficiency for the sand is smooth in both fixed and fluidized conditions. In contrast, the curves obtained for the PCM show abrupt changes in slope at the beginning and end of the phase change process. In the fixed bed (Figure 3.6(a)) appear four changes in the slope of the curve, which correspond with the phase change process detected by each one of the four thermocouples in the bed. The highest efficiency for the fixed bed case is found to occur when the thermocouple placed at 7.5 cm detects the phase change. Under fluidized conditions (Figure 3.6(b)), only one change in the slope is observed between 0.5 and 1.0 hours, because it is well mixed and the phase change transition occurs homogenously in the bed.

When the temperature in the bed is stabilized, the electric heaters stop heating the air and the blowing air continues to flow at the same rate as the original heated flow. To analyze this discharging process, the recovery efficiency, η_R, is defined as follows (Elsayed *et al.*, 1988)

$$\eta_R = \frac{E_d}{E_{d,max}} = \frac{\rho_s(1-\varepsilon)A_t \int_{x=0}^{x=H} (i_{b_{max}} - i_x)\,\mathrm{d}x}{\rho_s(1-\varepsilon)A_t \int_{x=0}^{x=H} (i_{max} - i_{end})\,\mathrm{d}x} = \frac{\int_{x=0}^{x=H} \int_{T_{b_x}}^{T_{b_{max}}} c_p\,\mathrm{d}T\,\mathrm{d}x}{\int_{x=0}^{x=H} \int_{T_{end}}^{T_{max}} c_p\,\mathrm{d}T\,\mathrm{d}x}, \tag{3.4}$$

where E_d names the energy obtained during the discharging period up to the time t, $E_{d,max}$ represents the maximum available energy at the discharge, T_{b_x} is the bed temperature at height x and time t, $T_{b_{max}}$ is the maximum bed temperature achieved at the end of the charging process, T_{max} corresponds to the supply air temperature at steady state conditions and T_{end} is the temperature of the bed at the end of the experiment.

Figures 3.7(a) and 3.7(b) represent the evolution of the recovery efficiency for the fixed and fluidized beds with sand and PCM, respectively.

The bed temperature for the four experiments does not decrease to the

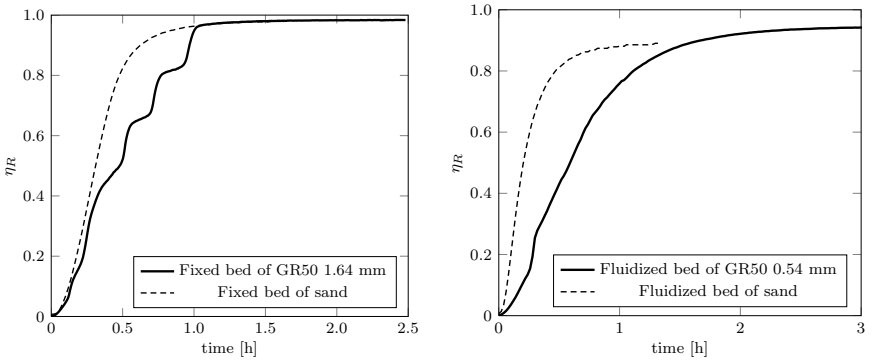

Figure 3.7: Evolution of recovery efficiency over time for the sand and the GR50 PCM in fixed and fluidized beds during the discharging periods.

initial temperature because the supplied air is heated by the blower, thereby achieving a higher temperature than the ambient temperature. The difference between the T_{end} and the room temperature depends on the flow rate. Thus, for the fluidized bed with sand, this difference is maximized when the flow rate is highest.

The recovery efficiency for the fixed beds (Figure 3.7(a)) shows better behavior for sand than GR50 during the first hour because of the time required for the solidification of the PCM. Thus, the 'steps' in the PCM curve correspond to the phase change. Nevertheless, after the first hour, the efficiency parameter is the same for both materials.

For the recovery efficiency in fluidized beds (Figure 3.7(b)), the efficiency during the first hour is higher for sand than for GR50, as also observed for the fixed beds. In contrast, when the recovery efficiency is stabilized in both fluidized beds, the PCM presents higher efficiency (0.94) than sand (0.89).

3.3.1 Influence of flow rate

To study the influence of flow rate on the performance of the fluidized bed with PCM, four different cases were studied. In all of these experiments, the mass of PCM was 5 kg and the air flow was heated from room temperature up to 65°C. The flow rates selected were 625, 500, 450 and 375 l/min, which correspond to an excess air velocity over the minimum fluidization conditions, U/U_{mf}, of 2.5, 2, 1.7 and 1.5, respectively.

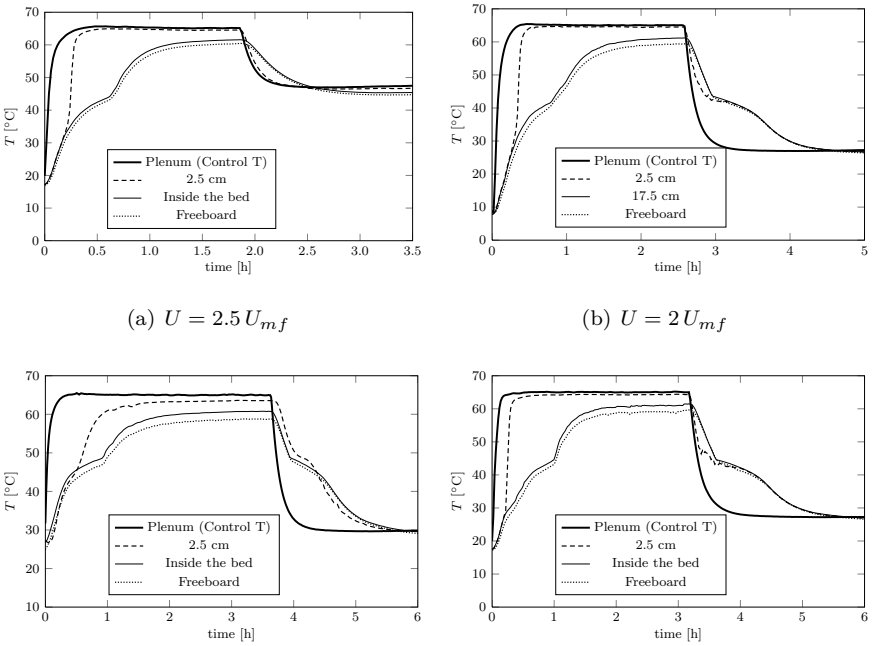

(a) $U = 2.5\,U_{mf}$ (b) $U = 2\,U_{mf}$

(c) $U = 1.7\,U_{mf}$ (d) $U = 1.5\,U_{mf}$

Figure 3.8: Temperature profiles for the fluidized bed with GR50 for different flow rates.

In Figure 3.8, the temperature distributions along the bed for the four experiments are presented. The temperatures plotted in this figure are the control temperature; the temperature measured by the first thermocouple, which is located 2.5 cm from the distributor; the mean temperature in the bed, which is calculated from data obtained by the other three thermocouples at 7.5, 12.5 and 17.5 cm; and the temperature of the air at the outlet section. The influence of the air jets on the temperature of the first thermocouple is also observed in the four cases shown in Figure 3.8.

Before proceeding to the analysis of these experimental results, it is convenient to introduce the following dimensionless bed average temperature

$$\overline{\theta}_b = \frac{\overline{T}_b - T_0}{T_{max} - T_0}, \tag{3.5}$$

where $\overline{T}_b$ is the average temperature of the bed, T_0 is the initial temperature of the bed and T_{max} is the supplied air temperature at steady state conditions

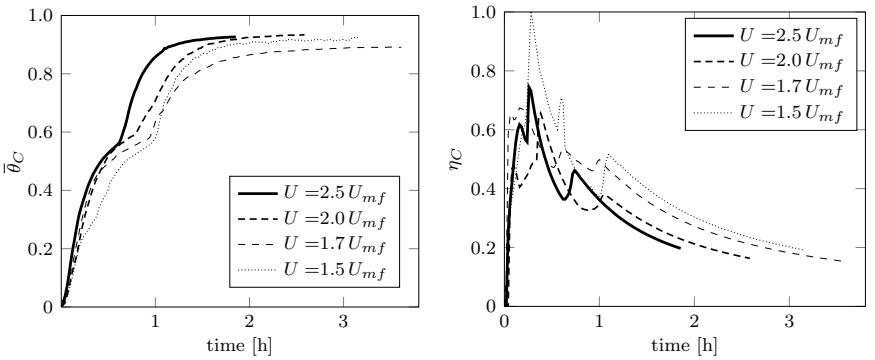

(a) Temperature profiles

(b) Charging efficiency

Figure 3.9: (a) Non-dimensional temperature profiles for the charging of GR50 at different flow rates. (b) Evolution of efficiency over time for the charging of GR50 at different flow rates.

(in this case, 65°C).

To analyze these experiments, η_C and η_R are calculated. In Figure 3.9(b), the efficiency during the charging process for the four experiments is shown. Furthermore, for better understanding, the dimensionless temperature for each charging test is presented in Figure 3.9(a).

The results of the efficiency evolution show that, disregarding the stabilization period, higher values of efficiency are reached once the supply air temperature attains its maximum difference with respect to the bed temperature. When the maximum steady temperature is reached in the bed, after approximately two hours of operation, the higher the air flow rate the lower the discharge efficiency because E_{in} increases for the same stored energy (see Equation (3.2)). However, a higher flow rate permits the set temperature to be achieved more quickly.

The dimensionless temperature and efficiency evolution during the recovery process are shown in Figure 3.10. The dimensionless temperature for the discharging process when $U/U_{mf} = 2.5$ (Figure 3.10(a)) shows that no phase change occurs because the blower heats the air flow above the phase change temperature. Thus, the recovery efficiency is not plotted for this case in Figure 3.10(b).

Regarding the charging process, similar efficiencies are observed at the end

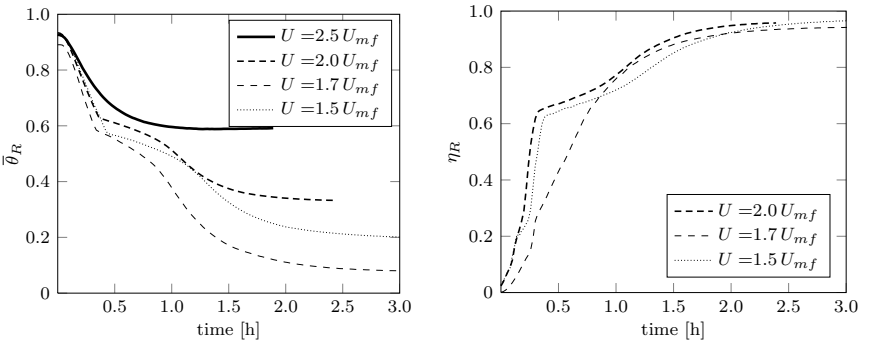

(a) Temperature profiles

(b) Discharging efficiency

Figure 3.10: (a) Non-dimensional temperature profiles for the discharging process of GR50 at different flow rates. (b) Evolution of efficiency over time for the discharging process of GR50 at different flow rates.

of the recovery process for the different flow rates, and the phase change occurs sooner at a higher flow rate.

3.3.2 Influence of bed height

The influence of the bed height in the fluidized bed filled with PCM is investigated. Three experiments are performed at various bed heights. The air is heated from room temperature up to 65°C, and the flow rate selected (500 l/min) is the same for all experiments. The three chosen heights are 100, 200 and 300 mm, which correspond to 0.5, 1 and 1.5 times the diameter of the bed, respectively. In Figure 3.11, the temperature distributions along the bed for the three experiments are presented.

The dimensionless temperature and efficiency for the charging process are presented in Figure 3.12. The time required to achieve a certain temperature is longer when the mass of the material is higher because the input energy is the same for the three different cases. However, increased charging efficiency is obtained when the mass is higher (see Figure 3.12(b)) as there is more material available to store heat while the input energy is the same. When the bed reaches a steady state, the maximum temperature attained decreases as the bed height increases, possibly because of small thermal losses to the ambient surroundings, although the bed is insulated. When the bed height is doubled (or tripled), the

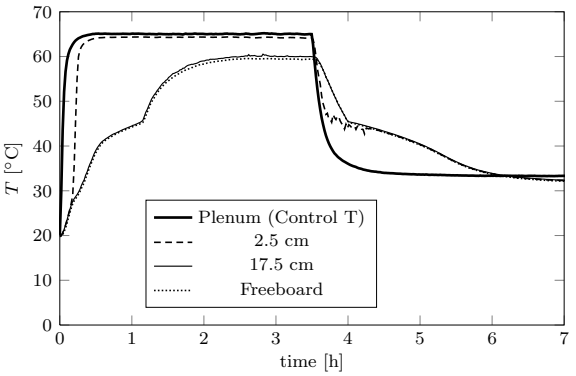

(a) $H = 1.5\,D$

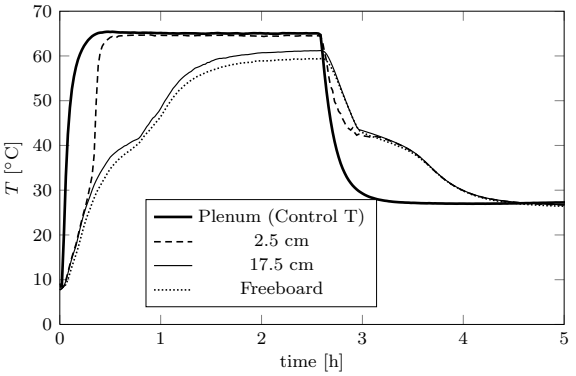

(b) $H = 1\,D$

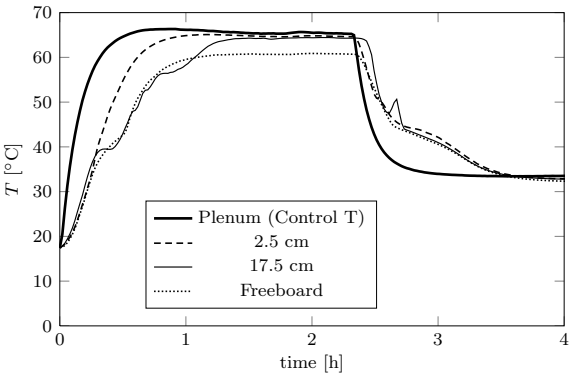

(c) $H = 0.5\,D$

Figure 3.11: Temperature profiles for the fluidized bed with GR50 for different bed heights.

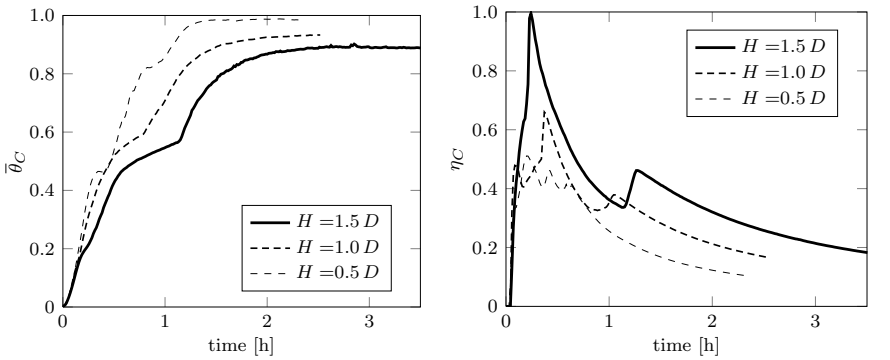

(a) Temperature profiles

(b) Charging efficiency

Figure 3.12: (a) Non-dimensional temperature profiles for the charging process of GR50 for different bed heights. (b) Evolution of efficiency with time for the charging process of GR50.

heat transfer area for heat losses is also doubled (or tripled), thereby increasing the thermal losses. For the bed height of $0.5D$, the bed temperature undergoes fluctuations that may be caused by the proximity of the thermocouple to the freeboard, where the bursting bubbles may affect the measurements.

In Figure 3.13, the dimensionless temperature and evolution efficiency during the recovery process are shown. Figure 3.13(a) shows that it takes more time to discharge the bed when the mass is higher, and better recovery efficiency coefficients are obtained when less mass is introduced (see Figure 3.13(b)). This last effect is a result of the higher thermal losses to the ambient surroundings from the larger beds, which results in a lower bed temperature at the beginning of the recovery process. Therefore, less of the energy supplied by the inlet gas during the charging process is recovered by the system.

3.3.3 Cycling behavior

Micro-encapsulated PCM may be prone to fracture and cracking because of collisions and shearing when fluidized by air. There are different studies in the literature concerning the stability of micro-PCMs in slurries (Delgado *et al.*, 2012; Giro-Paloma *et al.*, 2012; Yang *et al.*, 2003) and they conclude that rupture of the micro-capsules in slurries is reduced diminishing the particle size and increasing the thickness of the encapsulation. Nevertheless, the different

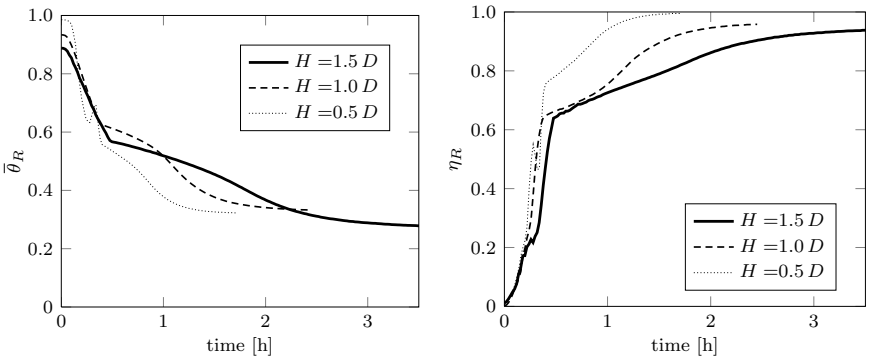

(a) Temperature profiles

(b) Discharging efficiency

Figure 3.13: (a) Non-dimensional temperature profiles for the discharging process of the GR50 for different bed heights. (b) Evolution of efficiency with time for the discharging process of GR50 for different bed heights.

phenomena that influence on the stability of micro-PCM slurries are different to those appearing in a bubbling fluidized bed and a direct comparison is not possible. The micro-PCMs used typically in slurries have a size around or under 10 μm whereas we are using particles of $\overline{d}_p = 0.54$ mm. Also the particle concentration in slurries is usually much lower than in fluidized beds, which is around 60%.

In fluidized beds the attrition is the phenomenon responsable for particle fragmentation. Two different attrition mechanisms can be observed (Werther & Reppenhagen, 2003): abrasion and fragmentation. In the first, particles of much smaller size are removed from the particle surface. As a result, the particle size distribution is slightly modified although the percentage of fines is increased. The final size distribution is bimodal. In the second mechanism, the original particles break into particles of similar size. The particle size distribution is notably broader with a distinctly smaller mean particle size. Ray & Jiang (1987) and Pis *et al.* (1991) concluded that the dominant mechanism in most fluidized bed applications is abrasion.

To study the cycling behavior and the attrition of the PCM, 15 heating and cooling cycles are conducted under the same conditions ($U = 500$ l/min, GR50 heated up to 65°C). Samples of 250 g of GR50 were extracted from the bed after certain cycles to study the particle size evolution. Some of the cycling

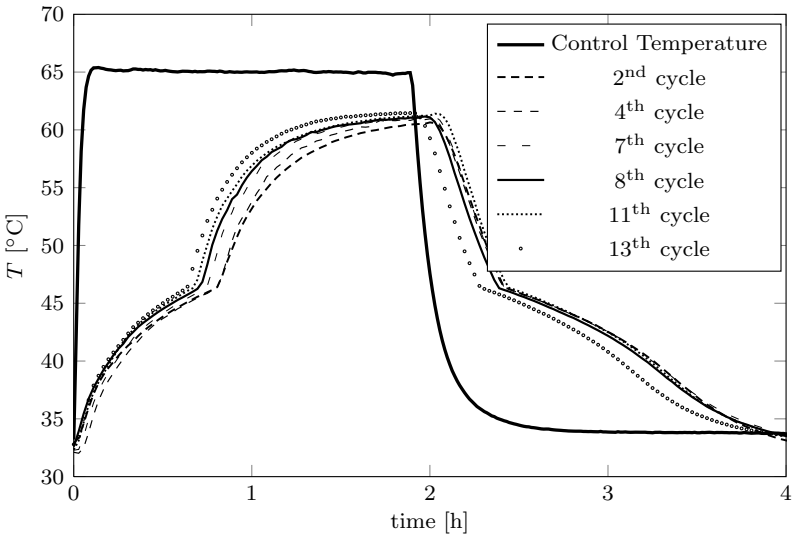

Figure 3.14: Temperature profiles for different cycles under the same conditions for the PCM in a fluidized bed.

curves are presented in Figure 3.14. The uniformity of the temperature in the bed measured during thermal cycling indicates that the fluidization quality of the PCM used in this study is not affected by the number of cycles and that the cycling stability is ensured. No loss of heat storage or recovery capacity during thermal cycling appears. Furthermore, the set temperature (65°C) is achieved sooner in the sequence of cycles. One reason could be the small differences between the size distributions in the sequence of cycles. When the number of cycles is increased, the particles become smaller, the heat transfer area increases, and hence, the heat transfer improves.

The particle size distributions after each cycle have been determined by sieve analysis. Figure 3.15 represents the cumulative distribution function showing the weight percent of particles passing through a sieve of a given aperture between the initial distribution and the end of two different cycles. The variation observed in the particle size distribution indicates that abrasion is present in the fluidized bed with GR50. The mean particle size is slightly reduced, the external surface of the particles is eroded increasing the content of fines in the bed but the PCM remains encapsulated. In Figure 3.15 it is observed that the percentage of fines is not augmented because no cyclone or dispositive has been used to collect them, so they are probably lost during the fluidized bed

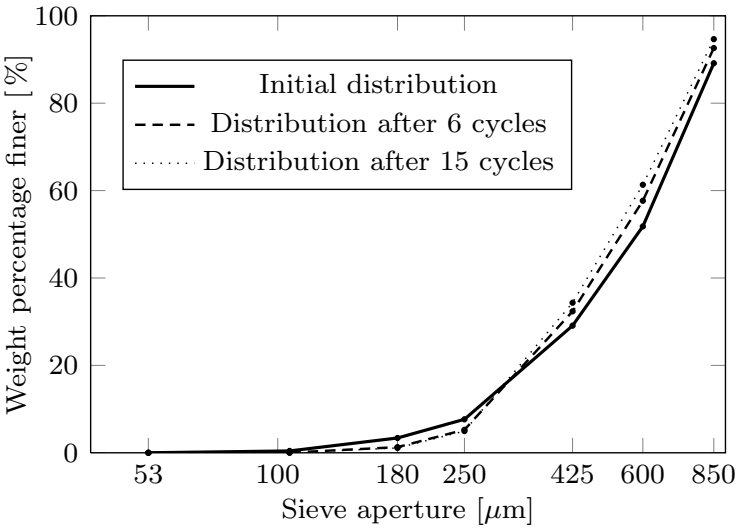

Figure 3.15: Cumulative distribution function showing the weight percent of particles passing through a sieve of a given aperture at the beginning, middle and end of the cycling tests.

operation. The rate of erosion reduces with time because the rugosities of the particles are filed and the surface is smoothed (see Section 2.3.3). Only if the thickness of the encapsulation is not large enough the abrasion could provoke the lost of PCM. If the PCM leaks out when it is in liquid form it can stick a group of particles, forming agglomerates similar to the ones observed by other researchers in slurries (Giro-Paloma *et al.*, 2012). If this happens the bed would be probably defluidized because the air flow rate could not fluidize particles of such size, but this problem is not observed in our work. If the PCM studied in this work is going to be used in an actual process, probably the material will suffer more than 15 cycles. For a specific application, the PCM should be previously tested under the same charging-discharging times and temperatures of the application, which could be different from the ones used in this work. The number of cycles that the PCM keeps its properties must be large enough to be economically profitable in comparison with a conventional storage facility. Nevertheless, this number of cycles strongly depends on the application and has to be studied for each particular case.

3.4 Conclusions

In this paper, the performance of an air-fluidized bed of micro-encapsulated PCM as a thermal storage system is studied. Its performance is compared to that of other storage methods: a fluidized bed of sand and fixed beds with sand and PCM. It is concluded that the PCM is an alternative material that can be used to increase the efficiency of storing thermal energy in the form of latent heat in fluidized bed systems.

Under the experimental conditions tested in this work, greater charging efficiencies are observed for the PCM than sand in fixed and fluidized beds. Furthermore, when the charging efficiency is stabilized, the PCM shows similar results for both beds. The PCM also presents better recovery efficiency for both beds after the solidification time.

The study of the influence of the bed height shows that it takes longer to achieve a certain temperature when more mass is used, but higher efficiency values are obtained. The analysis of the influence of the flow rate shows that a higher flow rate permits the set temperature to be achieved more quickly. At the end of the charging process, similar efficiencies are measured at the different flow rates studied. The cycling study reveals that the PCM suffers attrition during the fluidization process, although no loss of PCM is observed under the experimental conditions tested in this work (75 hours of continuous operation with 15 charging-discharging cycles).

Notation

A_t	cross section of the bed [m^2]
c_p	specific heat[$J \cdot kg^{-1} \cdot K^{-1}$]
$\overline{d}_p$	mean particle diameter [mm]
d_i	internal diameter of the bed [mm]
E	energy [J]
H	height of the bed [mm]
h_{ls}	PCM latent heat of fusion [$J \cdot kg^{-1}$]
i	specific energy stored in the bed [$J \cdot kg^{-1}$]
k_e	effective thermal conductivity [$W \cdot m^{-1} \cdot K^{-1}$]
m	mass [kg]
$\dot{m}$	mass flow rate [$kg \cdot s^{-1}$]
T	temperature [°C]
t	time [s]

U	superficial gas velocity [m·s^{-1}]
U_{mf}	minimum fluidization velocity [m·s^{-1}]

Greek symbols

ρ	density[kg·m^{-3}]
σ_{dp}	standard deviation of the mean particle diameter [mm]
Δp	pressure drop [Pa]
$\overline{\theta}$	dimensionless temperature
η	efficiency
ε	voidage of the bed

Subscripts

0	initial
b	bed
C	charging
D	discharging
end	end of the discharging process
in	inlet
l	liquid phase
s	solid phase
max	maximum value
x	at a specific bed height

References

Beasley, D.E. & Clark, J.A. 1984 Transient response of a packed bed for thermal energy storage. *International Journal of Heat and Mass Transfer* 27, 1659–1669.

Benmansour, A., Hamdan, M.A. & Bengeuddach, A. 2006 Experimental and numerical investigations of solid particles thermal energy storage unit. *Applied Thermal Engineering* 26, 513–518.

Brown, R.C., Rasberry, J.D. & Overmann, S.P. 1998 Microencapsulated phase-change materials as heat transfer media in gas fluidized beds. *Powder Technology* 98, 217–222.

Cabeza, L.F., Castell, A., Barreneche, C., de Gracia, A. & Fernández, A.I. 2011 Materials used as pcm in thermal energy storage in buildings: A review. *Renewable & Sustainable Energy Reviews* 15, 1675–1695.

Delgado, M., Lázaro, A., Mazo, J. & Zalba, B. 2012 Review of phase change materials emulsions and microencapsulated phase change material slurries: materials, heat transfer studies and applications. *Renewable & Sustainable Energy Reviews* 16, 253–273.

Dhifaoui, B., Jabrallah, S. Ben, Belghith, A. & Corriou, J.P. 2007 Experimental study of dynamic behaviour of a porous medium submitted to a wall heat flux in view of thermal energy storage by sensible heat. *International Journal of Thermal Sciences* 46, 1056–1063.

Elsayed, M.M., Megahed, I.E. & El-Refaee 1988 Experimental testing of fluidized beds thermal storage. *Solar & Wind technology* 5, 15–25.

Geldart, D. 1973 Types of gas fluidization. *Powder Technology* 7, 285–292.

Geldart, D. 1986 *Gas Fluidization Technology*. John Wiley & Sons.

Giro-Paloma, J., Oncins, G., Barreneche, C., Martínez, M., Fernández, I. & Cabeza, L.F. 2012 Physico-chemical and mechanical properties of microencapsulated phase change material. *Applied Energy* 109, 441–448.

Hänchen, M., Brückner, S. & Steinfeld, A. 2011 High temperature thermal storage using a packed bed of rocks. heat transfer analysis and experimental validation. *Applied Thermal Engineering* 31, 1798–1806.

Kathuria, D.G. & Saxena, S.C. 1987 A variable thickness two-dimensional bed for investigating gas-solid fluidized bed hydrodynamics. *Powder Technology* 53, 91–96.

Kunii, D. & Levenspiel, O. 1991 *Fluidization Engineering*. Butterworth-Heinemann.

Merry, N. & Rubinsky, B. 1989 Energy storage in a fluidized bed. *Transactions of the ASME. Journal of Heat Transfer* 111, 726–730.

Nagano, K., Takeda, S., Mochida, T. & Shimakura, K. 2004 Thermal characteristics of a direct heat exchange system between granules with phase change material and air. *Applied Thermal Engineering* 24, 2131–2144.

Pis, J.J., Fuertes, A.B., Artos, V., Suárez, A. & Rubiera, F. 1991 Attrition of coal ash particles in a fluidized bed. *Powder Technology* 66, 41–46.

Rady, M. 2009*a* Granular phase change materials for thermal energy storage: experiments and numerical simulations. *Applied Thermal Engineering* 29, 3149–3159.

Rady, M. 2009*b* Study of phase changing characteristics of granular composites using differential scanning calorimetry. *Energy Conversion and Management* 50, 1210–1217.

Ray, Y.C. & Jiang, T.S. 1987 Particle attrition phenomena in a fluidized bed. *Powder Technology* 49, 193–206.

Rees, A.C., Davidson, J.F, Dennis, J.S., Fennell, P.S., Gladden, L.F., Hayhurst, A.N., Mantle, M.D., Mu̇ller, C.R. & Sederman, A.J. 2006 The nature of the flow just above the perforated plate distributor of a gas-fluidised bed, as imaged using magnetic resonance. *Chemical Engineering Journal* 61, 6002–6015.

Regin, A.F., Solanki, S.C. & Saini, J.S. 2008 Heat transfer characteristics of thermal energy storage system using pcm capsules: A review. *Renewable and Sustainable Energy Reviews* 12, 2438–2458.

Regin, A.F., Solanki, S.C. & Saini, J.S 2009 An analysis of a packed bed latent heat thermal energy storage system using pcm capsules: Numerical investigation. *Renewable Energy* 34, 1765–1773.

Sozen, Z.Z., Grace, J.R. & Pinder, K.L. 1988 Thermal energy storage by agitated capsules of phase change material: pilot scale experiments. *Industrial and Engineering Chemistry Research* 27, 679–684.

Wagialla, K.M., Fakeeha, A.H., Elnashaire, S.S.E.H. & Almaktary, A.Y. 1991 Modeling and simulation of energy storage in fluidized beds using the two-phase model. *Energy Sources* 13, 189–201.

Werther, J. & Reppenhagen, J. 2003 *Handbook of fluidization and fluid-particle systems, chapter 8*. Marcel Dekker Inc., New York.

Xia, L., Zhang, P. & Wang, R.Z. 2010 Numerical heat transfer analysis of the packed bed latent heat storage system based on an effective packed bed model. *Energy* 35, 2022–2032.

Yang, R., Xu, R. H. & Zhang, Y. 2003 Preparation, physical property and thermal physical property of phase change microcapsule slurry and phase change emulsion. *Solar Energy Materials & Solar Cells* 80, 405–416.

Zalba, B., Marín, J.M., Cabeza, L.F. & Mehling, H. 2003 Review on thermal energy storage with phase change: materials, heat transfer analysis and applications. *Applied Thermal Engineering* 23, 251 – 283.

CHAPTER
FOUR

Modeling and experiments of energy storage in a packed bed with PCM

This work presents a numerical and experimental study of the transient response of a packed bed filled with a granular phase change material (PCM). The proposed numerical model accounts for the progressive evolution of the enthalpy with temperature during the phase change rather than using a constant phase change temperature. This temperature-dependent enthalpy is included in the model as an apparent specific heat that is dependent on temperature according to the measurements obtained by differential scanning calorimetry (DSC). The model also includes the energy stored in the wall, which has been shown to have a non-negligible effect in several experimental facilities.

The equations presented are non-dimensionalized, which results in the same differential equation system regardless of whether a granular PCM is present. In this manner, the same numerical method can be used in cases with or without a granular PCM. Numerical and experimental results are obtained for a conventional granular material (sand) and two commercial granular PCMs with different phase change temperatures. The numerical and experimental heating results exhibit good agreement, and the energy stored in the wall of the bed represents between 8.5 and 17% of the energy stored in the granular material.

4.1 Introduction

The energy storage process reduces the rate mismatch between energy supply and energy demand. Energy can be stored in a material in the form of sensible or latent heat. Water, rock beds and PCMs are the most suitable media for energy storage. Packed beds are typically used in air-based storage systems. Because the inlet fluid temperature typically varies, it is necessary to determine the transient response of packed beds. The use of a PCM as the storage medium

offers several advantages compared to using sensible heat to store a large amount of energy in a small volume or heat charging/discharging at a nearly constant temperature.

Thermal storage models in packed beds include single-phase models, in which the bed is approximated by a quasi-homogeneous medium (Vortmeyer & Schaefer, 1974), and separate-phase models, which were first studied by Schumann (1929), where two energy conservation equations are obtained for the solid and fluid phases and are coupled by a heat exchange term. Among these models, the concentric dispersion model considers a temperature gradient inside the solid spheres (Xia *et al.*, 2010). Furthermore, one- and two-dimensional models (Beasley & Clark, 1984) can be distinguished depending on whether the radial temperature profile is considered.

A review on the mathematical modeling of PCMs has been published by Dutil *et al.* (2011). In particular, fixed-grid methods for solid-liquid phase change problems formulate the governing equations for the entire region of the PCM, including the solid and liquid phases (Faghri & Zhang, 2006). These methods include the following: i) the enthalpy method, in which the energy equation is considered in terms of enthalpy, ii) the equivalent heat capacity method, which converts the latent heat into an equivalent heat capacity of the PCM in the phase change temperature range and iii) the temperature transforming model, which was proposed by Cao & Faghri (1990). The enthalpy method assumes an isothermal phase transition, whereas the equivalent heat capacity and temperature transforming models consider that phase change occurs in a temperature range, where the enthalpy variation with temperature is assumed to be linear. Peng *et al.* (2014) modeled the transient behavior of a packed bed of PCM capsules for high-temperature thermal storage using molten salts as the heat transfer fluid. The radial temperature distribution inside the capsules was included due to the size of the capsules. Rady (2009*a*) presented experiments and numerical simulations of the charging process in a small, fixed bed with an internal diameter of 4.5 cm using air as the heat transfer fluid and particles with a smaller particle diameter (1-3 mm), which allowed the temperature variations within the solids to be neglected. Izquierdo-Barrientos *et al.* (2013) used this material with a smaller particle size (mean diameter of 0.5 mm) in a fluidized bed and observed greater storage efficiencies compared to a typical material, such as sand, in fixed and fluidized beds.

The numerical model presented in this work accounts for the heat stored in the walls of the container. Regarding the phase change process, other re-

searchers have included the effect of the latent heat of melting using an effective heat capacity within the selected melting range (Farid *et al.*, 1998). The researchers have observed that the best agreement between the numerical and experimental results is obtained when the effective heat capacity is calculated from DSC measurements at a heating rate close to the experimental conditions (Arkar & Medved, 2005; Rady, 2009*b*). In this manner, a variable temperature-dependent enthalpy, which was obtained from DSC measurements, is introduced in the model.

The materials used in this work and the experimental set-up are described in the following section. Then, the numerical model of the energy storage in a fixed bed is explained. Finally, the experimental and numerical results are compared, and the main conclusions of the work are summarized.

4.2 Materials and experimental apparatus

The materials used in this study are sand, which is a typical material used for sensible energy storage, and two granular phase-changing composites with different temperature transitions. Both granular PCMs consist of paraffin, which is the PCM, bounded within a secondary supporting structure of SiO_2, which ensures that the paraffin does not leak from the granulate when in liquid form. Table 4.1 presents several properties of the sand and PCMs, such as the density ρ, thermal conductivity k and mean diameter of the particles $\overline{d}_p$ with its standard deviation σ_{dp}.

The granular PCMs are commercially available (Rubitherm® GR50 and GR80) and similar to those used by Rady (2009*a*) and Izquierdo-Barrientos *et al.* (2013) in their studies. The phase change temperature T_{pc} is approximately 50°C for GR50 and 80°C for GR80. The mean particle diameters of GR50 and GR80 are 1.64 and 1.58 mm, respectively, which is suitable for use in a fixed bed. Figure 4.1(a) shows the specific heat evolution with temperature for the granular PCMs, which was measured by DSC with a slow heating rate of 0.5°C/min (Rady, 2009*a*,*b*), which ensures thermal equilibrium in the sample during the DSC measurements. The phase changes of GR50 and GR80 are clearly distinguished at approximately 50°C and 80°C, respectively. The specific heat of the sand was also measured, and a mean value of 0.776 kJ/(kg °C) was obtained for the temperature range used in this work. Figure 4.1(b) presents the enthalpy variation as a function of temperature calculated from the DSC measurements.

Material	ρ [kg/m^3]	k [W/m·K]	$\overline{d}_p$ [mm]	σ_{dp} [mm]
Sand*	2632.3	4.2	0.57	0.070
GR50	1512.8	4.0	1.64	0.196
GR80	1618.0	4.0	1.58	0.187

Table 4.1: Material properties.*This sand corresponds to Sand 3 from Table 2.2.

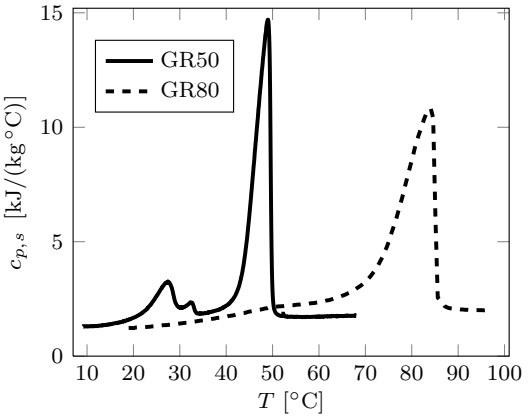

(a)

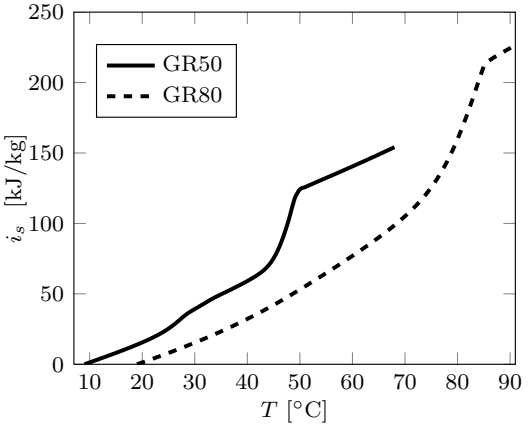

(b)

Figure 4.1: Specific heat (a) and enthalpy variation (b) as a function of temperature for the granular PCMs, GR50 and GR80.

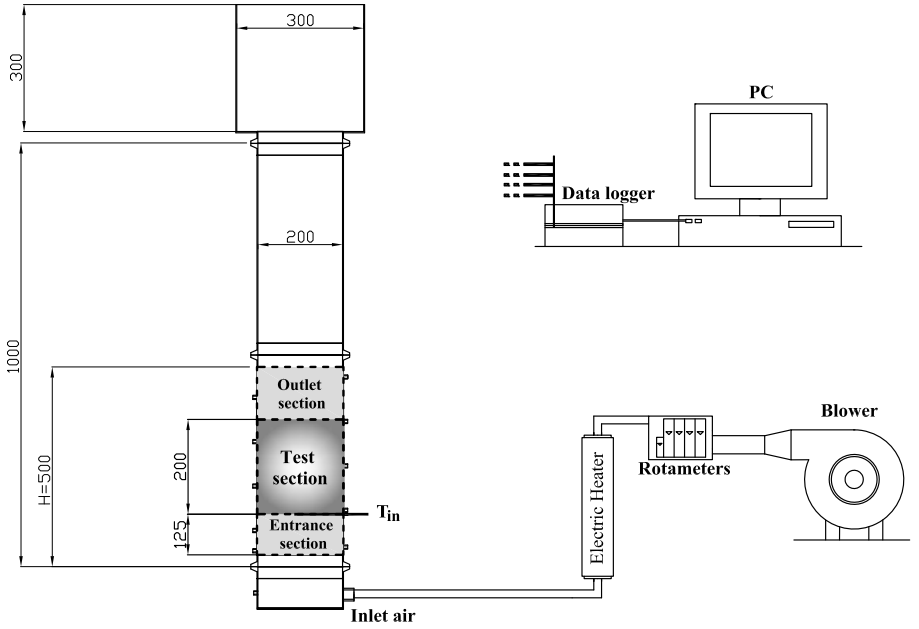

Figure 4.2: Scheme of the experimental apparatus. Dimensions in mm.

Figure 4.2 shows a scheme of the experimental apparatus used for the heating experiments. The bed consists of a cylindrical tube made from stainless steel with 2-mm-thick walls and filled with particles. The air enters the plenum of the column and flows into the bed through a distribution plate. The instrumentally monitored section of the test apparatus has a height of 500 mm and an internal diameter of $d_i = 200$ mm and is insulated with 2-cm-thick glass wool. For every case, the bed was filled with material up to a height of $H = 0.5$ m. For the sand, its height was equivalent to a mass of 18 kg because it has a higher density, whereas the masses of the granular PCMs were approximately 10 kg. The bed is composed of a 12.5-cm-long entrance section to develop the fluid velocity profile before the fluid enters the test section (Thoméo *et al.*, 2004), where it is measured. The test section is 20 cm long and corresponds to the numerical domain. The air flow is produced by a blower with a variable mass flow rate and is heated by electrical heaters before flowing into the column. Type K thermocouples were used to measure the temperature at specific locations inside the test section and within the plenum chamber.

The bed temperature was uniform and equal to the ambient temperature T_0 at the beginning of every experiment. Before beginning the temperature

measurements, the blower is switched on and air is introduced into the column at the desired rate. During this process, the blower heats the air to a temperature greater than the ambient temperature due to the compression process. The entire bed reaches this temperature after approximately 2 h. Once the bed reaches the steady state, the electric heaters are switched on with the required power. The air is heated up to a temperature greater than the T_{pc} of each PCM (65°C for GR50 and 95°C for GR80) by regulating the electrical resistance power with a PID controller, which is controlled using the reading of the thermocouple placed at the exit of the electric heaters.

4.3 Heat transfer model in a packed bed

The proposed two-phase model is explained in the following sections. First, the model is described for a packed bed without phase change in the granular material, and then, the modifications required for the solid phase to include the phase change are described.

4.3.1 Packed bed model without phase change in the granular material

The equations that govern the heat transfer in a packed bed are based on the study by Rady (2009*a*); however, the equations have been modified to include the energy stored in the wall of the bed. In this manner, a new term in the gas equation is added to account for the energy transferred from the bed to wall. Furthermore, the energy conservation equation of the wall is incorporated. The three conservation equations are

$$\rho_a\,\varepsilon\,c_{p,a}\frac{\partial T}{\partial t} = \varepsilon\,k_{a,x}\frac{\partial^2 T}{\partial x^2} + h\,a_p\,(\theta - T) - \rho_a\,\varepsilon\,c_{p,a}\,u\,\frac{\partial T}{\partial x} - \\ - a_{wi,b}\,h_w\,(T - \psi)\,, \tag{4.1}$$

$$\rho_s\,(1-\varepsilon)\,c_{p,s}\frac{\partial \theta}{\partial t} = (1-\varepsilon)\,k_{s,x}\frac{\partial^2 \theta}{\partial x^2} - h\,a_p\,(\theta - T)\,, \tag{4.2}$$

$$\rho_w c_{p,w}\frac{\partial \psi}{\partial t} = k_w\frac{\partial^2 \psi}{\partial x^2} + a_{wi,w}\,h_w\,(T - \psi) - a_{wo,w}\,U_\infty\,(\psi - T_0)\,, \tag{4.3}$$

where T is the air temperature, θ is the solid temperature, ψ is the wall temperature, ε is the voidage in the bed, $a_p = (6\,(1-\varepsilon))/d_p$ is the superficial particle area per unit of bed volume, $a_{wi,b} = 4/d_i$ is the inner wall surface area per unit of bed volume, $a_{wi,w} = 4\,d_i/(d_o^2 - d_i^2)$ is the inner wall surface area per unit

volume of bed wall, $a_{wo,w} = 4d_o/(d_o^2 - d_i^2)$ is the outer wall surface area per unit volume of the bed wall, U_∞ is the overall heat transfer coefficient from the outer surface of the wall to the ambient and u is the interstitial gas velocity, which is related to the superficial velocity as $U = \varepsilon\, u$. The correlation proposed by Galloway & Sage (1970) for a particular type of packing and the constants adjusted by Beasley & Clark (1984) were used to calculate the interphase heat transfer coefficient, h. The model proposed by Izquierdo-Barrientos *et al.* (2014) and explained in Chapter 7 was used to calculate the convective heat transfer from the bed to the inner surface of the bed, h_w, because the authors validated their results with the same material used in this work.

The thermal conductivities, $k_{a,x}$ and $k_{s,x}$, are the effective conductivities in the axial direction for the gas and solid phases, respectively. In Equations (4.1) and (4.2), the conductivities $k_{a,x}$ and $k_{s,x}$ are averaged over the volumes occupied by the gas and particles, respectively. In contrast, in the literature, the effective conductivities are typically averaged over the bed volume. Following the work of Wakao & Kaguei (1982), $k_{a,x}$ can be obtained as follows

$$k_{a,x} = \begin{cases} 0.7\, k_a & \text{for} \quad Re_p \leq 0.8 \\ \dfrac{0.5\, Pr\, Re_p\, k_a}{\varepsilon} & \text{for} \quad Re_p > 0.8 \end{cases} \tag{4.4}$$

where k_a is the air conductivity, Re_p is the particle Reynolds number based on the superficial velocity and particle diameter and Pr is the Prandtl number. The solid effective conductivity $k_{s,x}$ is calculated from the following relationship

$$k_{s,x} = \frac{k_e^0 + 0.5\, Pr\, Re_p\, k_a - k_{a,x}\, \varepsilon}{1 - \varepsilon}, \tag{4.5}$$

where k_e^0 is the stagnation effective thermal conductivity calculated from the study of Krupiezka (1967)

$$\frac{k_e^0}{k_a} = \left(\frac{k_s}{k_a}\right)^m \quad \text{with} \quad m = 0.280 - 0.757 \log \varepsilon - 0.057 \log\left(\frac{k_s}{k_a}\right), \tag{4.6}$$

and k_s is the solid conductivity.

The boundary conditions and initial conditions to solve the differential equation system formed by Equations (4.1), (4.2) and (4.3) are summarized in Table 4.2.

The proposed differential equation system can be transformed into a non-dimensional equation by introducing non-dimensional variables

$$\hat{T} = \frac{T - T_0}{T_{max} - T_0}, \quad \hat{\theta} = \frac{\theta - T_0}{T_{max} - T_0}, \quad \hat{\psi} = \frac{\psi - T_0}{T_{max} - T_0}, \quad \hat{t} = t\,\frac{u}{H}, \quad \hat{x} = \frac{x}{H}.$$

	Gas phase	Solid phase	Wall
Initial condition (t=0)	$T = T_0$	θ=T_0	ψ=T_0
Boundary condition (x=0)	$T = T_{in}$	$\frac{\partial^2\theta}{\partial x^2} = 0$	$\frac{\partial^2\psi}{\partial x^2} = 0$
Boundary condition (x=H)	$\frac{\partial^2 T}{\partial x^2} = 0$	$\frac{\partial^2\theta}{\partial x^2} = 0$	$\frac{\partial^2\psi}{\partial x^2} = 0$

Table 4.2: Initial conditions and boundary conditions for Equations (4.1), (4.2) and (4.3).

With these changes, the non-dimensional temperatures vary between 0, when the temperature is equal to the ambient temperature (minimum temperature) T_0, and 1, when the temperature is equal to T_{max}, which is the maximum temperature of the introduced air.

As a result, the original system is converted into

$$\frac{\partial\hat{T}}{\partial\hat{t}} = Fo_a \frac{\partial^2\hat{T}}{\partial\hat{x}^2} + Bi_a\, Fo_a \left(\hat{\theta} - \hat{T}\right) - \frac{\partial\hat{T}}{\partial\hat{x}} - Bi_{wi,b}\, Fo_a \left(\hat{T} - \hat{\psi}\right), \tag{4.7}$$

$$\frac{\partial\hat{\theta}}{\partial\hat{t}} = Fo_s \frac{\partial^2\hat{\theta}}{\partial\hat{x}^2} - Bi_s\, Fo_s \left(\hat{\theta} - \hat{T}\right), \tag{4.8}$$

$$\frac{\partial\hat{\psi}}{\partial\hat{t}} = Fo_w \frac{\partial^2\hat{\psi}}{\partial\hat{x}^2} + Bi_{wi,w}\, Fo_w \left(\hat{T} - \hat{\psi}\right) - Bi_{wo,w}\, Fo_w \left(\hat{\psi} - \hat{T}_0\right), \tag{4.9}$$

where Fo_a, Fo_s and Fo_w represent the Fourier numbers of the air, solid phase and wall, respectively, and Bi corresponds to Biot numbers, which are defined as

$$Fo_a = \frac{\alpha_a}{u\,H}, \quad Fo_s = \frac{\alpha_s}{u\,H}, \quad Fo_w = \frac{\alpha_w}{u\,H},$$
$$Bi_a = \frac{h\,a_p\,H^2}{k_{a,x}\,\varepsilon}, \quad Bi_{wi,b} = \frac{h_w\,a_{wi,b}\,H^2}{k_{a,x}\,\varepsilon}, \quad Bi_s = \frac{h\,a_p\,H^2}{k_{s,x}\,(1-\varepsilon)},$$
$$Bi_{wi,w} = \frac{h_w\,a_{wi,w}\,H^2}{k_w}, \quad Bi_{wo,w} = \frac{U_\infty\,a_{wo,w}\,H^2}{k_w\,\varepsilon}$$

where α_a and α_s are the thermal diffusivity of the air and solid calculated with their respective effective conductivities, $k_{a,x}$ and $k_{s,x}$.

The proposed model includes an equation for the wall of the column, which is typically neglected in the packed bed models published in literature, with a few exceptions (Beasley & Clark, 1984). However, the effect of the wall heat

	Gas phase	Solid phase	Wall
Initial condition ($\hat{t}=0$)	$\hat{T}=0$	$\hat{\theta}=0$	$\hat{\psi}=0$
Boundary condition ($\hat{x}=0$)	$\hat{T}=1$	$\frac{\partial^2\hat{\theta}}{\partial\hat{x}^2}=0$	$\frac{\partial^2\hat{\psi}}{\partial\hat{x}^2}=0$
Boundary condition ($\hat{x}=1$)	$\frac{\partial^2\hat{T}}{\partial\hat{x}^2}=0$	$\frac{\partial^2\hat{\theta}}{\partial\hat{x}^2}=0$	$\frac{\partial^2\hat{\psi}}{\partial\hat{x}^2}=0$

Table 4.3: Initial conditions and boundary conditions for Equations (4.7), (4.8) and (4.9) in non-dimensional form.

capacity has a significant effect in the present bed, as it is 16.2% of the sand heat capacity and 7.6% of the GR50 mean heat capacity for the considered test section.

The initial conditions and boundary conditions in non-dimensional form are presented in Table 4.3.

4.3.2 Packed bed model with phase change in the granular material

When a phase change process is included in the granular material, the energy equation of the solid phase (4.2) must be written in terms of the enthalpy, which yields the following expression

$$\rho_s\,(1-\varepsilon)\,\frac{\partial i_s}{\partial t}=(1-\varepsilon)\,k_{s,x}\frac{\partial^2\theta}{\partial x^2}-h\,a_p\,(\theta-T)\,, \tag{4.10}$$

where

$$i_s=\int_{T_0}^{T_{max}} c_{p,s}\,\mathrm{d}\theta+i_{s_0} \tag{4.11}$$

is the enthalpy of the solid phase (plotted in Figure 4.1(b)), $c_{p,s}$ is the apparent specific heat of the granular PCM (represented in Figure 4.1(a)) and i_{s0} is the enthalpy at the reference temperature T_0. Equation (4.10) can be non-dimensionalized by introducing the non-dimensional enthalpy

$$\hat{i}_s=\frac{i_s-i_{s_0}}{\bar{c}_{p,s}\,(T_{max}-T_0)}=\int_0^{\hat{\theta}}\hat{c}_{p,s}\,\mathrm{d}\hat{\theta}, \tag{4.12}$$

where

$$\bar{c}_{p,s} = \frac{1}{T_{max} - T_0} \int_{T_0}^{T_{max}} c_{p,s} \, \mathrm{d}\theta \tag{4.13}$$

is the average apparent specific heat in the range of temperatures of the experiments and

$$\hat{c}_{p,s} = \frac{c_{p,s}}{\bar{c}_{p,s}} \tag{4.14}$$

is a non-dimensional specific heat, which is defined as the ratio of the specific heat at a certain temperature and the average specific heat defined previously.

In this manner, the non-dimensional solid equation for the granular material with phase change is

$$\frac{\partial \hat{i}_s}{\partial \hat{t}} = \overline{Fo}_s \frac{\partial^2 \hat{\theta}}{\partial \hat{x}^2} - Bi_s \, \overline{Fo}_s \left(\hat{\theta} - \hat{T} \right), \tag{4.15}$$

where $\overline{Fo}_s$ corresponds to the Fourier number defined before, although the average specific heat of the PCM, $\bar{c}_{p,s}$, is used instead of the constant specific heat $c_{p,s}$.

A comparison of Equations (4.8) and (4.15) demonstrates that both equations have the same form and both non-dimensional variables $\hat{\theta}$ and $\hat{i}_s$ are bounded between 0 and 1. Therefore, the same numerical procedure can be used to solve both equations, as explained in the following section.

4.3.3 Numerical solution for the heat transfer model

The system of differential equations formed by Equations (4.7), (4.8) and (4.9), i.e., when there is no phase change in the granular material, or by Equations (4.7), (4.9) and (4.15), i.e., when phase change occurs, can be numerically solved by an explicit finite difference technique. The results are obtained with a spatial step of $\Delta x = 1$ cm and a temporal step of $\Delta t = 0.1 \Delta x \, \varepsilon / U$, which ensures convergence of the numerical method. The temporal derivatives were approximated by a fourth-order Runge-Kutta method, and the spatial derivatives were approximated using an up-wind scheme.

The non-dimensionalization of the enthalpy proposed and the use of a function for the apparent specific heat obtained from DSC measurements result in Equation (4.15) for the PCM, which has the exact same form as Equation (4.8) for the sand. When the solid is a PCM, the enthalpy is calculated at each time

step from Equation (4.15). Then, the solid temperature is obtained from Figure 4.1(b). The data represented in this figure were interpolated using a cubic spline interpolation.

4.4 Results and discussion

4.4.1 Numerical results

Figure 4.3(a) shows the numerical results of the temperature evolution for the inlet air T_{in}, gas phase T, solid phase θ and wall when the bed is filled with sand. The voidage selected ε is 0.4, and the chosen flow rate is $\dot{V}$=450 l/min. The numerical domain is 20 cm long and extends from a height of 12.5 cm above the distributor after the entrance section (Thoméo *et al.*, 2004). The inlet air temperature T_{in} is the temperature measured in the middle of the bed at the beginning of the domain (x=0). The temperature profiles increase progressively along the height of the bed. This behavior is typical of a plug flow system, where the front travels in the axial direction. The difference between the gas and solid temperature profiles is negligible. Furthermore, the wall temperature has nearly the same profile as the gas and solid, although displaced approximately 1°C lower.

The energy stored in the material and in the wall is calculated using the following expression

$$E_{stored} = \frac{m}{H} \int_{x=0}^{x=H} (i_x - i_0)\, \mathrm{d}x, \tag{4.16}$$

where H is the height of the test section, m is the mass of the solid phase or the wall for the test section (7.2 and 2.2 kg, respectively), and i_x is the enthalpy calculated at each spatial step.

Figure 4.3(b) presents the energy stored in the solid phase (sand) and wall as a function of time. The sand stores an estimated 23 MJ of energy, whereas the wall stores 3.9 MJ of energy (17% of the heat stored in the sand).

The numerical results for the temperature profiles and the energy stored when the bed is filled with PCM are shown in Figure 4.4. In Figure 4.4(a), the temperature profiles plotted are similar to those obtained for sand. The plug flow behavior of the system is preserved, which is characteristic of the thermal storage in packed beds. Moreover, the phase change of the material is revealed with the abrupt change in slope at approximately 47°C, which corresponds to the phase change of GR50. During this process, the material is able to store

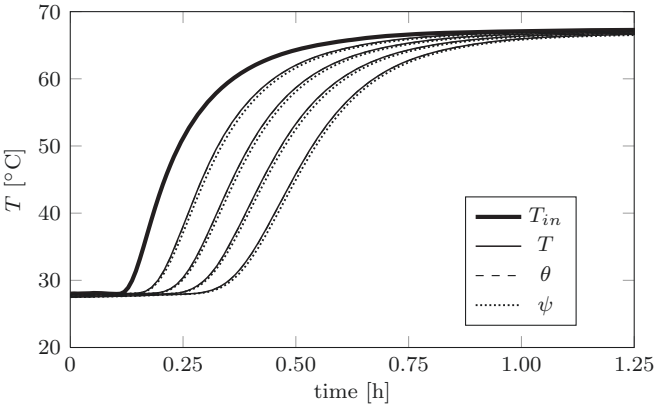

(a) Temperature profiles

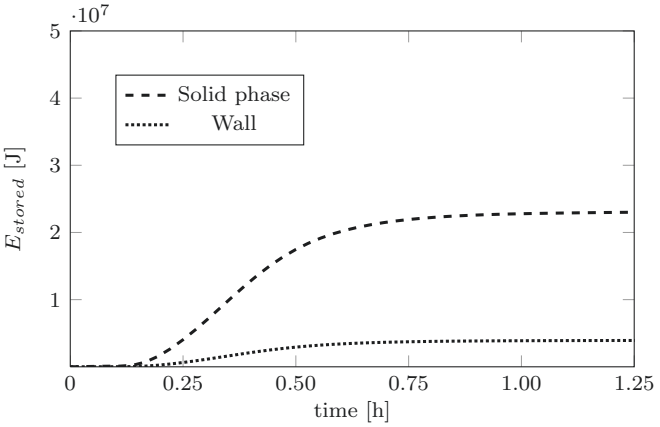

(b) Energy stored

Figure 4.3: (a) Temperature profiles modeled for the gas phase T, solid phase θ and wall ψ for the sand at the following axial positions: $x = 5$ cm, $x = 10$ cm, $x = 15$ cm and $x = 20$ cm. $\dot{V} = 450$ l/min and $\varepsilon = 0.4$. (b) Energy stored in the solid phase and the wall.

energy at a nearly constant temperature. Additionally, different phase change velocities occur along the bed. For example, at a height of $x = 5$ cm, the phase change process occurs in a short interval of time, approximately 0.5 h, whereas at a height of $x = 20$ cm, the phase change process takes nearly 1 h. This difference between phase change velocities is due to the more progressive heating of the particles placed at a greater height as a result of being located

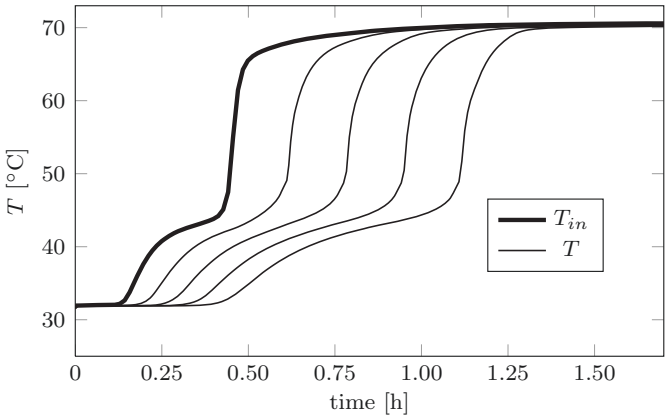

(a) Temperature profiles

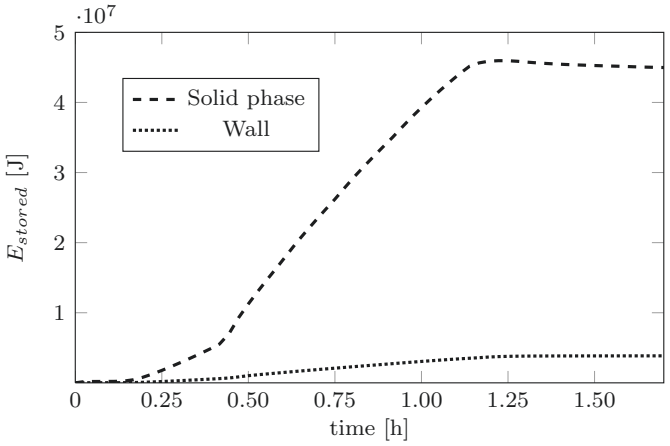

(b) Energy stored

Figure 4.4: (a) Temperature profiles modeled for the gas phase T for GR50 at the following axial positions: $x = 5$ cm, $x = 10$ cm, $x = 15$ cm and $x = 20$ cm. $\dot{V} = 450$ l/min and $\varepsilon = 0.4$. (b) Energy stored in the solid phase and the wall.

far away from the inlet air.

Regarding the energy stored in the solid phase and wall shown in Figure 4.4(b)), the energy stored in the wall is 8.5% of the energy stored in the PCM, i.e., 45 MJ, which was calculated for the corresponding mass of the test section (4 kg). This percentage, although smaller than that for sand, is still significant and confirms the importance of including the energy conservation equation for

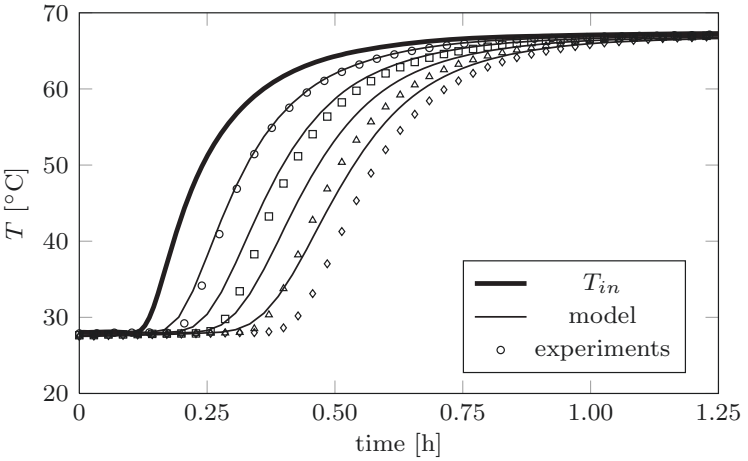

Figure 4.5: Measured (markers) and modeled (continuous lines) temperature profiles for sand at the following axial positions: $x = 5$ cm, $x = 10$ cm, $x = 15$ cm and $x = 20$ cm. $\dot{V} = 450$ l/min and $\varepsilon = 0.4$.

the wall.

The evaluation of the energy stored per unit mass for the sand and PCM between the temperature range of 32-70°C shows that the sand is able to store 3.2 MJ/kg, whereas the PCM can store 11.2 MJ/kg (3.5-fold more than sand). The percentage of energy stored in latent form (between 40 and 50°C) for the PCM is 60%, which corresponds to 6.7 MJ/kg, which is more than the sand can store. This increased storage capacity is due to the ability of the PCM to store energy in a small volume.

4.4.2 Comparison with the experimental results

Figure 4.5 shows the evolution of the experimental temperatures symbolized by markers and the numerical temperature evolution represented by continuous lines for sand. The numerical results were obtained following the procedure detailed in section 4.3.3, and the case study is the same as that described in Figure 4.3(a).

A comparison of the experimental and numerical results indicates that the temperature profiles follow the same trend, although they begin to deviate after $x = 5$ cm. This discrepancy may be due to the uncertainty in the calculation of the stagnation effective thermal conductivity k_e^0. If this value is overestimated,

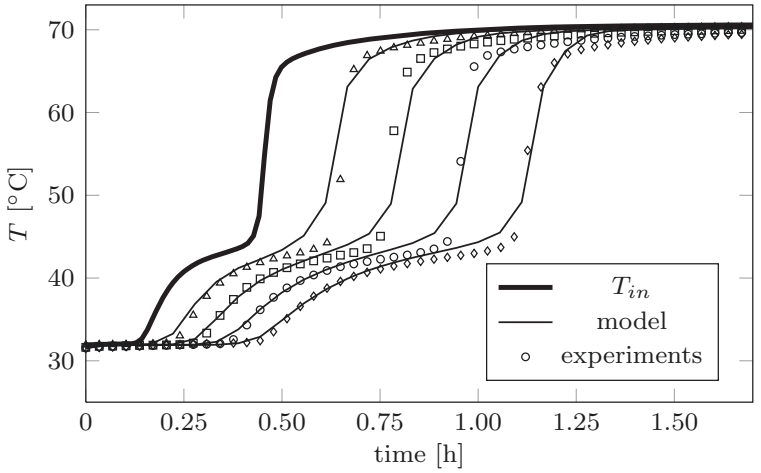

Figure 4.6: Measured (markers) and modeled (continuous lines) temperature profiles for GR50 at the following axial positions: $x = 5$ cm, $x = 10$ cm, $x = 15$ cm and $x = 20$ cm. $\dot{V} = 450$ l/min and $\varepsilon = 0.4$.

the velocity of the heat wave front increases, and hence, the maximum temperature at a certain height in the bed is reached before that in the experiments (Kubie & Broughton, 1975). The rate at which the curves are propagated is controlled by the equivalent thermal conductivity.

The results for GR50 and GR80 for the same flow rate ($\dot{V} = 450$ l/min) are presented in Figure 4.6 and 4.7, respectively.

The abrupt change in slope at approximately 47°C in Figure 4.6 and at approximately 78°C in Figure 4.7 corresponds to the phase change of each material. Due to the phase change, the system requires more time to reach the steady state when heating PCM compared to when using sand. For both PCMs, the plug flow behavior is conserved, and good agreement between the numerical experimental is obtained.

According to Arkar & Medved (2005), the shape of the apparent specific heat curves depend on the DSC heating rate; in particular, during melting, the peak temperature (temperature peak of the DSC curve) shifts toward the lower temperatures at the lower heating rates, and the peak becomes narrower and higher. Therefore, the authors suggest that the apparent specific heat function should be measured at approximately the same heating or cooling rate in the actual application. The same conclusions were also reached by Rady (2009*b*).

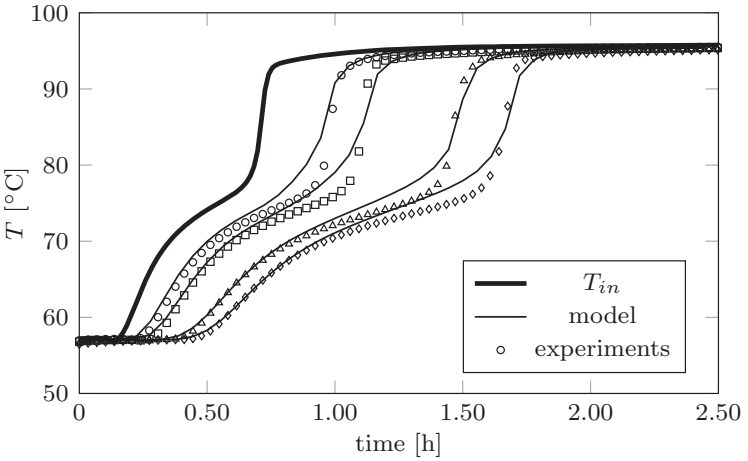

Figure 4.7: Measured (markers) and modeled (continuous lines) temperature profiles for GR80 at the following axial positions: x=6 cm, x=9.5 cm, x=16.5 cm and x=20 cm. $\dot{V} = 450$ l/min and $\varepsilon = 0.5$.

In addition, DSC measurements performed at a high heating rate should be corrected by accounting for the instrument thermal resistance effects because these effects significantly influence the functional dependence of the enthalpy on temperature during the phase change (Rady, 2009*b*). These corrections are negligible at low heating and cooling rates of 0.5°C/min. In view of these observations, the small discrepancies between the experimental measurements and model predictions when approaching the peak temperature could be attributed to the slightly different heating rate in the DSC measurements and experiments. An exact match of both heating rates is hardly possible because it presents fluctuations during the experiment.

4.4.3 Influence of the flow rate

The same experiments were conducted for different flow rates and compared with their corresponding numerical outputs. The results for GR50 for a flow rate of $\dot{V}$=250 l/min are plotted in Figure 4.8, and similar results with the previous results were obtained. More time is required to reach steady state and obtain a uniform temperature along the bed when considering a smaller flow rate.

Figure 4.9 presents the results for GR50 at a higher flow rate, $\dot{V}$=650 l/min.

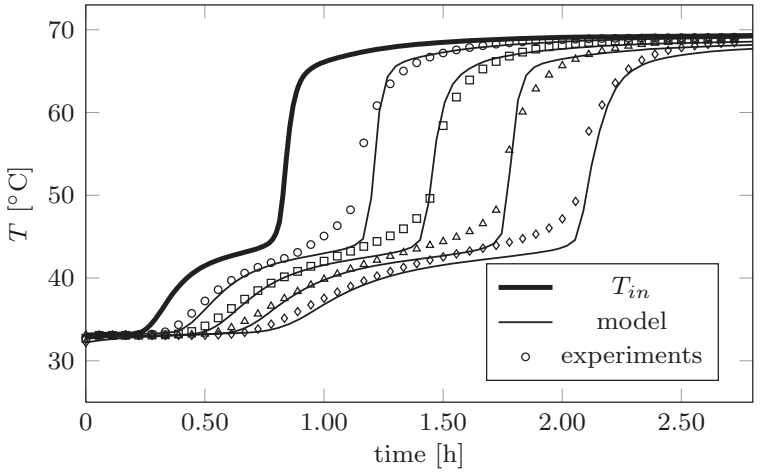

Figure 4.8: Temperature profiles for GR50 at the following axial positions: $x = 5$ cm, $x = 10$ cm, $x = 15$ cm and $x = 20$ cm. $\dot{V} = 250$ l/min and $\varepsilon = 0.4$.

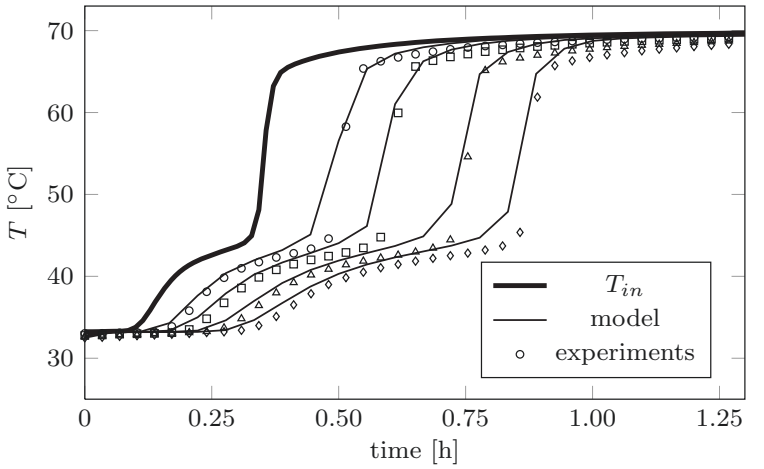

Figure 4.9: Temperature profiles for GR50 at the following axial positions: $x = 6$ cm, $x = 10$ cm, $x = 16$ cm and $x = 20$ cm. $\dot{V} = 650$ l/min and $\varepsilon = 0.4$.

As before, there is nearly no difference between the experimental and numerical results. Thus, the proposed model is suitable for predicting heating temperature profiles for granular PCMs at different flow rates in fixed beds.

4.5 Conclusions

In this paper, numerical and experimental investigations were performed for a phase change thermal energy storage unit using granulate material. The proposed numerical model accounts for the progressive evolution of the enthalpy with temperature during the phase change.

The equations presented were non-dimensionalized, which results in the same differential equation system regardless of whether the granular material contains PCM. The model quantifies the energy stored in the wall, which can represent between 8 and 17% of the energy stored in the material.

The transient response of the packed bed was compared with experimental measurements, and a good agreement for different flow rates was confirmed. Therefore, it may be concluded that the numerical model proposed significantly accurate prediction of the temperature distributions within the bed during charging processes.

Notation

a	superficial area per unit volume [m^{-1}]
Bi	Biot number [-]
c_p	specific heat [$\mathrm{J{\cdot}kg^{-1}{\cdot}K^{-1}}$]
d	diameter [m]
E_{stored}	energy stored [J]
Fo	Fourier number [-]
H	height of the bed [m]
h	interphase heat transfer coefficient [$\mathrm{W{\cdot}m^{-2}{\cdot}K^{-1}}$]
h_w	convective heat transfer coefficient from the bed to the inner surface of the bed [$\mathrm{W{\cdot}m^{-2}{\cdot}K^{-1}}$]
i	enthalpy [J]
k	thermal conductivity [$\mathrm{W{\cdot}m^{-1}{\cdot}K^{-1}}$]
$k_{a,x}$	effective thermal conductivity in the axial direction for the gas [$\mathrm{W{\cdot}m^{-1}{\cdot}K^{-1}}$]
$k_{s,x}$	effective thermal conductivity in the axial direction for the solid phase [$\mathrm{W{\cdot}m^{-1}{\cdot}K^{-1}}$]
k_e^0	stagnation effective thermal conductivity [$\mathrm{W{\cdot}m^{-1}{\cdot}K^{-1}}$]
m	mass [kg]
Pr	Prandtl number [-]
Re	Reynolds number [-]

T	air temperature [°C]
T_{pc}	phase change temperature [°C]
U	superficial gas velocity [m·s^{-1}]
U_∞	overall heat transfer coefficient [W·m^{-2}·K^{-1}]
u	interstitial gas velocity [m·s^{-1}]
$\dot{V}$	flow rate [m^3·s^{-1}]

Greek symbols

α	thermal diffusivity [m^2·s^{-1}]
ρ	density [kg·m^{-3}]
σ_{dp}	standard deviation of the mean particle diameter [m]
θ	solid temperature [°C]
ψ	wall temperature [°C]
ε	voidage in the bed [-]
Δt	time step [s]
Δx	spatial step [m]

Subscripts

0	ambient/initial
a	air
b	bed
i	internal
in	inlet
o	outer
p	particle
s	solid
w	wall
wi	inner wall
wo	outer wall
x	axial position

References

Arkar, C. & Medved, S. 2005 Influence of accuracy of thermal property data of a phase change material on the result of a numerical model of a packed bed latent heat storage with spheres. *Thermochimica Acta* 438, 192–201.

Beasley, D.E. & Clark, J.A. 1984 Transient response of a packed bed for thermal energy storage. *International Journal of Heat and Mass Transfer* 27, 1659–1669.

Cao, Y. & Faghri, A. 1990 A numerical analysis of phase change problems including natural convection. *ASME Journal of Heat Transfer* 112, 812–816.

Dutil, Y., Rousse, D.R., Salah, N. Ben, Lassue, Stéphane & Zalewski, Laurent 2011 A review on phase-change materials: Mathematical modeling and simulations. *Renewable and Sustainable Energy Reviews* 15, 112–130.

Faghri, A. & Zhang, Y. 2006 In *Transport Phenomena in Multiphase Systems* (ed. Amir Faghri & Yuwen Zhang), pp. 1–106. Boston: Academic Press.

Farid, M.M., Hamad, F.A. & Abu-Arabi, M. 1998 Melting and solidification in multi-dimensional geometry and presence of more than one interface. *Energy Conversion and Management* 39, 809–818.

Galloway, T.R. & Sage, B.H. 1970 A model of the mechanism of transport in packed, distended, and fluidized beds. *Chemical Engineering Science* 25, 495–516.

Izquierdo-Barrientos, M.A., Sobrino, C. & Almendros-Ibáñez, J.A. 2013 Thermal energy storage in a fluidized bed of pcm. *Chemical Engineering Journal* 230, 573–583.

Izquierdo-Barrientos, M.A., Sobrino, C. & Almendros-Ibáñez, J.A. 2014 Modeling of the heat transfer coefficient in fixed and fluidized beds with pcm. In *Eurotherm Seminar 99: Advances in Thermal Energy Storage*. Lleida.

Krupiezka, R. 1967 Analysis of thermal conductivity in granular materials. *International Chemical Engineering* 7, 122–144.

Kubie, J. & Broughton, J. 1975 A model of heat transfer in gas fluidized beds. *International Journal of Heat and Mass Transfer* 18, 289 – 299.

Peng, H., Dong, H. & Ling, X. 2014 Thermal investigation of pcm-based high temperature thermal energy storage in packed bed. *Energy Conversion and Management* 81, 420–427.

Rady, M. 2009*a* Granular phase change materials for thermal energy storage: experiments and numerical simulations. *Applied Thermal Engineering* 29, 3149–3159.

Rady, M. 2009*b* Study of phase changing characteristics of granular composites using differential scanning calorimetry. *Energy Conversion and Management* 50, 1210–1217.

Schumann, T.E.W. 1929 Heat transfer: A liquid flowing through a porous prism. *Journal of the Franklin Institute* 208, 405–416.

Thoméo, J.C., Rouiller, C.O. & Freire., J. 2004 Experimental analysis of heat transfer in packed beds with air flow. *Industrial and Engineering Chemistry Research* 43, 4140–4148.

Vortmeyer, D. & Schaefer, R.J. 1974 Equivalence of one- and two-phase models for heat transfer processes in packed beds: one dimensional theory. *Chemical Engineering Science* 29, 485–491.

Wakao, N. & Kaguei, S. 1982 *Heat and Mass Transfer in Packed Beds*. Gordon and Braech. Science Publishers New York.

Xia, L., Zhang, P. & Wang, R.Z. 2010 Numerical heat transfer analysis of the packed bed latent heat storage system based on an effective packed bed model. *Energy* 35, 2022–2032.

CHAPTER

FIVE

Energy storage with PCM in fluidized beds: modeling and experiments

In recent years, the development of phase change materials (PCMs) has introduced new ways to increase the energy storage capacity of a system due to the high latent heat and high storage density of these materials. The aim of this work is to model the charging process of a fluidized bed with PCMs operating as an energy storage device. The temperature in the bed during the charging process of the fluidized bed has been modeled using the two phase theory of fluidization. The dense phase is taken to be perfectly mixed, and the bubble phase is taken to be in plug flow. The numerical model presented takes into account the fact that the phase change process of the bed material occurs over a temperature range and also estimates the energy stored in the wall of the bed and in the distributor plate. The energy equation of the dense phase is numerically solved in enthalpy form, considering the dependence of enthalpy on temperature for phase changes occurring over a range of temperatures. The model's validity is verified against experimental data for two granular materials: sand, a typical material used in fluidized beds, and a granular PCM with a mean particle diameter of 0.54 mm and a phase change temperature of approximately 50°C. For the sand, the temperature profiles obtained numerically perfectly agree with the values measured experimentally. In the case of the granular PCM, the fitting of the curves is improved when slow and similar heating rates are selected for the experiments and for the DSC measurements used to determine the PCM enthalpy-temperature curve.

5.1 Introduction

Time-dependent energy resources require effective storage methods to reduce the mismatch between supply and demand. Sensible heat storage is the most

common method of thermal storage, although the latent heat method provides a much higher energy storage density with small temperature swings. Due to these advantages, much research has been focused on studying, theoretically and experimentally, the performance of energy storage methods employing PCMs, especially regarding their application in packed beds (Farid *et al.*, 2004; Benmansour *et al.*, 2006; Regin *et al.*, 2009). Compared with packed beds, fluidized beds have the advantage of a higher rate of heat transfer between the carrying fluid and the storage medium, as well as presenting a uniform temperature along the bed.

In spite of the advantages of fluidized beds over fixed beds, only a few studies have examined fluidized beds as heat storage devices. Elsayed *et al.* (1988) tested an air-sand fluidized bed for thermal storage, in which the bed was heated or cooled by a flow of air. They observed that the bed always behaves as a well mixed tank. Sozen *et al.* (1988) presented an experimental investigation using 25-mm-diameter PCM spheres in a water fluidized bed, showing that with cycling, fluidization yielded less of a loss in heat storage efficiency than was observed under fixed bed conditions. Izquierdo-Barrientos *et al.* (2013) presented heating experiments using a granular PCM of 0.54 mm mean diameter in an air fluidized bed, obtaining higher charging efficiencies than in sand beds and stable behavior after 75 hours of continuous operation.

The unsteady state behavior of fluidized bed thermal storage systems has been modeled in a limited number of studies in the literature, and only for sensible heat. Wagialla *et al.* (1991) used the two phase theory of fluidization to simulate the transient response of a bed of alumina particles fluidized by a hot air stream and verified the results with experimental data. They neglected the energy stored in the bubble phase, which made it possible to obtain an analytical expression for the bubble phase temperature. A similar model developed by El-Halwagi *et al.* (1991) was used to study the influence of different parameters (gas flow rate, mass of solids and bed aspect ratio) on the performance of the system as a heat regenerator.

In this paper, a model for the transient response of a fluidized bed containing PCM is presented and verified by experimental measurements. The fluidized bed is modeled using the two phase theory of fluidization, assuming that the emulsion phase is perfectly mixed and assuming plug flow in the bubble phase. It is assumed that all gas in excess of what is required for minimum fluidization passes through the bed as bubbles, which exchange heat with the dense phase as they rise. The energy equation for the emulsion phase is calculated employing

the enthalpy method, given that the phase transition occurs over a temperature range (Faghri & Zhang, 2006). The heat accumulated in the stainless steel vessel and in the plate distributor is included in the simulations. Previous results from the work of Kunii & Levenspiel (1968), who proposed a correlation for the heat transfer from the bubble phase to the emulsion phase, and Izquierdo-Barrientos *et al.* (2014*a*), who measured and modeled the heat transfer coefficient to an immersed surface in bubbling fluidized beds of sand and granular PCM, are used in this work.

5.2 Materials and experimental apparatus

Heating experiments for sand and a PCM in a fluidized bed have been carried out to validate the model proposed in this study. Figure 5.1 shows a schematic of the set up. It consists of a cylindrical stainless steel bed with a 2 mm wall thickness filled with particles. The air enters the plenum of the column and then flows into the bed through a 1.5-mm-thick distribution plate with 300 orifices with a 2 mm diameter, resulting in an open area of 3%. The distributor has been designed to have a pressure drop equal to 30% of the bed pressure drop (Kunii & Levenspiel, 1991). In this way, the air is uniformly distributed in the bed. A fine-mesh screen is mounted at the bottom of the distributor plate to prevent solid particles from entering the plenum chamber. The instrumental test section is 500 mm in height, has an internal diameter of 200 mm and is insulated with glass wool with a thickness of 2 cm. The piping is insulated with a 1-cm-thick thermal insulator. The freeboard of the column is divided into two parts, one cylinder with an internal diameter of 200 mm and another with an internal diameter of 300 mm. The purpose of this division is to assure a homogeneous velocity distribution of air at the exit from the test section and to reduce the elutriation and entrainment of particles from the bed.

The air flow is produced by a blower with a variable mass flow rate and is heated by electrical heaters before flowing to the column. For the PCM experiments, the column is filled with 5 kg of PCM, whereas 7.25 kg is used for the experiments with sand. The fixed bed height is $H = 200$ mm for all the experiments. Type K thermocouples are used to measure the temperature at specific locations inside the test section. Air temperature is also measured at the inlet and outlet of the test section. These thermocouples are connected to a data acquisition system for continuous monitoring and recording of the data.

The materials used for the experiments are sand and a granular phase chang-

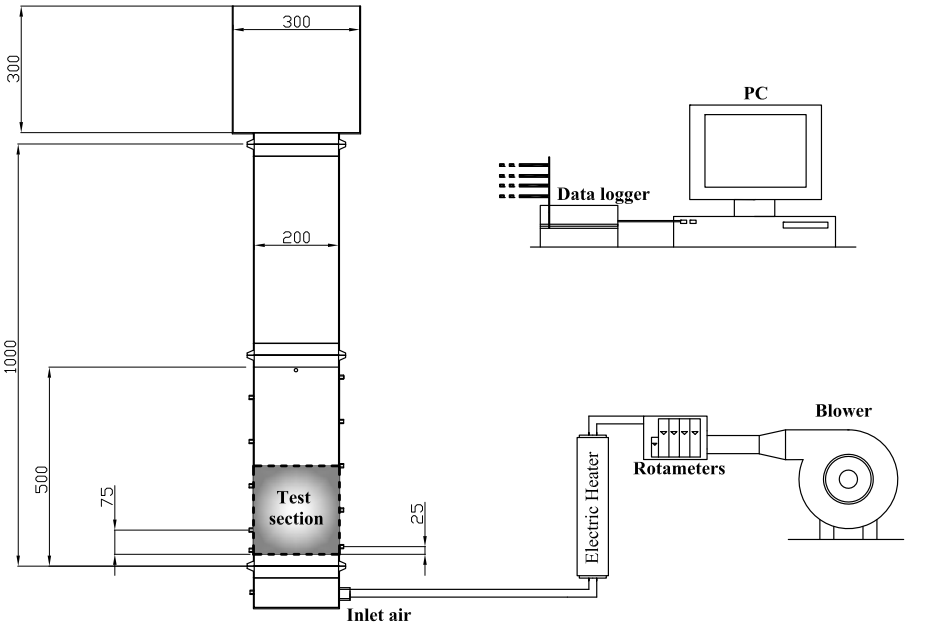

Figure 5.1: Schematic representation of the experimental apparatus. Dimensions in mm.

ing composite (Rubitherm® GR50), with a phase change temperature T_{pc} interval of 45-51°C, according to the manufacturer. Both the sand and the GR50 material correspond to group B of Geldart's classification (Geldart, 1973). This means that they fluidize easily with vigorous bubbling action and that the bubbles grow large (Kunii & Levenspiel, 1991).

Table 5.1 gives several properties of the sand and PCM, such as density ρ, thermal conductivity k, mean particle diameter $\overline{d}_p$ and standard deviation σ_{dp}, and minimum fluidization velocity U_{mf}. Moreover, the variation of specific heat with the temperature obtained by differential scanning calorimetry (DSC) is plotted for each material in Figure 5.2(a). These data are obtained with a heating rate of 0.5°C/min (Rady, 2009). For the PCM, the curve of the specific heat versus temperature shows a clear peak between 40 and 50°C, where the phase change process occurs. By contrast, the curve for the sand is approximately linear with an average value of $c_p = 0.776$ kJ/(kg·K) in the range of temperatures shown in Figure 5.2(a). In addition, the variation of enthalpy with temperature for the PCM is presented in Figure 5.2(b). Both materials have a similar mean particle size, although the density of the GR50 is

Material	ρ [kg/m^3]	k [W/m·K]	$\overline{d}_p$ [mm]	σ_{dp} [mm]	U_{mf}[m/s]
Sand*	2632.3	4.2	0.57	0.07	0.27
GR50	1550.5	4.0	0.54	0.08	0.13

Table 5.1: Properties of the materials studied.*This sand corresponds to Sand 3 from Table 2.2.

approximately half that of the sand. Consequently, the minimum fluidization velocity of the GR50 is 0.13 m/s, much lower than that of the sand (0.27 m/s).

5.3 Heat transfer model in a fluidized bed

In the following sections, the two phase fluidized model is described. First, the model is explained for a fluidized bed without a phase change in the granular material; then, the modifications needed in the emulsion phase to include the phase change are explained.

5.3.1 Fluidized bed model without phase change in the dense phase

The two phase model considers a fluidized bed as a bubble phase and a surrounding suspension phase consisting of solid particles and gas, known as the dense or emulsion phase. The energy conservation equations are based on a heat balance involving the dense phase (assuming a uniform temperature), a differential element in the bubble phase (assuming plug flow) and the container walls.

The heat accumulated in the dense phase is equal to the net enthalpy flow of the fluidizing gas (which is assumed to leave the bed at the dense phase temperature), the heat transferred from the dense phase to the bubble phase and the heat transferred from the dense phase to the container walls (Wagialla *et al.*, 1991). Following this statement, the heat balance for the dense phase is expressed as

$$(\rho_a\,\varepsilon\,c_{p,a} + \rho_s\,(1-\varepsilon)\,c_{p,s})A_d\,H\,\frac{\partial T_d}{\partial t} = G_d\,\rho_a\,c_{p,a}\,(T_{in} - T_d) + \\ + \int_0^H P_b\,h_b\,(T_b - T_d)\,\mathrm{d}x + A_{wi}\,h_w(T_w - T_d), \tag{5.1}$$

where T_d is the dense phase temperature, T_b is the bubble phase temperature,

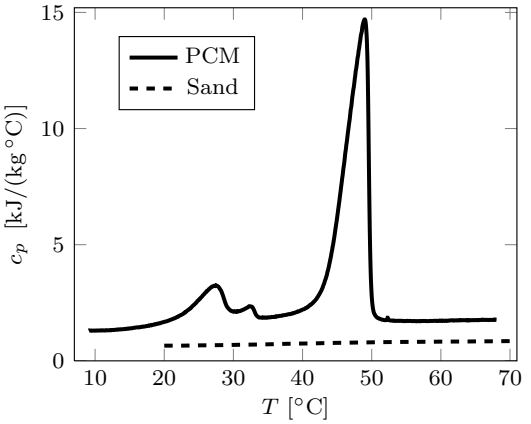

(a)

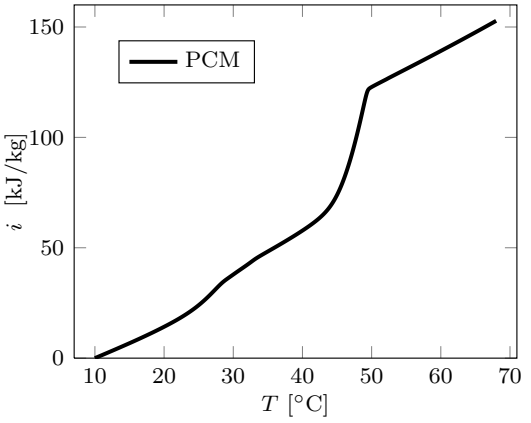

(b)

Figure 5.2: (a) Specific heat variation with temperature for the sand and the PCM (c_p=$\partial i/\partial T$) and (b) enthalpy variation with temperature for the PCM.

T_w is the container wall temperature, T_{in} is the gas temperature at the inlet of the bed, H is the bed height, ε is the voidage in the bed, A_d is the cross sectional area of the dense phase, A_{wi} is the internal surface area of the container wall, P_b is the perimeter of the cross sectional area of the bubbles and h_b is the convective heat transfer coefficient between the bubbles and the dense phase. The convective heat transfer coefficient between the dense phase and the container wall, h_w, has been calculated using the model proposed by Izquierdo-Barrientos *et al.* (2014*b*), explained in Chapter 7. The volumetric flow rate through the dense phase $G_d = A\,U_{mf}$ has been calculated by assuming that the dense phase remains at minimum fluidization conditions while all gas in excess of U_{mf} passes through the bed as bubbles.

The heat transfer coefficient from the bubbles to the dense phase h_b has been calculated from the total heat interchange across the bubble cloud boundary per unit of bubble phase (Kunii & Levenspiel, 1991):

$$H_{bc} = 4.5\left(\frac{U_{mf}\,\rho_a\,c_{p,a}}{d_b}\right) + \frac{5.85\,(k_a\,\rho_a\,c_{p,a})^{1/2}\,g^{1/4}}{d_b^{5/4}}, \tag{5.2}$$

where g corresponds to gravity and d_b is the diameter of a sphere with the same volume as the spherical cup bubble calculated by finding the average value of the expression presented by Darton *et al.* (1977) along the bed height. The first term of Equation (5.2) corresponds to transfer by bulk gas flow and the second to transfer by convection. Under the experimental conditions of this work, the latter term is almost one order of magnitude lower than the former.

Using correlation (5.2), the heat transfer coefficient from the bubble phase to the dense phase per unit length $P_b\,h_b$ that appears in the second term on the right hand side of Equation (5.1) can be calculated as

$$P_b h_b = \frac{S_b}{H}\frac{H_{bc} V_b}{S_b}, \tag{5.3}$$

where S_b is the bubble surface and V_b corresponds to the bubble volume. Using the expression $\delta = V_b/V = A_b/A$, where V is the bed volume and A is the cross sectional area of the bed, Equation (5.3) can be rewritten as

$$P_b h_b = H_{bc}\,\delta\,A. \tag{5.4}$$

The parameter δ corresponds to the volume fraction of the bed in bubbles, which, according to the two phase model, can be calculated as

$$\delta = \frac{U - U_{mf}}{U_b}, \tag{5.5}$$

where U is the superficial gas velocity and U_b is the rising velocity of bubbles given by the expression (Davidson & Harrison, 1963)

$$U_b = U - U_{mf} + 0.711\,(g\,d_b)^{1/2}\,. \tag{5.6}$$

The heat balance for a differential element of the bubble phase yields the equation

$$A_b\,\rho_a\,c_{p,a}\frac{\partial T_b}{\partial t} = -G_b\,\rho_a\,c_{p,a}\frac{\partial T_b}{\partial x} + P_b\,h_b\,(T_d - T_b)\,, \tag{5.7}$$

where $A_b = A\delta$ is the cross sectional area of the bubble phase and $G_b = A\,(U - U_{mf})$ is the volumetric flow rate through the bubble phase. In this way, the heat accumulated in a bubble phase element is equal to the net enthalpy flow of the fluidizing gas and the heat interchanged with the dense phase.

The heat accumulated in the wall of the bed is defined as the heat transferred by the dense phase and the heat lost to the ambient surroundings, leading to

$$\rho_w\,c_{p,w}\,A_w\,H_w\frac{\partial T_w}{\partial t} = A_{wi}\,h_w\,(T_d - T_w) + A_{wo}\,U_{wo}\,(T_0 - T_w)\,, \tag{5.8}$$

where T_0 is the ambient temperature, A_w is the cross sectional area of the container wall, H_w is the height of the wall and U_{wo} is the global heat transfer coefficient between the container wall and the ambient surroundings.

The boundary and initial conditions used to solve the differential equation system formed by Equations (5.1), (5.7) and (5.8) are summarized in Table 5.2.

Initial condition ($t = 0$)	Boundary condition ($x = 0$)
$T_d = T_b = T_w = T_0$	$T_b = T_{in}$

Table 5.2: Initial and boundary conditions for Equations (5.1), (5.7) and (5.8).

The proposed differential equation system can be transformed into a non-dimensional system by introducing the following non-dimensional variables

$$\hat{T}_d = \frac{T_d - T_0}{T_{max} - T_0}, \quad \hat{T}_b = \frac{T_b - T_0}{T_{max} - T_0}, \quad \hat{T}_w = \frac{T_w - T_0}{T_{max} - T_0},$$
$$\hat{T}_{in} = \frac{T_{in} - T_0}{T_{max} - T_0}, \quad \hat{t} = t\,\frac{U}{\varepsilon\,H}, \quad \hat{x} = \frac{x}{H}.$$

With this change, the non-dimensional temperatures vary between 0, when the temperature is equal to the ambient temperature (minimum temperature)

T_0, and 1, when the temperature is equal to T_{max}, which is the maximum temperature of the introduced air. As a result, the original system takes the form

$$\frac{\partial \hat{T}_d}{\partial \hat{t}} = \hat{U}_d R_{a-s}\left(\hat{T}_{in} - \hat{T}_d\right) + \int_0^1 St_{b-s}\left(\hat{T}_b - \hat{T}_d\right) d\hat{x} + St_{wi-s}\left(\hat{T}_w - \hat{T}_d\right) \tag{5.9}$$

$$\frac{\partial \hat{T}_b}{\partial \hat{t}} = -\hat{U}_b \varepsilon \frac{\partial \hat{T}_b}{\partial \hat{x}} + St_{b-a}\left(\hat{T}_d - \hat{T}_b\right) \tag{5.10}$$

$$\frac{\partial \hat{T}_w}{\partial \hat{t}} = St_{wi-w}\left(\hat{T}_d - \hat{T}_w\right) + St_{wo-w}\left(\hat{T}_0 - \hat{T}_w\right) \tag{5.11}$$

where St represents different Stanton numbers, $\hat{U}_b$ is the dimensionless superficial velocity of the bubble, $\hat{U}_d$ is the dimensionless velocity of the dense phase and R_{a-s} is the ratio of the volumetric heat capacities of the air and the solids, defined as

$$St_{b-s} = \frac{P_b h_b H \varepsilon}{\rho_s (1-\varepsilon) c_{p,s} A_d U}, \quad St_{wi-s} = \frac{A_{wi}\, h_w \varepsilon}{A_d (1-\varepsilon) \rho_s c_{p,s} U},$$
$$St_{b-a} = \frac{P_b h_b H \varepsilon}{A_b \rho_a c_{p,a} U}, \quad St_{wi-w} = \frac{A_{wi} h_w H \varepsilon}{A_w \rho_w c_{p,w} U H_w},$$
$$St_{wo-w} = \frac{A_{wo} U_{wo} H \varepsilon}{A_w \rho_w c_{p,w} U H_w}, \quad \hat{U}_b = \frac{G_b}{A_b U},$$
$$R_{a-s} = \frac{\varepsilon \rho_a c_{p,a}}{(1-\varepsilon)\rho_s c_{p,s}}, \quad \hat{U}_d = \frac{G_d}{A_d U}.$$

The initial and boundary conditions in non-dimensional form are included in Table 5.3.

Initial condition ($\hat{t}=0$)	Boundary condition ($\hat{x}=0$)
$\hat{T}_d = \hat{T}_b = \hat{T}_w = 0$	$\hat{T}_b = 1$

Table 5.3: Dimensionless initial and boundary conditions for Equations (5.9), (5.10) and (5.11).

5.3.2 Fluidized bed model with phase change in the dense phase

When the dense phase contains granular PCM whose phase change occurs over a temperature range, the phase change process can be introduced using an

apparent specific heat, which is a function of temperature (Figure 5.2(a)) Thus, the energy equation of the dense phase for a conventional granular material (Equation (5.1)), neglecting the heat capacity of the gas in comparison with the heat capacity of the solid, is transformed into

$$\rho_s\,(1-\varepsilon)\,A_d\,H\frac{\partial i_d}{\partial t} = G_d\rho_a\,c_{p,a}\,(T_{in}-T_d) + \\ + \int_0^H P_b h_b\,(T_b-T_d)\,\mathrm{d}x + A_{wi}\,h_{wi}\,(T_w-T_d)\,, \tag{5.12}$$

where i_d represents the enthalpy of the solid.

Equation (5.12) can be non-dimensionalized by introducing the dimensionless variable enthalpy

$$\hat{i}_d = \frac{i_d - i_{d_0}}{\bar{c}_{p,s}\,(T_{max}-T_0)} = \int_0^{\hat{\theta}} \hat{c}_{p,s}\,\mathrm{d}\hat{\theta}, \tag{5.13}$$

where

$$\bar{c}_{p,s} = \frac{1}{T_{max}-T_0}\int_{T_0}^{T_{max}} c_{p,s}\,\mathrm{d}\theta \tag{5.14}$$

is the average apparent specific heat in the range of temperatures of the experiments and

$$\hat{c}_{p,s} = \frac{c_{p,s}}{\bar{c}_{p,s}} \tag{5.15}$$

is a non-dimensional specific heat defined as the ratio of the specific heat at a certain temperature and the average specific heat defined previously. Using the non-dimensional variables, Equation (5.12) is converted into the non-dimensional

$$\frac{\partial \hat{i}_d}{\partial \hat{t}} = \hat{U}_d\overline{R}_{a-s}\left(\hat{T}_{in}-\hat{T}_d\right) + \int_0^1 \overline{St}_{b-s}\left(\hat{T}_b-\hat{T}_d\right)\mathrm{d}\hat{x} + \overline{St}_{wi-s}\left(\hat{T}_w-\hat{T}_d\right), \tag{5.16}$$

where $\hat{U}_d$, $\overline{R}_{a-s}$, $\overline{St}_{b-s}$ and $\overline{St}_{wi-s}$ are the previously defined dimensionless numbers, in which the constant specific heat of the sand $c_{p,s}$ is replaced by the average specific heat of the PCM, $\bar{c}_{p,s}$, defined in Equation (5.14).

The energy balance presented in Equation (5.9) has the same structure as Equation (5.16), but the latter is described as a function of enthalpy. Thus, for each time step, values for $\hat{i}_d$ are calculated, and then the temperature of the dense phase T_d is determined from the calculated enthalpy using the specific heat function obtained with the DSC (Figure 5.2(a)). Therefore, the numerical method used to solve the system of equations is the same, even though there is a phase change in the granular material.

5.3.3 Numerical solution for the heat transfer model

The system of differential equations formed by Equations (5.9), (5.10) and (5.11) for the conventional granular material, sand, or by Equations (5.10), (5.11) and (5.16) for the granular PCM can be numerically solved by an explicit finite difference technique. The results are obtained with a spatial step of $\Delta x = 1$ cm and a temporal step of $\Delta t = 0.2\Delta x\varepsilon/U$, which ensures the convergence of the numerical method. The temporal derivatives are approximated by the fourth-order Runge-Kutta method, and the spatial derivatives are approximated using an up-wind scheme.

When the solid enthalpy is obtained from Equation (5.16), the solid temperature is obtained from Figure 5.2(b). The data represented in this figure have been interpolated using cubic spline interpolation.

5.4 Results

Figure 5.3 illustrates the evolution of the experimental and numerical temperatures for the sand. The selected flow rate is $G_{1,sand}$= 1000 l/min, which corresponds to an excess air velocity over minimum fluidization conditions of approximately $U/U_{mf} = 2$. The ambient temperature is $T_0 = 18°$C. The temperature of the feed gas differs from that of the gas that leaves the distributor plate and enters the bed, and hence the influence of the distributor plate needs to be considered. This fact has been observed by other researchers (Hoebink & Rietema, 1980; Heertjes *et al.*, 1953). The influence of the distributor plate has been characterized experimentally in this work, and the temperature difference between the gas at the plenum chamber and at the bed inlet, after the distributor plate, has been measured in the empty vessel at different gas flow rates. This temperature difference has been subtracted from the temperature measured in the plenum chamber T_{plenum} to estimate the value of the inlet air temperature for the different cases studied, which corresponds to T_{in} in the graphs. The global heat transfer coefficient U_{wo} is 3 W/m^2·K. This parameter has been calculated as the value that satisfies the steady state temperature of the bed and is suitable for all the flow rates used.

Because of the plug flow behavior of the bubble phase, its temperature evolution T_b is plotted at different heights: $x = 3$ cm, $x = 5$ cm and $x = 7$ cm. Above a bed height of 10 cm, there is nearly no difference between the bubble and dense phase temperatures. As expected, the system behaves as a well mixed

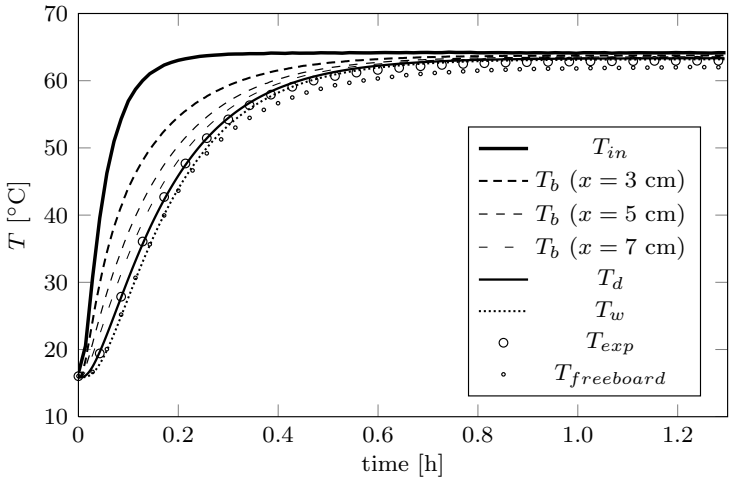

Figure 5.3: Temperature evolution of the inlet air T_{in}, the bubble phase at different heights T_b, the dense phase T_d, the temperature of the wall T_w, the experimental temperature of the dense phase T_{exp} and the temperature measured in the freeboard $T_{freeboard}$ when the bed is filled with sand and the flow rate is $G_{1,sand} = 1000$ l/min.

tank, and the dense phase temperature T_d is uniform along the bed height. The experimental temperature of the dense phase T_{exp} is measured along the axis of the bed at three different heights. Because the values of T_{exp} at different heights are the same, only one of the temperature profiles is plotted in the subsequent figures.

From the results in Figure 5.3, it can be concluded that there is good agreement between the experimental and numerical data for the dense phase.

The same experiments have been performed at different flow rates, $G_{2,sand} = 700$ l/min and $G_{3,sand} = 875$ l/min, which correspond to excess air velocities over a minimum fluidization of approximately $U_{2,sand} = 1.5\,U_{mf}$ and $U_{3,sand} = 1.75\,U_{mf}$. The results are plotted in Figure 5.4(a) and 5.4(b), showing analogous behavior to the case previously presented. The temperature of the dense phase predicted by the model is adjusted properly to the experimental measurements. The temperature of the wall vessel follows the temperature of the dense phase with a small delay.

Figure 5.5 shows the numerical and experimental results obtained for the bed filled with granular PCM when the flow rate corresponds to $G_{1,PCM} = 500$ l/min ($U_{1,PCM} = 2\,U_{mf}$). The coefficient U_{wo} varies between 0.77 and 6

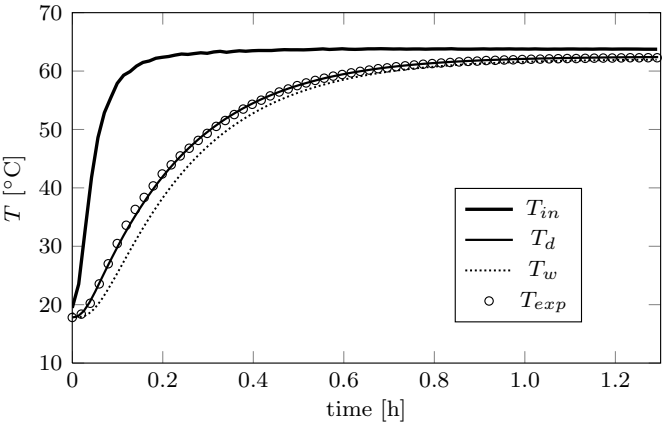

(a) $G_{2,sand} = 700$ l/min

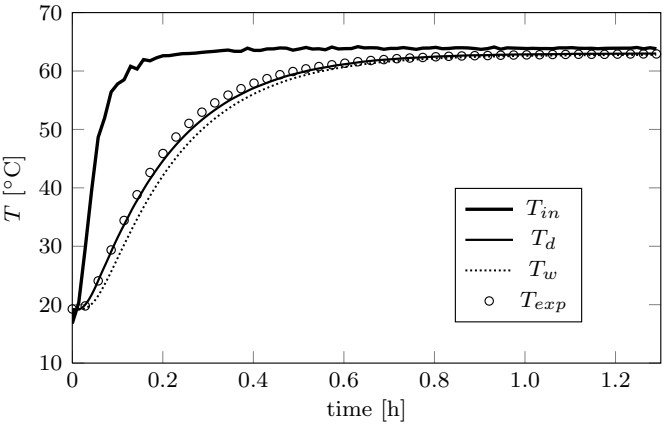

(b) $G_{3,sand} = 875$ l/min

Figure 5.4: Evolution of the inlet air temperature T_{in}, the dense phase temperature T_d, the temperature of the wall T_w and the experimental temperature of the dense phase T_{exp} for a flow rate of (a) $G_{2,sand} = 700$ l/min and (b) $G_{3,sand} = 875$ l/min when the bed is filled with sand.

W/m^2·K, depending on the air flow rate. The same uniform behavior is observed in the dense phase as is observed for sand, with a homogeneous temperature along the bed. Furthermore, the phase change process is clearly reflected in the change in slope of the curves near the phase change temperature interval of (40-50°C). In this case, there are discrepancies between the experimental and

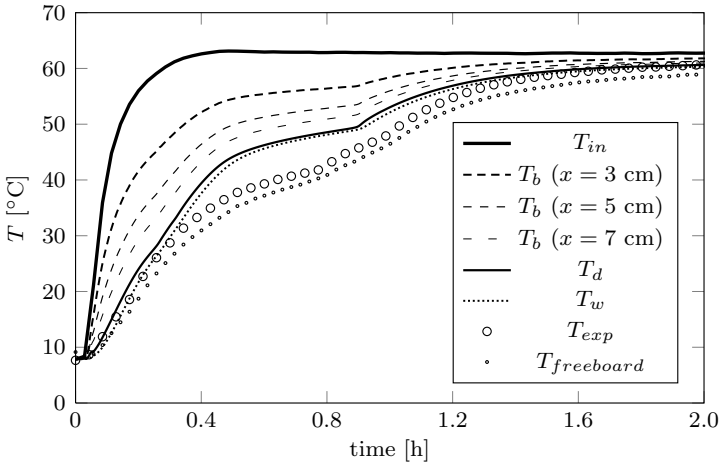

Figure 5.5: Temperature evolution of the inlet air T_{in}, the bubble phase at different heights T_b, the dense phase T_d, the temperature of the wall T_w, the experimental temperature of the dense phase T_{exp} and the temperature measured in the freeboard $T_{freeboard}$ when the bed is filled with PCM and the flow rate is $G_{1,PCM} = 500$ l/min.

numerical data, especially during the phase change process. These discrepancies are attributed to the difference between the heating rate of the material during the experiment, which is approximately 1.5°C/min, and the rate used during the DSC measurements, 0.5°C/min, to obtain the enthalpy-temperature curve used in the model (Figure 5.2). Rady (2009) found that high heating rates promote the development of thermal non-equilibrium effects inside the sample material and result in an increase in the temperature range for melting. It is also observed that the shape of the enthalpy variation curve with temperature depends on the heating rate, calling for functions derived for heating rates similar to those experienced in the actual application.

Two more experiments have been carried out for the flow rates $G_{2,PCM} = 375$ l/min and $G_{3,PCM} = 625$ l/min, which correspond to excess air velocities over minimum fluidization of approximately $U_{2,PCM} = 1.5\,U_{mf}$ and $U_{3,PCM} = 2.5\,U_{mf}$. The results are plotted in Figure 5.6, showing a similar behavior to the case for $G_{1,PCM} = 500$ l/min. The model predicts higher temperatures at all times, except for at $G_{2,PCM} = 375$ l/min after the phase change, where the temperatures predicted by the model are slightly lower than the experimental data.

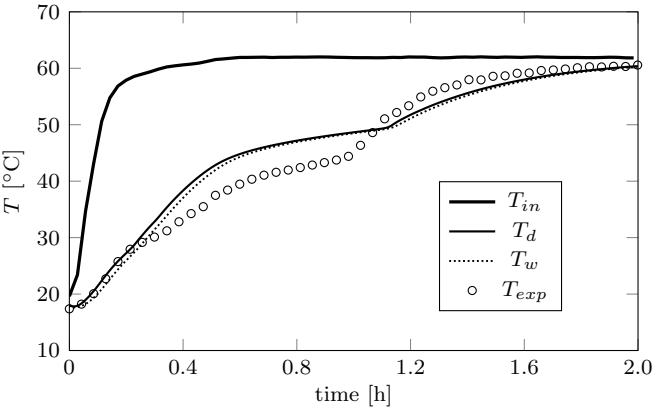

(a) $G_{2,PCM} = 375$ l/min

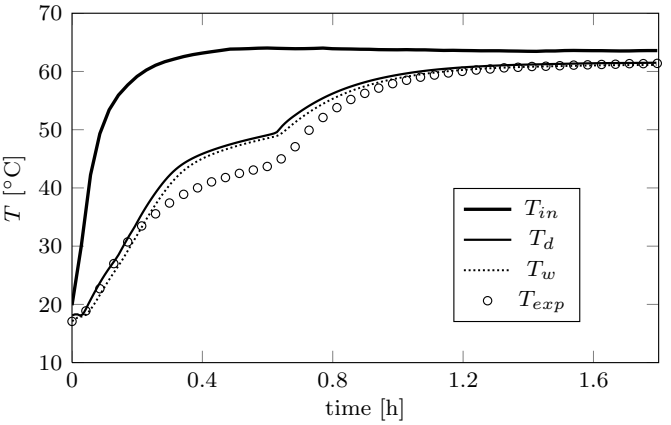

(b) $G_{3,PCM} = 625$ l/min

Figure 5.6: Evolution of the inlet air temperature T_{in}, the dense phase temperature T_d, the temperature of the wall T_w and the experimental temperature of the dense phase T_{exp} for a flow rate of (a) $G_{2,PCM} = 375$ l/min and (b) $G_{3,PCM} = 625$ l/min when the bed is filled with PCM.

5.4.1 Influence of the heating rate

To study the influence of the heating rate, charging experiments with the PCM at a low air heating rate of approximately 0.2°C/min are carried out. For this slow air heating rate, there is a low rate of heat accumulation in the distributor plate, which causes a negligible temperature difference (less than 0.5°C)

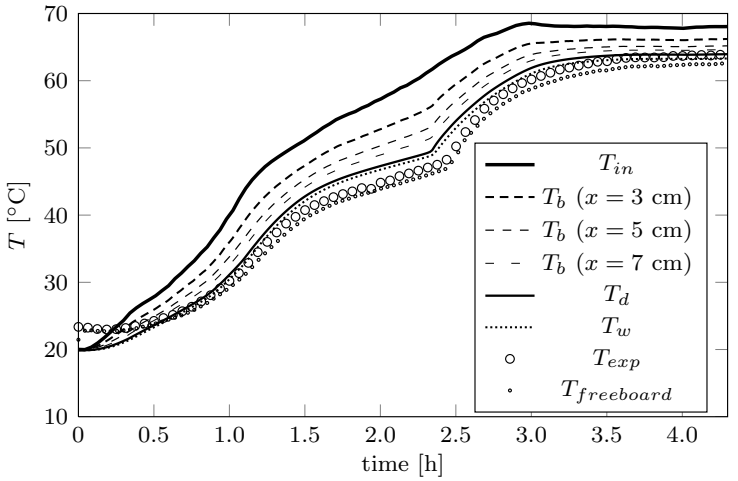

Figure 5.7: Temperature evolution of the inlet air T_{in} with a heating rate of 0.2°C/min, temperature of the dense phase T_d, temperature of the wall T_w, bubble phase temperature at different heights T_b, experimental temperature of the dense phase T_{exp} and temperature measured in the freeboard $T_{freeboard}$ when the bed is filled with PCM.

between the gas in the plenum chamber and the gas at the bed inlet. Therefore, under these experimental conditions, T_{in} is not corrected, and its value is assumed to be equal to the temperature measured in the plenum chamber.

Figure 5.7 presents the temperature profiles for the PCM with a flow rate of $G_{1,PCM} = 500$ l/min and an air heating rate of 0.2°C/min. It is evident that there is a better agreement between the experimental and numerical data.

The same experiments are repeated for flow rates of $G_{2,PCM} = 375$ l/min and $G_{3,PCM} = 625$ l/min (see Figure 5.8), also obtaining good concordance between the experiments and the model. It can be seen that higher charging times are needed at lower flow rates.

For the low heating rates shown in this section, the experimental and numerical results present better agreement because the heating rate is similar to the 0.5°C/min applied in the DSC measurements for the determination of the enthalpy-temperature curves. This low heating rate assures thermal equilibrium in the sample introduced in the DSC.

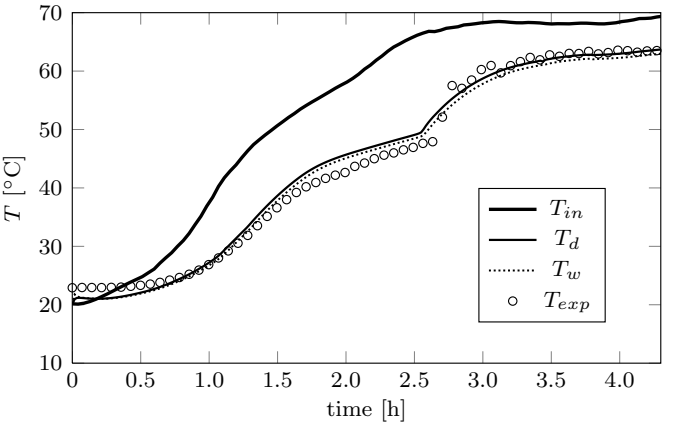

(a) $G = 375$ l/min

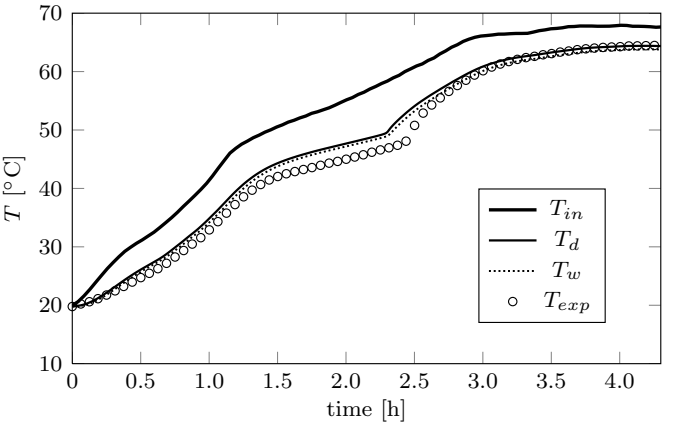

(b) $G = 625$ l/min

Figure 5.8: Temperature evolution of the inlet air T_{in} with a heating rate of 0.2°C/min, temperature of the dense phase T_d, temperature of the wall T_w and experimental temperature of the dense phase T_{exp} for a flow rate of (a) $G_{2,PCM} = 375$ l/min and (b) $G_{3,PCM} = 625$ l/min.

5.4.2 Heat accumulation in the distributor plate

When the heating rate designed for the experiments is high and there is no possibility to experimentally characterize the influence of the distributor plate, the temperature of the air entering the bed can be estimated by introducing the

energy balance equation for the distributor plate into the model. Neglecting convective heat transfer and assuming that the air leaves the distributor at the temperature of the distributor plate T_{dist} (Hoebink & Rietema, 1980), the energy balance for the distributor plate yields the expression

$$m_{dist}\, c_{p,dist} \frac{\partial T_{dist}}{\partial t} = G\, \rho_a\, c_{p,a}\, (T_{plenum} - T_{dist}) + A_{dist}\, U_{dist}\, (T_0 - T_{dist})\,, \quad (5.17)$$

where m_{dist} and $c_{p,dist}$ are the mass and specific heat of the distributor plate, T_{plenum} is the temperature at the plenum chamber and A_{dist} is the heat transfer area between the distributor and the ambient environment. U_{dist} is the heat transfer coefficient between the distributor and the ambient environment, given that the product $A_{dist}U_{dist} = 0.37$ W/K.

Non-dimensionalizing the Equation (5.17) using

$$\hat{T}_{dist} = \frac{T_{dist} - T_0}{T_{max} - T_0}, \quad \hat{T}_{plenum} = \frac{T_{plenum} - T_0}{T_{max} - T_0},$$

the result is

$$\frac{\partial \hat{T}_{dist}}{\partial \hat{t}} = R_{a-dist} \left(\hat{T}_{plenum} - \hat{T}_{dist} \right) + St_{dist-dist} \left(\hat{T}_0 - \hat{T}_{dist} \right). \quad (5.18)$$

The non-dimensional parameters R_{a-dist} and $St_{dist-dist}$ correspond to the expressions

$$R_{a-dist} = \frac{A\, \varepsilon\, H\, \rho_a\, c_{p,a}}{m_{dist}\, c_{p,dist}}, \qquad St_{dist-dist} = \frac{A_{dist}\, U_{dist}\, \varepsilon\, H}{m_{dist}\, c_{p,dist} U}.$$

The solution to Equation (5.18) is

$$\hat{T}_{dist} = \left(\hat{T}_0 - \frac{b}{a} \right) e^{-a\hat{t}} + \frac{b}{a} \quad (5.19)$$

where $a = R_{a-dist} + St_{disto-dist}$ and $b = R_{a-dist}\, \hat{T}_{in} + St_{dist-dist}\, \hat{T}_0$.

When simulating experiments in which the heat accumulation in the distributor plate cannot be neglected, the temperature of the gas that leaves the distributor and enters the bed, T_{in}, can be significantly different from the temperature measured in the plenum chamber, T_{plenum}. Assuming that T_{in} has the same value as the distributor plate temperature, it can be calculated using Equation (5.19).

The comparison between the numerical results for the PCM charging process calculated using different methods to estimate the inlet air temperatures is presented in Figure 5.9, where the temperature measured in the plenum chamber

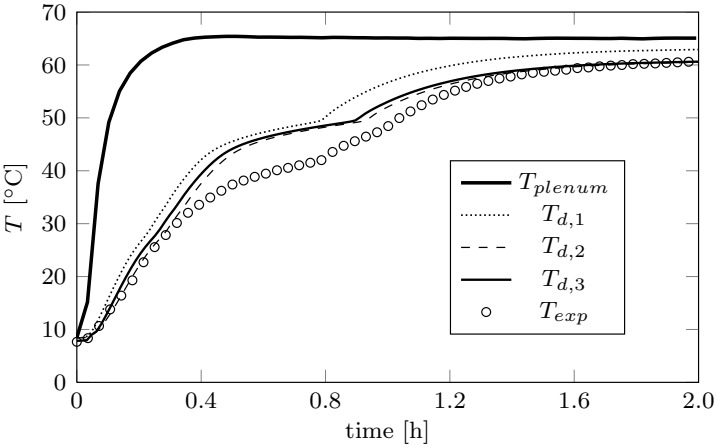

Figure 5.9: Temperature evolution of the air measured in the plenum chamber T_{plenum}, the dense phase temperature obtained by applying three different methods for the estimation of the inlet air temperature ($T_{d,1}$, $T_{d,2}$ and $T_{d,3}$) and the dense phase temperature measured experimentally (T_{exp}) when the bed is filled with PCM at a gas flow rate of $G_{1,PCM} = 500$ l/min.

is defined as T_{plenum}, and T_{exp} corresponds to the same experimental measurements presented in Figure 5.5 for the flow rate $G_{1,PCM} = 500$ l/min. The product $A_{dist}U_{dist} = 0.37$ W/K is estimated according to these experimental conditions. The numerical results of the dense phase temperature T_d are shown for the following methods: (i) $T_{d,1}$ is the result obtained if the inlet air temperature is taken as the temperature measured in the plenum chamber, (ii) $T_{d,2}$ is the result obtained if the inlet air temperature is taken as the distributor temperature calculated using equation (5.19) and (iii) $T_{d,3}$ is the result obtained if the inlet air temperature is experimentally determined by subtracting the temperature drop across the distributor from the temperature measured in the plenum chamber.

It is evident that the dense phase temperature, $T_{d,1}$, obtained using the temperature measured in the plenum chamber as an estimation of the inlet air temperature, is always higher than the experimentally measured temperature because the temperature drop across the distributor, which has a significant value at this heating rate, is not accounted for. By contrast, the results for $T_{d,2}$ and $T_{d,3}$, where the influence of the distributor is considered experimentally and numerically, are similar and agree well with the experimental measure-

ments. This confirms that the temperature of the air entering the bed can be estimated numerically by including Equation (5.18) in the model proposed. The discrepancies found between the model and experimental results during the phase change process are due to the high heating rate of the PCM at these experimental conditions, as explained before.

5.5 Conclusions

A numerical model for heat transfer in a fluidized bed with granular PCM material has been presented. The proposed non-dimensionalization of the energy equations results in the same differential equation system regardless of whether the granular material contains PCM. In this manner, the same numerical procedure can be used in cases with or without PCM. Furthermore, the model takes into account the energy stored in the wall and the air temperature drop across the distributor plate.

The comparison between the numerical and experimental data shows good agreement for the conventional material, sand. When there is a phase change in the granular material, the model properly predicts the experimental results if the heating rate of the bed is slow (0.2°C/min) because the enthalpy-temperature curve introduced in the model has been obtained in a DSC that also has a slow heating rate to ensure equilibrium conditions in the sample.

The solution of the distributor plate energy equation makes possible to properly estimate the inlet air temperature, whose value is significantly different from the gas temperature measured at the plenum chamber if the heating rate is high.

Notation

A	cross sectional area of the bed [m^2]
c_p	specific heat [$J \cdot kg^{-1} \cdot K^{-1}$]
d	diameter [m]
G	volumetric flow rate [$m^3 \cdot s^{-1}$]
g	gravity [$m \cdot s^{-2}$]
H	height of the bed [m]
H_{bc}	heat interchange across the bubble cloud boundary per unit volume of bubble phase [$W \cdot m^{-3} \cdot K^{-1}$]
H_w	height of the wall [m]

h_b	convective heat transfer coefficient between the bubbles and the dense phase [W·m^{-2}·K^{-1}]
h_w	convective heat transfer coefficient between the dense phase and the container wall [W·m^{-2}·K^{-1}]
i	enthalpy [J]
k	thermal conductivity [W·m^{-1}·K^{-1}]
m	mass [kg]
P_b	perimeter of the cross sectional area of bubbles [m]
S_b	bubble surface [m^2]
St	Stanton number [-]
T	temperature [°C]
T_{pc}	phase change temperature [°C]
U	superficial gas velocity [m·s^{-1}]
U_b	rising velocity of bubbles [m·s^{-1}]
U_{dist}	heat transfer coefficient between the distributor and the ambient surroundings [W·m^{-2}·K^{-1}]
U_{mf}	minimum fluidization velocity [m·s^{-1}]
U_{wo}	global heat transfer coefficient between the container wall and the ambient surroundings [W·m^{-2}·K^{-1}]
V	bed volume [m^3]
V_b	bubble volume [m^3]

Greek symbols

ρ	density [kg·m^{-3}]
σ_{dp}	standard deviation of the mean particle diameter [m]
ε	voidage in the bed [-]
δ	volume fraction of bed consisting of bubbles [-]
Δt	time step [s]
Δx	spatial step [m]

Subscripts

0	ambient/initial
a	air
b	bubble
d	dense phase
$dist$	distributor
in	inlet
max	maximum value
p	particle

pc	phase change
s	solid
w	wall
wi	inner wall
wo	outer wall

References

Benmansour, A., Hamdan, M.A. & Bengeuddach, A. 2006 Experimental and numerical investigations of solid particles thermal energy storage unit. *Applied Thermal Engineering* 26, 513–518.

Darton, R.C., LaNauze, R.D., Davidson, J.F. & Harrison, D. 1977 Bubble growth due to coalescence in fluidized beds. *Transactions of the Institution of Chemical Engineers* 55, 274–280.

Davidson, J.F. & Harrison, D. 1963 *Fluidised particles*. Cambridge University Press.

El-Halwagi, A.M., El-Rifai, M.A. & El-Halwagi, M.M. 1991 Maximization of thermal efficiency of fluidized-bed heat regenerators. *Heat Recovery Systems and CHP* 11, 141–148.

Elsayed, M.M., Megahed, I.E. & El-Refaee 1988 Experimental testing of fluidized beds thermal storage. *Solar & Wind technology* 5, 15–25.

Faghri, A. & Zhang, Y. 2006 In *Transport Phenomena in Multiphase Systems* (ed. Amir Faghri & Yuwen Zhang), pp. 1–106. Boston: Academic Press.

Farid, M.M., Khudhair, A.M., Razack, S.A.K. & Al-Hallaj, S. 2004 A review on phase change energy storage: materials and applications. *Energy Conversion and Management* 45, 1597–1615.

Geldart, D. 1973 Types of gas fluidization. *Powder Technology* 7, 285–292.

Heertjes, P.M., de Boer, H.G.J. & de Haas van Dorsser, A.H. 1953 Temperature and humidity measurements in a drying fluidized bed. *Chemical Engineering Science* 2, 97–107.

Hoebink, J.H.B.J. & Rietema, K. 1980 Drying granular solids in fluidized beds i: Description on basis of mass and heat transfer coefficients. *Chemical Engineering Science* 35, 2135–2139.

Izquierdo-Barrientos, M.A., Sobrino, C. & Almendros-Ibáñez, J.A. 2013 Thermal energy storage in a fluidized bed of pcm. *Chemical Engineering Journal* 230, 573–583.

Izquierdo-Barrientos, M.A., Sobrino, C. & Almendros-Ibáñez, J.A. 2014*a* Modeling of the heat transfer coefficient in fixed and fluidized beds with pcm. In *Eurotherm Seminar 99: Advances in Thermal Energy Storage*. Lleida.

Izquierdo-Barrientos, M.A., Sobrino, C. & Almendros-Ibáñez, J.A. 2014*b* Modeling the heat transfer coefficient between a surface and fixed and fluidized beds with pcm. *Submitted to International Journal of Heat and Mass Transfer* .

Kunii, D. & Levenspiel, O. 1968 Bubbling bed model for kinetic processes in fluidized plate. gas-solid mass and heat transfer and catalytic reactions. *Industrial and Engineering Chemistry Process Design and Development* 7, 481–492.

Kunii, D. & Levenspiel, O. 1991 *Fluidization Engineering*. Butterworth-Heinemann.

Rady, M. 2009 Study of phase changing characteristics of granular composites using differential scanning calorimetry. *Energy Conversion and Management* 50, 1210–1217.

Regin, A.F., Solanki, S.C. & Saini, J.S 2009 An analysis of a packed bed latent heat thermal energy storage system using pcm capsules: Numerical investigation. *Renewable Energy* 34, 1765–1773.

Sozen, Z.Z., Grace, J.R. & Pinder, K.L. 1988 Thermal energy storage by agitated capsules of phase change material: pilot scale experiments. *Industrial and Engineering Chemistry Research* 27, 679–684.

Wagialla, K.M., Fakeeha, A.H., Elnashaire, S.S.E.H. & Almaktary, A.Y. 1991 Modeling and simulation of energy storage in fluidized beds using the two-phase model. *Energy Sources* 13, 189–201.

CHAPTER
SIX

Experimental heat transfer coefficients between a surface and fixed and fluidized beds with PCM

This work presents an experimental study to determine the capacity of a phase change material (PCM) in granular form to be used in fixed and bubbling fluidized beds for thermal energy storage. The experimental measurements are focused on determination of the heat transfer coefficient between a heated surface immersed in the bed and the granular PCM. The flow rate is varied to quantify its influence on the heat transfer coefficient. The PCM used is Rubitherm® GR50 with a phase change temperature of approximately 50°C. The PCM is available in two different particle sizes, 0.54 mm and 1.64 mm, of which the finer is used in the fluidized bed and the coarser is used in the fixed bed. In addition, the results obtained for the PCM are compared with the heat transfer coefficients measured for sand, a material commonly used for thermal storage.

In comparing the heat transfer coefficients for fixed and fluidized beds, the heat transfer coefficients in the fluidized bed with PCM are nearly three times higher than those for the fixed bed at the same gas flow rate. This increase in the heat transfer is a result of two main factors: first, the continuous renewal of PCM particles from the heated surface when they are fluidized, and second, the large quantities of energy in latent form absorbed by the PCM.

6.1 Introduction

The development of renewable energy technologies, such as solar thermal energy technology, has accompanied the evolution of new and more efficient energy storage systems in order to equilibrate the energy supply with its demands.

The integration of phase change materials (PCMs) in these systems improves the energy storage capacity for the same volume and makes it possible for the system to be maintained in a narrow temperature range (Mehling & Cabeza, 2008). There are different ways of incorporating PCMs in storage tanks. For example, in domestic hot water tanks, a macroencapsulated PCM is typically located at the top of the tank to improve the stratification in the tank and increase the energy density of the hottest region of the deposit (Talmatsky & Kribus, 2008). When the heat transfer fluid is air instead of water, packed beds of micro- and macroencapsulated PCMs have traditionally been utilized. More recently, Izquierdo-Barrientos *et al.* (2013) studied the performance of a fluidized bed with a granular PCM (with a particle size of 0.54 mm) as an energy storage device. They observed a higher efficiency during the storage process compared with traditional packed beds.

In gas-particle systems, heat transfer can occur between the gas and the solid or between the gas or solid particles and a solid surface. Knowledge of this bed-to-surface heat transfer coefficient is essential for optimal design of the storage systems from which thermal energy is removed. Because of its engineering importance, the heat transfer coefficient has been measured by many researchers for different geometries and operating conditions in fixed and fluidized beds of rocks, sand or glass beads (Kunii & Levenspiel, 1991*b*; Kunii & Smith, 1960; Kunii & Suzuki, 1966; Botterill & Desai, 1972; Chen, 1976; Ozkaynak & Chen, 1980; Mickley & Trilling, 1949; Al-Busoul & Abu-Ein, 2003; Karamavruc & Clark, 1996; Khan & Turton, 1992).

Alternatively, fluidized beds are widely used in heat recovery processes because of their ability to achieve intense heat transfer and provide a uniform temperature within the bed. A number of experimental investigations have been reported on the measurement of the heat transfer rate between a horizontal tube and fluidized beds (Lese & Kermode, 1972; Bartel & Genetti, 1973; Priebe & Genetti, 1977; Grewal *et al.*, 1979; Doherty *et al.*, 1986). However, none of these studies used a granular material with a PCM inside the bed. The difficulty in establishing a reliable value for the heat transfer coefficient stems from the fact that it depends on a large number of systems and operating parameters. The simple and pioneering model of Mickley & Fairbanks (1955) establishes that when a group of particles in a fluidized bed come in contact with the heat transfer surface, transient conduction occurs during the residence time of the particles until the particles are displaced by the action of the bubbles. Thus, the average heat transfer coefficient, h_w, in a fluidized bed

is typically computed as follows

$$h_w = h_s\,(1 - \delta_w) + h_g\,\delta_w, \tag{6.1}$$

where δ_w is the fraction of bubbles in the bed and h_g is the heat transfer coefficient of the gas in the bubble phase, which is orders of magnitude lower than the heat transfer coefficient of the particles, h_s. According to Mickley & Fairbanks (1955), h_s can be calculated as

$$h_s = \frac{2}{\sqrt{\pi}}\sqrt{\frac{k\,\rho\,c_p}{t_s}}. \tag{6.2}$$

Equation (6.2) shows that the rate of heat transfer to a wall surface is proportional to the square root of the specific heat, c_p, of the particulate material. Therefore, the use of granules with a core composed of PCM is expected to enhance the convection coefficient because of their large equivalent heat capacity during the phase change of the material, which is defined as

$$\bar{c}_{p_{pcm}} = \frac{1}{\Delta T}\int_{T_0}^{T_0+\Delta T} c_{p_{pcm}}(T)\,\mathrm{d}T, \tag{6.3}$$

where $c_{p_{pcm}}(T)$ is the specific heat of the granular PCM, T_0 is the initial temperature of the phase change and $T_0 + \Delta T$ is the end temperature.

Rady (2009*a*) used a granular PCM (Rubitherm® GR42) with a particle size in the range of 1-3 mm in a fixed bed for thermal energy storage, and Regin *et al.* (2009) reviewed the development and advantages of the heat transfer characteristics of a thermal energy storage system using PCM capsules. Nevertheless, no extensive research on evaluating the convective heat transfer coefficient has been performed. Most of the experimental studies and the proposed models in the literature concerning heat transfer between a surface and solid particles have been focused on the case in which the heat transferred to the particles increases the internal energy of the solids in sensible form, i.e., increasing its temperature. In a recent study, Izquierdo-Barrientos *et al.* (2013) successfully used a commercial PCM with a smaller particle size of $0.2-0.6$ mm in a bubbling fluidized bed. However, only Brown et al. (Brown *et al.*, 1998) measured heat transfer coefficients in a microencapsulated phase-change material fluidized bed (octadecane encapsulated in a gelatin shell with a size range of

300-600 μm), and heat transfer enhancements approximately 30% larger than the single-phase values were observed.

The objective of this work is to measure the heat transfer coefficient between a surface and particles in both fixed and fluidized beds filled with a granular PCM that changes its phase (solid-liquid transition) at a certain temperature. In addition, the results obtained are compared with the heat transfer coefficients for a fixed and a fluidized bed filled with sand, a material commonly used in both technologies for thermal storage. Described herein are the experimental procedure and set-up and the properties of the materials studied, followed by the main experimental results, and finally a summary of the main conclusions of the work.

6.2 Materials and experimental apparatus

The materials used in this study are sand and a granular phase change composite. The granular PCM consists of paraffin, which is the material that changes its phase, bounded within a secondary supporting structure of SiO_2, which ensures that the paraffin does not leak from the granulate when in its liquid form. This material is commercialized by Rubitherm® and is similar to that used by Rady (2009*a*) and Izquierdo-Barrientos *et al.* (2013) in their studies. This PCM is available in two sizes involving particle diameters of 1-3 mm and 0.2-0.6 mm. The finer grade is used in the fluidized bed because the particle size is appropriate for obtaining a bubbling fluidization of Geldart B particles (Geldart, 1973), whereas the coarser grade is employed in the fixed bed conditions to achieve high gas velocities without exceeding the minimum fluidization velocity. Table 6.1 presents several properties of the sand and PCM, such as the density ρ, thermal conductivity k, mean diameter of the particles $\overline{d}_p$ with its standard deviation σ_{dp} and the approximate mass m used for each experiment.

Figure 6.1 shows the specific heat evolution with temperature for the PCM and the sand, which were measured by differential scanning calorimetry (DSC) with a slow heating rate of 0.5°C/min (Rady, 2009*a*,*b*), which ensures thermal equilibrium in the sample during the DSC measurements. The phase change of the PCM is clearly distinguished at approximately 50°C, which is its phase change temperature T_{pc}. The mean specific heat of the sand is 0.776 kJ/(kg °C) for the temperature range used in this work.

Figure 6.2 shows a schematic of the experimental apparatus used for the heating experiments. The bed consists of a cylindrical tube made from stain-

Material	Bed	ρ [kg/m^3]	k [W/m·K]	$\overline{d}_p$ [mm]	σ_{dp} [mm]	m [kg]
Sand*	Fixed	2632.3	4.2	0.91	0.125	13
	Fluidized	2632.3	4.2	0.76	0.068	9
GR50	Fixed	1512.8	4.0	1.64	0.196	8
	Fluidized	1550.5	4.0	0.54	0.082	5

Table 6.1: Material properties.*The sand used in the fixed bed corresponds to Sand 2 from Table 2.2 and the sand used in the fluidized bed to Sand 1 (also in Table 2.2).

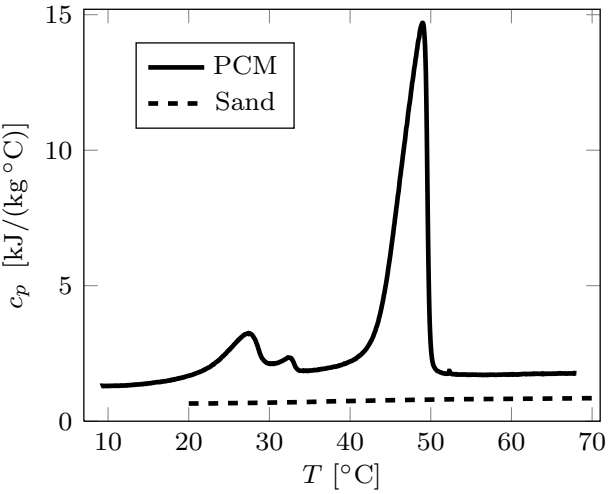

Figure 6.1: Specific heat as a function of temperature for the PCM-GR50 and the sand.

less steel with 2-mm-thick walls and filled with particles. The air enters the plenum of the column and flows into the bed through a distribution plate. The instrumentally monitored section of the test apparatus has a height of 500 mm and an internal diameter of $d_i = 200$ mm and is insulated with 2-cm-thick glass wool. The air flow is produced by a blower with a variable mass flow rate and can be heated by electrical heaters that are regulated by a PID controller before flowing into the column. Type K thermocouples are used to measure the temperature at specific locations inside the test section and within the plenum chamber. In the same locations, the heat transfer probe can be introduced, which consists of a cylindrical variable resistance of 200 W with three thermo-

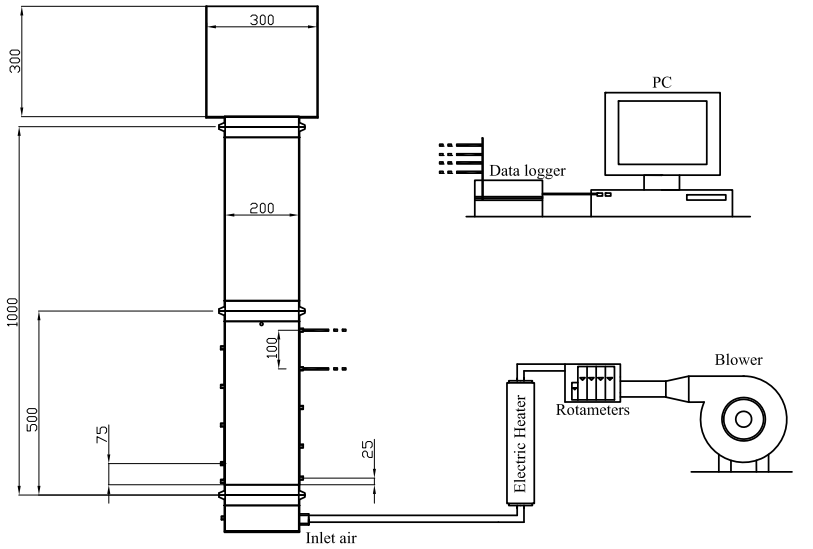

Figure 6.2: Schematic of the experimental apparatus. Dimensions in mm.

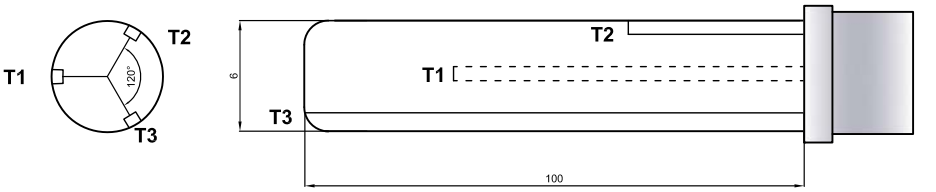

Figure 6.3: Schematic of the probe for measuring the heat transfer coefficient. Dimensions in mm.

couples distributed around its surface. This probe is similar to the one used by Masoumifard *et al.* (2008) and is schematically presented in Figure 6.3. The three thermocouples permit the measurement of the mean temperature of the resistance surface, T_w, as will be explained later on. The bed temperature, T_∞, is measured at the center of the bed at different heights above the distributor.

The bed temperature is uniform and equal to the ambient temperature $T_0 \simeq 18°\text{C}$ at the beginning of every experiment. Before beginning the temperature measurements, the blower is switched on, and air is introduced into the column at the desired rate. During this process, the blower heats the air to a temperature greater than the ambient temperature because of the compres-

sion process. This temperature is approximately 35°C. The entire bed reaches this temperature after approximately 2 h. Once the bed reaches steady state, the heat transfer probe is heated to a temperature higher than T_{pc}. For these conditions, the temperatures at different heights of the bed and the probe temperature are measured over a one-minute period at a frequency of 1 Hz.

This procedure is repeated two more times, rotating the heat transfer probe 120°, to obtain a total of 9 temperature measurements for the resistance surface. Thus, any possible variations of the local heat transfer coefficient with the tangential angle (Saxena *et al.*, 1979) are taken into account. Therefore, the temperature T_w is the mean value of these 9 measurements. This process is repeated at different superficial velocities.

For the fluidized bed experiments, the bed is filled with particles up to a height $H = 0.2$ m, and the heat transfer probe is placed 12.5 cm above the distributor (see Figure 6.4(a)). Unlike fluidized beds, the temperature distribution around the resistance in a fixed bed is not uniform, and natural convection may affect the value of the heat transfer coefficient. Thus, for the fixed bed, the same experiments described are performed for two different positions of the heat transfer probe: one at the bottom of the bed at a height of 2.5 cm above the distributor (see Figure 6.4(b)) and the other close to the freeboard of the bed at 22.5 cm above the distributor (see Figure 6.4(c)). The height of the bed for the fixed bed is increased, $H = 0.3$ m, to avoid the influence of the distributor when the probe is at the top and the influence of the freeboard when the probe is at the bottom.

The heat transfer coefficient is calculated following the expression

$$h_w = \frac{q}{a_w(T_w - T_\infty)}, \tag{6.4}$$

where a_w is the submerged area of the probe and q is the power transferred by the probe. The power supplied to the probe is varied during the experiments to obtain a temperature difference of $T_w - T_\infty \approx 20$°C, where $T_\infty \approx 35$°C. Thus, the entire temperature range of the phase change exhibited in Figure 6.1 is covered.

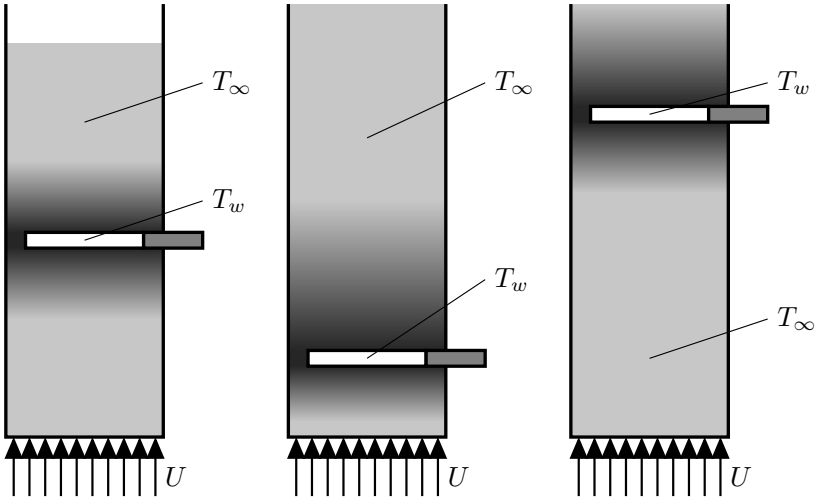

(a) Middle, $H = 0.2$ m (b) Down, $H = 0.3$ m (c) Up, $H = 0.3$ m

Figure 6.4: Positions of the heat transfer probe for the fluidized bed (a) and the fixed bed (b, c).

6.3 Experimental results and discussion

6.3.1 Fixed Bed

The total heat transfer coefficients obtained from the experiments (isolated points) and their linear regression (continuous line) for the sand and the PCM are plotted in Figure 6.5. When the flow rate is increased, the value of the heat transfer coefficient increases linearly for both materials. This tendency was previously observed by Yagi & Kunii (1962) and Kunii & Suzuki (1966). Furthermore, when the particles are surrounded by motionless fluid, the thermal conductivity of a layer of solids adjacent to the surface aids in the transport of heat. This heat transfer coefficient for the fixed bed with stagnant gas is increased by the gas flow through the bed.

The flow rates selected must be lower than the minimum fluidization velocity of each material, U_{mf}. For this reason, the maximum flow rate selected for the sand is $\dot{V} = 600$ l/min because its minimum fluidization velocity is approximately $\dot{V} = 750$ l/min. The minimum fluidization velocity for the coarser PCM is higher than the maximum flow rate our facility can supply ($\dot{V} = 1100$ l/min).

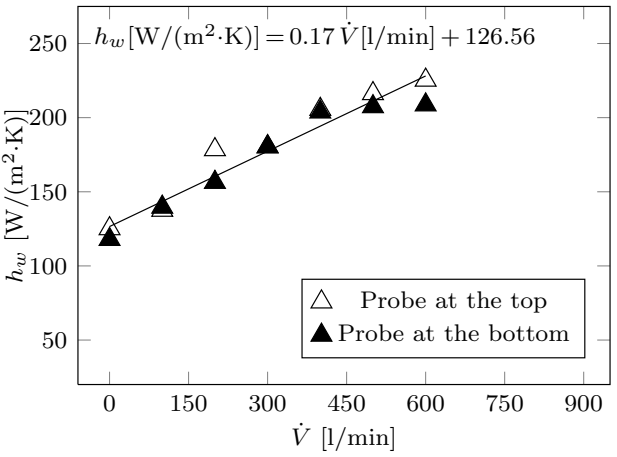

(a) Sand

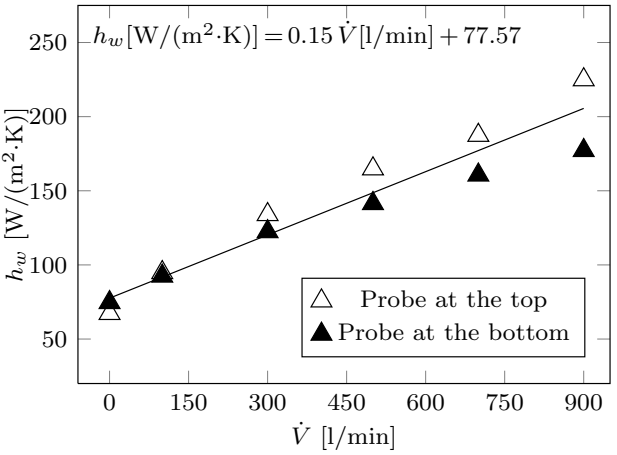

(b) PCM

Figure 6.5: Evolution of the heat transfer coefficient, h_w, in a fixed bed for different flow rates for (a) sand and (b) PCM.

Figure 6.5 shows that natural convection of the heated air slightly affects the results for the different positions of the probe. The values of the heat transfer coefficients obtained for the sand and the PCM are similar because both materials have similar thermal conductivities and particles in a fixed bed are motionless. The paraffin of the PCM particles touching the heated surface may be in liquid form if $T_w > T_{pc}$, but the particles far from the surface may be

in the solid phase if $T_\infty < T_{pc}$. Therefore, in a fixed bed, the benefit expected in the heat transfer coefficient resulting from the phase change of the PCM is limited because there is no movement of the particles surrounding the heated probe, and consequently no increase in the heat transfer coefficient is obtained.

6.3.2 Fluidized bed

The sand and the finer PCM correspond to group B according to Geldart's classification (Geldart, 1973), which indicates that these materials fluidize easily with vigorous bubbling action and that the bubbles grow large (Kunii & Levenspiel, 1991*a*). The same experiments performed for the packed bed were repeated for the sand and the PCM in the fluidized state, taking into account that the flow rates chosen have to exceed the minimum fluidization velocity for each material. For the sand used in the fluidized bed, the minimum fluidization velocity is $U_{mf} = 0.33$ m/s, which corresponds to a flow rate of 622 l/min. The minimum fluidization velocity of the finer GR50 is $U_{mf} = 0.13$ m/s, which corresponds to a flow rate of 250 l/min, much lower than that for the sand because the PCM has a lower density. Thus, the flow rates chosen for the experiments with GR50 are greater than 250 l/min and nearly the same as those selected for the fixed bed with the coarser PCM.

The measured heat transfer coefficients for the sand and the PCM in the fluidized bed are presented in Figure 6.6 as a function of the gas velocity. The corresponding excess air ratio, U/U_{mf}, at a given superficial velocity is also indicated in the upper abscissa. As concluded for the fixed bed case, the heat transfer coefficient increases when the flow rate increases (Kunii & Levenspiel, 1991*a*; Grewal & Saxena, 1980; Masoumifard *et al.*, 2008). It is also observed that at the same excess air velocity over minimum fluidization conditions, U/U_{mf}, better coefficients are obtained for the sand; however, sand requires a higher air flow and therefore has a higher energy cost. Moreover, for the same heat transfer coefficient, i.e., $h_w \approx 500$ W/m^{2}K, the flow rate required for the sand is ~ 800 l/min, whereas that for the PCM is only 300 l/min. This higher heat transfer coefficient for the PCM in comparison to the sand is due to the phase transition enabled by the continuous renewal of the PCM from the heated surface. This enhancement was not observed for the packed bed of the PCM because the particles at the surface were not regenerated.

The use of a finer PCM in the fluidized bed allows it to remain in a fluidized state with the same range of gas velocity as in the packed bed for the coarser

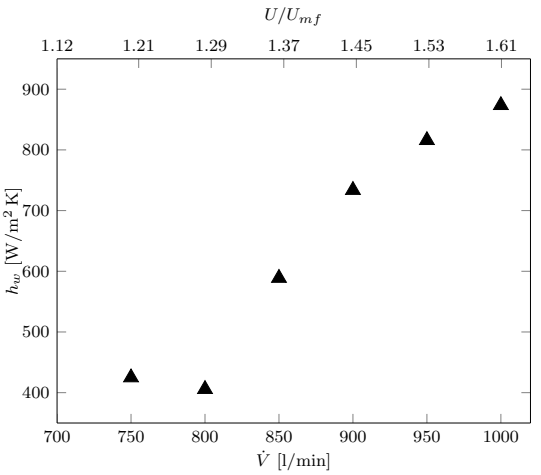

(a) Sand

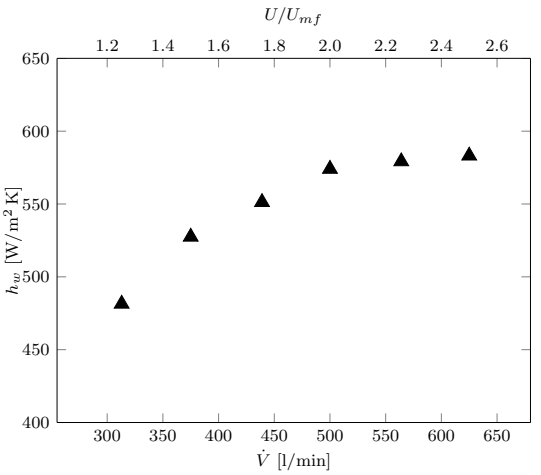

(b) PCM

Figure 6.6: Evolution of the heat transfer coefficient, h_w, in a fluidized bed for different flow rates for (a) sand and (b) PCM.

PCM. This material takes advantage of the higher heat transfer coefficients typically obtained in fluidized beds that are enhanced by the phase transition of the particles heated by the heat transfer surface.

A comparison of the heat transfer coefficient for the fixed bed of sand and for the fluidized bed of sand (Figure 6.5(a) and Figure 6.6(a)) shows, as observed

by other investigators (Xavier & Davidson (1985)), much higher values for the fluidized bed.

6.3.3 Measurements in a heating and cooling cycle

The variations of the heat transfer coefficient in the fluidized bed during the entire phase change process are not adequately represented in the previous results because the data were obtained at a constant bed temperature. To properly interpret the differences observed in h_w with the bed temperature, the heat transfer coefficient is measured during the heating of the bed from ambient temperature to a maximum temperature over T_{pc} and during the corresponding cooling period.

Although the heat transfer coefficient is measured under transient conditions, the characteristic time t of replacement of the particles that are touching the surface is on the order of ~ 1 s (Kunii & Levenspiel, 1991a), whereas the data for the heat transfer coefficient are averaged over one minute. During this time, the bed temperature does not vary appreciably; thus, the measurements are obtained under quasi-steady-state conditions.

Figure 6.7 represents the evolution of two temperatures: the temperature of the bed, T_∞, and the temperature of the supplied air, T_{air}, during a charging-discharging process in the fluidized bed together with the variation of the heat transfer coefficient. The temperature of the probe, T_w, is always higher than T_∞. The power supplied to the probe is 9 W. During the charging process, the values observed for the heat transfer coefficient are lower than those measured during the discharging process. When the granular PCM is in the liquid state during the heating period, a constant value of $h_w \approx 350$ W/m^{2}K is observed. In contrast, during the cooling process, once the material has reduced its temperature under T_{pc} and it is in the solid form, the heat transfer coefficient is more than two times higher. This result arises from the phase-change transition that takes place when the cold particles, which are continuously renewed, come in contact with the hot probe surface.

According to the model of Mickley & Fairbanks (1955), the heat transfer coefficient in a fluidized bed is proportional to the square root of the specific heat (see Equation (6.2)). If we compare the ratio between the heat transfer coefficients when the bed particle temperature is under the phase-change temperature of the PCM and when it is over, taking into account Equations (6.1)-(6.3) and

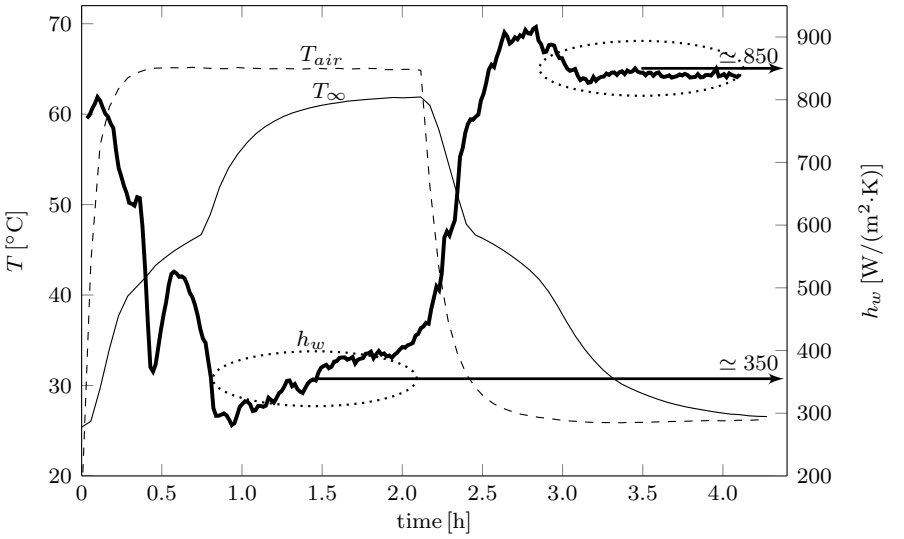

Figure 6.7: Evolution of the air supply temperature, bed temperature and convective heat transfer coefficient during a charging-discharging process. $\dot{V} = 500$ l/min.

assuming that $h_s \gg h_g$, we obtain the following equation

$$\frac{h_{T_\infty<T_{pc}}}{h_{T_\infty>T_{pc}}} = \frac{h_{s_{T_\infty<T_{pc}}}(1-\delta_w)+h_g\,\delta_w}{h_{s_{T_\infty>T_{pc}}}(1-\delta_w)+h_g\,\delta_w} \sim \frac{h_{s_{T_\infty<T_{pc}}}}{h_{s_{T_\infty>T_{pc}}}} \sim \sqrt{\frac{\bar{c}_{p_{pcm}}}{c_p}} \approx \sqrt{\frac{6300}{1700}} \approx 2, \tag{6.5}$$

where $c_{p_{pcm}}$ is the equivalent heat capacity of the PCM defined in Equation (6.3). The result is in accordance with the values for the heat transfer coefficient observed in Figure 6.7.

6.4 Conclusions

In this work, the heat transfer coefficient h_w has been measured for a PCM and sand in a fixed and fluidized bed with a heat transfer probe horizontally immersed. For both fixed and fluidized beds, the heat transfer coefficient increases with increasing flow rate. As expected, higher values of h_w are obtained for the fluidized bed than for the fixed bed because of the continuous regeneration of solids that come in contact with the surface of the probe.

In the fixed bed filled with PCM, only the particles surrounding the heating probe are able to change their phase; hence, no increase in the heat transfer coefficient is obtained from the phase change. Consequently, the comparison between the sand and the PCM shows similar results when they are used in fixed bed because they have similar conductivities. In the fluidized bed of PCM particles, the phase transition of the PCM particles increases the heat transfer coefficient, which is higher than the heat transfer coefficient of the fluidized bed of sand for the air flow rates used in the fluidized bed with PCM.

The experimental results show that the heat transfer coefficient in a fluidized bed with granular PCM is notably increased because of the latent energy stored by the PCM when the bed is at a temperature below the transition temperature. Under these conditions, the PCM inside the granular material changes its phase and absorbs the latent energy. The expected increase in the heat transfer coefficient is proportional to the square root of the ratio between the latent energy of the phase change and the sensible energy in the solid phase. For the granular PCM used in this work, the heat transfer coefficient when there is a phase change in the PCM is expected to double the coefficient when there is no phase change. The experimental observations are in agreement with this prediction.

Notation

a_w	submerged area of the probe [m^2]
c_p	specific heat [$J \cdot kg^{-1} \cdot K^{-1}$]
d	diameter [m]
H	height of the bed [m]
h_g	convective heat transfer coefficient of the gas [$W \cdot m^{-2} \cdot K^{-1}$]
h_s	convective heat transfer coefficient of the particles [$W \cdot m^{-2} \cdot K^{-1}$]
h_w	convective heat transfer coefficient from the bed to the inner surface of the bed [$W \cdot m^{-2} \cdot K^{-1}$]
k	thermal conductivity [$W \cdot m^{-1} \cdot K^{-1}$]
m	mass [kg]
q	power transferred by the probe [W]
t	time [s]
T	temperature [°C]
U	superficial gas velocity [$m \cdot s^{-1}$]
$\dot{V}$	flow rate [$m^3 \cdot s^{-1}$]

Greek symbols

δ_w	fraction of bubbles in the bed
ρ	density [kg·m^{-3}]
σ_{dp}	standard deviation of the mean particle diameter [m]

Subscripts

0	ambient/initial
air	air
b	bed
i	internal
mf	minimum fluidization
p	particle
pc	phase change
w	wall surface of the probe
∞	far from the surface of the probe

References

Al-Busoul, M. & Abu-Ein, S. 2003 Local heat transfer coefficient around a horizontal heated tube immersed in a gas fluidized bed. *Heat and Mass Transfer* 39, 355–358.

Bartel, W.J. & Genetti, W.E. 1973 Heat transfer from a horizontal bundle of bare and finned tubes in an air fluidized bed. *Chemical engineering progress symposium series* 69, 85–93.

Botterill, J.S.M. & Desai, M. 1972 Limiting factor in gas-fluidized bed heat transfer. *Powder Technology* 6, 231–238.

Brown, R.C., Rasberry, J.D. & Overmann, S.P. 1998 Microencapsulated phase-change materials as heat transfer media in gas fluidized beds. *Powder Technology* 98, 217–222.

Chen, J.C. 1976 Heat transfer to tubes in fluidized bed. In *National Heat Transfer Conference*. St. Louis MO.

Doherty, J.A., Verma, R.S., Shrivastava, S. & Saxena, S.C. 1986 Heat transfer from immersed horizontal tubes of different diameter in a gas fluidized bed. *Energy* 11, 773–783.

Geldart, D. 1973 Types of gas fluidization. *Powder Technology* 7, 285–292.

Grewal, N.S. & Saxena, S.C. 1980 Heat transfer between a horizontal tube and a gas-solid fluidized bed. *International Journal of Heat and Mass Transfer* 23, 1505–1519.

Grewal, N.S., Saxena, S.C., Dolidovich, A.F. & Zabrodsky, S.S. 1979 Effect of distributor design on heat transfer from an immersed horizontal tube in a fluidized bed. *Chemical Engineering Journal* 18, 197–201.

Izquierdo-Barrientos, M.A., Sobrino, C. & Almendros-Ibáñez, J.A. 2013 Thermal energy storage in a fluidized bed of pcm. *Chemical Engineering Journal* 230, 573–583.

Karamavruc, A.I. & Clark, N.N. 1996 A correction factor for one-dimensional heat transfer coefficients around a horizontal tube in a fluidized bed. *Powder Technology* 86, 209–217.

Khan, T. & Turton, R. 1992 The measurements of instantaneous heat transfer coefficients around the circumference of a tube immersed in a high temperature fluidized bed. *International Journal of Heat and Mass Transfer* 35, 3397–3406.

Kunii, D. & Levenspiel, O. 1991*a* *Fluidization Engineering*. Butterworth-Heinemann.

Kunii, D. & Levenspiel, O. 1991*b* A general equation for the heat transfer coefficient at wall surface of gas/solid contactors. *Industrial and Engineering Chemistry Research* 30, 136–141.

Kunii, D. & Smith, J.M. 1960 Heat transfer characteristics of porous rocks. *American Institute of Chemical Engineers Journal* 6, 71–78.

Kunii, D. & Suzuki, M. 1966 Heat transfer between wall surface and packed solids. In *International Heat Transfer Conference IV*, pp. 344–352.

Lese, H.K. & Kermode, R.I. 1972 Heat transfer from a horizontal tube to a fluidized bed in the presence of unheated tubes. *Canadian Journal of Chemical Engineering* 50, 44–48.

Masoumifard, N., Mostoufi, N., Hamidi, A.A. & Sotudeh-Gharebagh, R. 2008 Investigation of heat transfer between a horizontal tube and gas-solid fluidized bed. *International Journal of Heat and Fluid Flow* 29, 1504–1511.

Mehling, H. & Cabeza, L.F. 2008 *Heat and cold storage with PCM*. Springer.

Mickley, H.S. & Fairbanks, D.F. 1955 Mechanism of heat transfer to fluidized beds. *American Institute of Chemical Engineers Journal* 2, 374–384.

Mickley, H.S. & Trilling, C.A. 1949 Heat transfer characteristics of fluidized beds. *Industrial and Engineering Chemistry* 41, 1135–1147.

Ozkaynak, T.F. & Chen, J.C. 1980 Emulsion phase residence time and its use in heat transfer models in fluidized beds. *American Institute of Chemical Engineers Journal* 26, 544–550.

Priebe, S.J. & Genetti, W.E. 1977 Heat transfer from a horizontal bundle of extended surface tubes to an air fluidized bed. *Chemical Engineering Progress Symposium Series* 73, 38–43.

Rady, M. 2009*a* Granular phase change materials for thermal energy storage: experiments and numerical simulations. *Applied Thermal Engineering* 29, 3149–3159.

Rady, M. 2009*b* Study of phase changing characteristics of granular composites using differential scanning calorimetry. *Energy Conversion and Management* 50, 1210–1217.

Regin, A.F., Solanki, S.C. & Saini, J.S 2009 An analysis of a packed bed latent heat thermal energy storage system using pcm capsules: Numerical investigation. *Renewable Energy* 34, 1765–1773.

Saxena, S.C., Grewal, N.S., Gabor, J.D., Zabrodsky, S.S. & Galershtein, D.M. 1979 Heat transfer between a gas fluidized bed and immersed tubes. *Advances in Heat Transfer*, vol. 14, pp. 149 – 247. Elsevier.

Talmatsky, E. & Kribus, A. 2008 Pcm storage for solar dhw: An unfulfilled promise? *Solar Energy* 82, 861 – 869.

Xavier, A.M. & Davidson, J.F 1985 *Fluidization*, chap. Heat transfer in fluidized beds. Academic Press, London.

Yagi, S. & Kunii, D. 1962 Studies on heat transfer in packed beds. *International Development in Heat Transfer.* Part IV, 750–759.

CHAPTER

SEVEN

Modeling the heat transfer coefficient between a surface and fixed and fluidized beds with PCM

The objective of this work is to model the heat transfer coefficient between an immersed surface and fixed and bubbling fluidized beds of granular phase change material (PCM). The model consists of a two-region model with two different voidages in which steady and transient conduction problems are solved for the fixed and fluidized bed cases, respectively. The model is validated with experimental data obtained under fixed and fluidized conditions for sand, a common material used in fixed and fluidized beds for sensible heat storage, and for a granular PCM with a phase change temperature of approximately 50°C. The superficial gas velocity is varied to quantify its influence on the convective heat transfer coefficient for both materials.

The model proposed for the PCM properly predicts the experimental results, except for high flow rates, which cause the contact times between the surface and particles to be very small and lead the model to over-predict the results.

7.1 Introduction

Extensive research has been conducted evaluating the convective heat transfer coefficient in fixed and fluidized beds (Botterill & Desai, 1972; Chen, 1976; Mickley & Trilling, 1949; Kubie & Broughton, 1975; Lu *et al.*, 1993; Zhang *et al.*, 2013; Yagi & Kunii, 1960; Kunii & Suzuki, 1966). In many industrial processes, it is necessary to cool or heat packed or fluidized beds, and this procedure is usually accomplished by the insertion of heat transfer tubes carrying cooling or heating fluids into the bed. The heat transfer occurs between the particle/gas medium and the submerged tube surface (often referred to as the walls). A

knowledge of basic mechanisms of heat transfer in beds with immersed heat exchange walls is crucial for producing an optimum design for these systems.

Several experimental and theoretical studies have determined effective thermal conductivities in packed beds. Kunii & Smith (1960) published a theoretical study on the effective thermal conductivities of porous media filled with a stationary fluid. They based their work on the heat transfer model for packed beds developed by Yagi & Kunii (1957). In this work, the authors presented a theoretical model for the effective thermal conductivity and compared it with experimental results from other studies. Yagi *et al.* (1960) derived an experimental correlation for the axial effective thermal conductivity in packed beds. Wakao & Kaguei (1982) provided a comprehensive review of the evaluation of the particle-to-fluid heat transfer coefficient. Ranz & Marshall (1952) correlated the Nusselt number of the particle-to-fluid heat transfer with other dimensionless numbers for packed beds consisting of both single and multiple particles. To encompass a broad spectrum of conditions and operations, Kunii & Levenspiel (1991*b*) developed a general equation for the heat transfer coefficient at the wall surfaces of gas-solid contactors.

In fluidized beds, the heat transfer coefficient of an immersed surface is several times greater than that for a single-phase gas convection exchanger (Chen, 2003). Mickley & Fairbanks (1955) proposed one of the first models, the so-called "packet theory", for the heat transfer coefficient between a fluidized bed and a surface. This model treated the heat transfer from surfaces to fluidized beds as the result of the non-steady-state conduction of particle packets at the bed temperature, assuming uniform physical properties. The model successfully explained the role played by the particles in heat transfer processes. However, the model did not account for the non-uniform porosity near the solid wall and predicted infinitely large values of the heat transfer coefficient when the particle contact time on the heat transfer surface decreased. This model was later improved and developed by considering an additional time-independent resistance near the walls (Baskakov, 1964; Patel, 1967). This additional resistance was treated either as a contact resistance or a gas film with a thickness of $0.1 - 0.33 d_p$ by Flamant & Menigault (1987). Kubie & Broughton (1975) adopted the packet theory but included a variable property boundary layer to take into account the variation of properties in the packet near the surface due to the porosity variation. Most models required a degree of empiricism to agree with experimental data.

The heat transfer process is thought to be governed by the residence time

of the emulsion phase (packets) on the heat transfer surface. Existing models in the literature suggest a constant decrease of particle-wall contact time with an increase in the gas velocity. Ozkaynak & Chen (1980) studied the emulsion phase residence time and its use in heat transfer models in fluidized beds for a centrally located vertical tube. They concluded that for any given fluidization state, the local residence time of the emulsion phase on the tube has a characteristic log normal distribution. Molerus *et al.* (1995) and Wang & Rhodes (2003) estimated a monotonically decreasing trend of particle-wall contact time upon increasing the gas velocity in all fluidization regimes. Hamidipour *et al.* (2005), however, experimentally investigated particle-wall contact and found that the particle-wall contact time in a bed of sand particles decreased with increasing gas velocity in the bubbling regime of fluidization, reached a minimum at the onset of turbulent fluidization, and thereafter increased. However, Zarghami *et al.* (2007) experimentally demonstrated that the contact time increased in the bubbling and turbulent regimes upon increasing the gas velocity.

One of the most efficient methods of heat recovery from packed and fluidized beds utilizes horizontally immersed tubes. Information regarding heat transfer to cylinders in a packed bed is sparse when applied to small cylinder sizes (i.e., 1-10 mm). Penny *et al.* (2010) examined heat transfer to cylinders immersed in packed beds in size ranges appropriate for steel wire heat-treating applications and developed an appropriate correlation and an empirical correlation that relates the Nusselt number to relevant physical variables, such as the particle and sample diameters, effective thermal conductivity, and fluid velocity. A number of experimental and numerical investigations have been reported on the measurement of the heat transfer rate between a horizontal tube and fluidized beds (Wood *et al.*, 1978; Vreedenberg, 1958; Chandran *et al.*, 1980; Doherty *et al.*, 1986; Grewal & Saxena, 1979; Lese & Kermode, 1972; Bartel & Genetti, 1973; Priebe & Genetti, 1977; Masoumifard *et al.*, 2008).

The heat transfer coefficient depends on several parameters of the system, such as the size and properties of bed particles, properties of the heat transfer surface (e.g., its geometry, surface finish and orientation within the bed) and the distributor design. Operating parameters, such as temperature, pressure, and fluidizing velocity, also influence the heat transfer process. Doherty *et al.* (1986) studied the heat transfer from immersed horizontal tubes of different diameters in gas-fluidized beds. For smooth horizontal tubes, the heat transfer coefficient h_w decreased as the tube diameter increased. This is explained based on the concept that solid particles remain in the vicinity of the heat transfer tube

longer as the diameter increases. They found that in all cases, h_w increases with increasing flow rate until a maximum and thereafter slowly decreases. Also they concluded that h_w decreased with increases in the solid particle diameter for the same fluidizing velocity. This trend is in agreement with reported findings in the literature (Grewal & Saxena, 1980, 1977; Grewal *et al.*, 1979; Botterill, 1975; Masoumifard *et al.*, 2008; Kim *et al.*, 2003). Recent investigations of the heat transfer between horizontally immersed tubes and fluidized beds have focused on larger tubes, i.e., $D_t > 2.5$ cm ((Khan & Turton, 1992; Karamavruc & Clark, 1996; Li *et al.*, 1993)). Few studies have investigated heat transfer from horizontal tubes in the size range of $1 - 8$ mm (Friedman *et al.*, 2006).

Several researchers have evaluated the use of phase-change materials (PCMs) for thermal storage (Rady, 2009; Regin *et al.*, 2009; Nallusamy *et al.*, 2006; Oró *et al.*, 2013) due to their ability to store a large amount of energy in a small volume. Trp (2005) worked on an experimental and numerical investigation of transient heat transfer phenomena during paraffin melting and solidification in a shell-and-tube latent thermal energy storage unit to provide guidelines for evaluating the system performance and for the design optimization. Experimental and theoretical studies have demonstrated that convection coefficients in fluidized beds are dependent on the energy storage capacity of fluidized particles (Ziegler *et al.*, 1964; Molerus, 1992; Brown & Overmann, 1998). For this reason, an encapsulated PCM in granular form is expected to enhance the heat transfer rate due to its ability to store large quantities of energy in latent form. Brown *et al.* (1998) evaluated several types of microencapsulated products as heat transfer media in fluidized beds and observed heat transfer enhancements of 30%.

In this work, heat transfer coefficients between an immersed horizontal surface and a fixed or fluidized bed with a granular PCM are modeled. The model is also valid for a conventional granular material without PCM. The model of the heat transfer coefficient for a fixed bed is developed according to Yagi & Kunii (1962), whereas the model of the heat transfer coefficient for a fluidized bed is developed according to Kunii & Levenspiel (1991*a*). The effective thermal conductivity is a common parameter for both models and is a key parameter in the proper prediction of the heat transfer coefficient. The calculation of this effective thermal conductivity is first attempted. Then, models for heat transfer coefficients in the fixed and fluidized beds are described. Finally, a comparison between the proposed models and experimental results is performed.

7.2 Model for h_w between a surface and a bed of particles

Schwartz & Smith (1953) indicated that the void fraction near the wall surface of a packed bed was larger than in the core of the bed; one particle has only one contact point with the wall surface. Yagi & Kunii (1960) concluded that the region of the bed where the voidage is affected by the presence of the wall is extended to a distance of $d_p/2$. Yagi & Kunii (1962) and Benenati & Brosilow (1962) observed that the voidage in a fixed bed remained constant beyond this distance with a typical value of $\varepsilon_b = 0.4$. Kubie & Broughton (1975) proposed a voidage profile near the surface where the voidage varied between 1 at the surface and 0.4 at $x = 0.5\,d_p$. Consequently, it might be reasonable to assume a heat transfer model in which two zones are differentiated by the voidage ε. This model is illustrated in Figure 7.1.

In the same manner, the effective thermal conductivity can be separated into two effective thermal conductivity terms: in the bed and in the region adjacent to the surface. Several correlations are proposed in the literature to determine the equivalent conductivity of a packed bed of particles (Kunii & Smith, 1960; Yagi & Kunii, 1957, 1962; Krupiezka, 1967; Vortmeyer & Adam, 1984; Elsari & Hughes, 2002; Gonzo, 2002; Wen & Ding, 2006). Among these models, equations of the model proposed by Kunii et al. (Kunii & Smith, 1960; Yagi & Kunii, 1957, 1962) were chosen. This model is based on the assumption that the total heat transfer through the bed of particles can be divided into two components that flow in parallel

$$\dot{Q} = \dot{Q}_g + \dot{Q}_s, \tag{7.1}$$

where $\dot{Q}_g$ is the fraction of the heat flux through the gas phase and $\dot{Q}_s$ is the fraction of the heat flux through the solid phase. The radiative heat transfer is neglected for low temperatures.

Figure 7.2 shows a scheme of the thermal circuit of the heat transfer model where

$$\dot{q}_g = \frac{\dot{Q}_g}{A} = -k_g\,\varepsilon_b\,\frac{\partial T}{\partial x} = k_g\,\varepsilon_b\frac{\Delta T}{\Delta x} \tag{7.2}$$

and

$$\dot{q}_s = \frac{\dot{Q}_s}{A} = k_s\,(1-\varepsilon_b)\,\frac{\Delta T_s}{l_s} = k_g\,(1-\varepsilon_b)\,\frac{\Delta T_c}{l_v}. \tag{7.3}$$

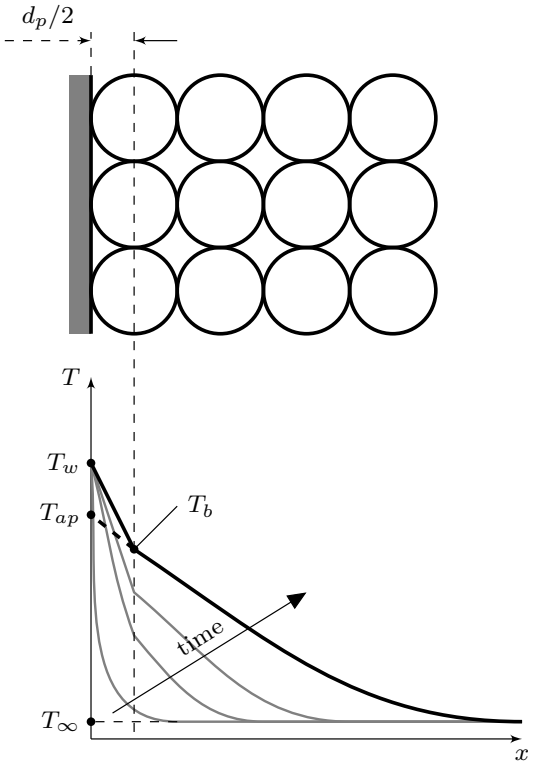

Figure 7.1: Temperature profile in a packed bed in the region near the wall, where T_w is the wall/surface temperature, T_b is the bed temperature at a distance $d_p/2$ from the surface, T_∞ is the bed temperature far from the wall and T_{ap} is the extrapolation of the temperature profile within the bed to $x = 0$ (apparent temperature).

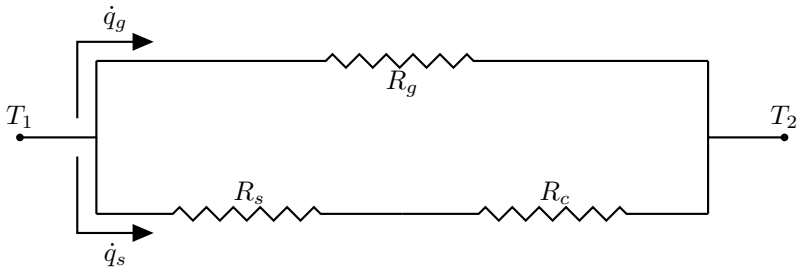

Figure 7.2: Equivalent thermal circuit of the heat transfer model through a bed of particles.

Here, k_s and k_g are thermal conductivities of the solid and gas phases, respectively, and ΔT is the temperature difference for each thermal resistance.

In Figure 7.2, R_g represents the equivalent resistance of the heat transferred through the gas phase, whereas R_s and R_c represent equivalent resistances for conduction through the solid phase and for conduction through the stagnant fluid near the contact points, respectively.

The resistances of the thermal circuit are obtained from Equations (7.2) and (7.3), yielding

$$R_g = \frac{\Delta x}{k_g\,\varepsilon_b}, \quad R_s = \frac{l_s}{k_s\,(1-\varepsilon_b)}, \quad R_c = \frac{l_v}{k_g\,(1-\varepsilon_b)}, \tag{7.4}$$

where Δx is the effective length between the center of two neighboring particles in the direction of the heat flow, l_s is the effective length of solid particles and l_v is the effective length of the fluid film near the stagnation point of two neighboring particles.

The equivalent resistance of the thermal circuit shown in Figure 7.2 is

$$R_{eq} = \frac{\Delta x}{k^0_{e,b}} = \left(\frac{1}{R_g} + \frac{1}{R_s + R_c}\right)^{-1}. \tag{7.5}$$

By introducing different resistances in the previous equation, an expression for the equivalent thermal conductivity of the bed with motionless fluid is obtained

$$\frac{k^0_{e,b}}{k_g} = \varepsilon_b + \frac{\beta_b\,(1-\varepsilon_b)}{\phi_b + \gamma_b \dfrac{1}{\kappa}}, \tag{7.6}$$

where $\kappa = k_s/k_g$, $\phi_b = l_v/d_p$, $\gamma_b = l_s/d_p$ and $\beta_b = \Delta x/d_p$ represent ratios

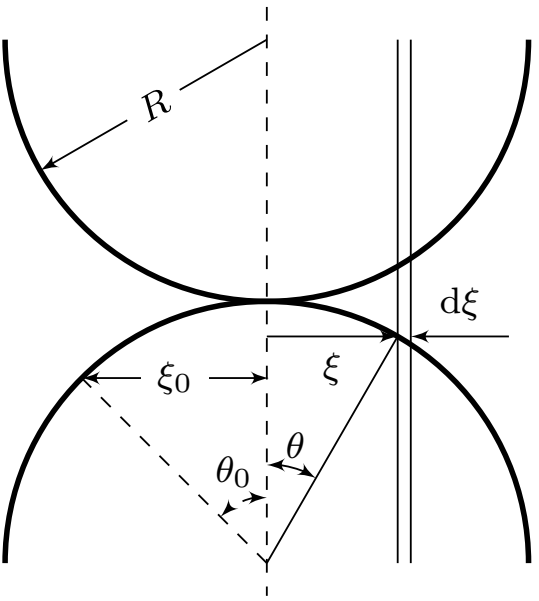

Figure 7.3: Scheme of two neighboring particles for determining $\dot{Q}_s$.

of distances between centers of adjacent particles to particle diameters, which, according to Kunii & Smith (1960), can be assumed to equal one.

The scheme of two neighboring particles is shown in Figure 7.3 where the area defined by the radius ξ_0 corresponds to the contact point between the two particles.

The heat flow through the solid phase is

$$\dot{Q}_s = \int_0^{\xi_0} \mathrm{d}\dot{Q}_s, \tag{7.7}$$

where

$$d\dot{Q}_s = 2\,\pi\,\xi\,d\xi \frac{\Delta T}{\frac{2\,R_p\,\cos\theta}{k_s} + \frac{2\,R_p\,(1-\cos\theta)}{k_g}}. \tag{7.8}$$

In Equation (7.8), the area defined by $\mathrm{d}\xi$ is $\mathrm{d}A = 2\,\pi\,\xi\,\mathrm{d}\xi$, ΔT is the temperature difference between the center of the two particles and $R_p = d_p/2$ is the particle radius. Taking into account that $\xi = R_b\,sin\theta$, the integration of Equation (7.8) yields

$$\dot{Q}_s = \pi\,R_b\,k_g\,\Delta T \left(\frac{\kappa}{\kappa-1}\right)^2 \left[\ln\left(\kappa-(\kappa-1)\cos\theta_0\right) - \frac{\kappa-1}{\kappa}\left(1-\cos\theta_0\right)\right]. \tag{7.9}$$

For the thermal model described in Figure 7.2, the heat flux through the solid phase can also be expressed as

$$\dot{Q}_s = \frac{\pi \left(R_b \sin\theta_0\right)^2 \Delta T}{\frac{l_s}{k_s} + \frac{l_v}{k_g}}. \tag{7.10}$$

To solve the system of Equations (7.9) and (7.10), where there are 3 unknowns, (l_s, l_v and $\dot{Q}_s$), the procedure of Kunii & Smith (1960) is followed. Kunii & Smith (1960) assumed that l_s was the length of a cylinder with the same volume as one particle; therefore, $\gamma = 2/3$ and $l_s = (2/3)d_p$. The expression for ϕ_b is (Kunii & Smith, 1960)

$$\phi_b = \frac{l_v}{d_p} = \frac{1}{2}\left(\frac{\kappa-1}{\kappa}\right)^2 \frac{\sin^2\theta_0}{\ln\left(\kappa-(\kappa-1)\cos\theta_0\right) - \frac{\kappa-1}{\kappa}\left(1-\cos\theta_0\right)} - \frac{2}{3}\frac{1}{\kappa}. \tag{7.11}$$

Equation (7.11) is represented in Figure 7.5(a) as a dashed line. For values of κ less than 10^{-1}, i.e., for thermal conductivities of the particles less than that of the gas, Equation (7.11) predicts very high values of ϕ_b. Equivalent lengths l_v of hundreds (or even thousands) of factors of the particle diameter are not physically realistic.

Instead of considering the length l_s equal to the length of one cylinder with the same volume of the particle (Kunii & Smith, 1960), it seems more reasonable to assume that the sum of both lengths, l_s and l_v, is equal to the particle diameter. With this approach, a new model to determine the two lengths l_s and l_v is presented, where

$$l_v + l_s = d_p \tag{7.12}$$

and thus,

$$\phi_b + \gamma_b = 1. \tag{7.13}$$

Under these statements and following a similar line of reasoning as Kunii & Smith (1960), a new expression for ϕ_b is obtained

$$\phi_b = \frac{l_v}{d_p} = \frac{1}{2}\left(\frac{\kappa-1}{\kappa}\right) \frac{\sin^2\theta_0}{\ln\left(\kappa-(\kappa-1)\cos\theta_0\right) - \frac{\kappa-1}{\kappa}\left(1-\cos\theta_0\right)} - \frac{1}{\kappa-1}. \tag{7.14}$$

This expression is plotted in Figure 7.5(b). In this case, the value of ϕ_b is less than one, i.e., $l_v < d_p$, for any value of κ.

To obtain the required ϕ_b, the angle θ_0 must be determined. This angle is related to the number of contact points n between two neighboring particles and follows the expression (Kunii & Smith, 1960)

$$\sin^2\theta_0 = \frac{1}{n}. \tag{7.15}$$

To estimate n, two particle arrangements should be considered: one for the most open packing and one for close packing (Kunii & Smith, 1960). It was assumed that actual packed beds with particle size distributions may be composites of both packing states. Thus, the correct value for ϕ_b is an additive function between ϕ_1 and ϕ_2

$$\phi_b = \phi_2 + (\phi_1 - \phi_2)\,\frac{\varepsilon_b - \varepsilon_2}{\varepsilon_1 - \varepsilon_2}, \tag{7.16}$$

where ϕ_1 is obtained for the less packed bed with $n_1 = 1.5$; $\varepsilon_1 = 1 - \pi/6$ and ϕ_2 are obtained for the close packed bed with $n_2 = 4\sqrt{3}$; and $\varepsilon_2 = 1 - \sqrt{2}\,\pi/6$.

To obtain the equivalent thermal conductivity in the region adjacent to the heat transfer surface, a similar line of reasoning as that used for Equation (7.6) is followed, which yields

$$\frac{k^0_{e,w}}{k_g} = \varepsilon_w + \frac{\beta_w\,(1-\varepsilon_w)}{\phi_w + \gamma_w\,\dfrac{1}{\kappa}}, \tag{7.17}$$

where the subscript w indicates that all variables are evaluated in the region adjacent to the wall surface. As stated in Yagi & Kunii (1962), the region of the bed where the voidage is affected by the presence of the wall is extended to a distance of $d_p/2$. As a consequence, for a thickness of $d_p/2$, $\beta_w = 1/2$.

The heat flux through the particles near the wall surface can be calculated following a similar line of reasoning. When the particles touch the surface, it is assumed that the angle θ_0, which defines the region of contact, is equal to $\pi/2$, i.e., $\xi_0 = d_p/2$, and extends to a region of length $d_p/2$ (see Figure 7.4).

Given these premises, then

$$\begin{aligned}\dot{Q}_s =& \int_0^{\xi_0} 2\,\pi\,\xi\,d\xi \frac{\Delta T}{\dfrac{R_p\,\cos\theta}{k_s} + \dfrac{R_p\,(1-\cos\theta)}{k_g}} \\ =& \pi\,d_p\,k_g\,\Delta T \left(\frac{\kappa}{\kappa-1}\right)^2 \left[\ln\kappa - \frac{\kappa-1}{\kappa}\right].\end{aligned} \tag{7.18}$$

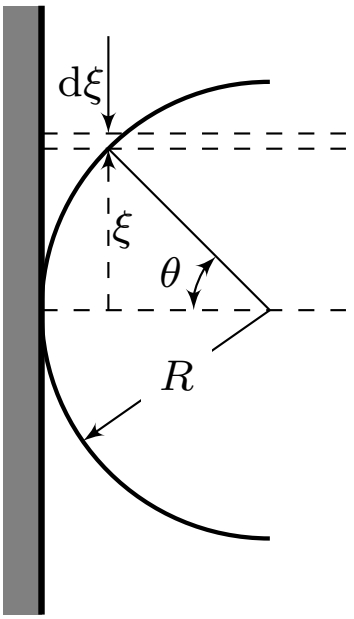

Figure 7.4: Scheme for determining $\dot{Q}_s$ at the wall surface.

The heat flux can also be expressed as

$$\dot{Q}_s = \frac{\frac{\pi}{4} d_p^2 \, \Delta T}{\frac{l_{s,w}}{k_s} + \frac{l_{v,w}}{k_g}}, \tag{7.19}$$

where $l_{s,w}$ and $l_{v,w}$ are the effective length of solid particles and the fluid film at the wall surface, respectively.

Combining Equations (7.18) and (7.19), the expression of ϕ_w is

$$\phi_w = \frac{l_{v,w}}{d_p} = \frac{1}{4} \left(\frac{\kappa - 1}{\kappa} \right)^2 \frac{1}{\ln \kappa - \frac{\kappa - 1}{\kappa}} - \frac{1}{3} \frac{1}{\kappa}. \tag{7.20}$$

Figure 7.5(a) shows the variation of ϕ_w with κ according to the previous equation. For values of κ less than 10^{-1}, Equation (7.20) results in negative values, which are physically unrealistic.

As before, an alternative model for determining the two lengths $l_{s,w}$ and $l_{v,w}$ is applied

$$l_{s,w} + l_{v,w} = \Delta x_w = d_p/2, \tag{7.21}$$

and thus,

$$\gamma_w + \phi_w = \beta_w = 1/2. \tag{7.22}$$

Equation (7.21) indicates that the lengths of the two branches of the thermal circuit shown in Figure 7.2 are equal to half of one diameter, which is the distance from the surface where a different voidage is assumed.

Thus, the expression of ϕ_w is

$$\phi_w = \frac{l_{v,w}}{d_p} = \frac{1}{4}\left(\frac{\kappa-1}{\kappa}\right)\frac{1}{\ln\kappa - \dfrac{\kappa-1}{\kappa}} - \frac{1}{2\,(\kappa-1)}. \tag{7.23}$$

Figure 7.5 shows variations of ϕ_b and ϕ_w with κ for the two models. The original equations proposed by Yagi & Kunii (1957, 1962), with $\gamma_b = 2/3$ and $\gamma_{b,w} = 1/3$, predict values greater than one or negative for $\phi_{b,w}$, which is physically unrealistic. For the model, we propose that these values are less than one, i.e., l_v and $l_{v,w}$ are less than the particle diameter.

7.2.1 Fixed Bed

As stated by Yagi & Kunii (1960), the convective heat transfer coefficient between a wall surface and a packed bed h_w can be expressed as

$$\frac{h_w\, d_p}{k_g} = \frac{h_w^0\, d_p}{k_g} + a_w\, Re\, Pr, \tag{7.24}$$

where k_g is the thermal conductivity of the gas, h_w^0 is the wall film coefficient with a motionless fluid and Re and Pr are the Reynolds and Prandtl numbers, respectively. The parameter a_w depends on flow conditions, the Reynolds number and particle sizes; its value varies, depending on the material and experimental conditions.

It is assumed that particles in contact with the wall surface are surrounded by stagnant, motionless fluid (Yagi & Kunii, 1962).

According to Yagi & Kunii (1962), the heat transfer coefficient between a surface and a packed bed with a stagnant fluid h_w^0 can be obtained

$$-k_{e,w}^0 \left.\frac{\partial T}{\partial x}\right|_{x=0} = -k_{e,b}^0 \left.\frac{\partial T}{\partial x}\right|_b = h_w^0\,(T_w - T_{ap})\,, \tag{7.25}$$

where $k_{e,w}^0$ and $k_{e,b}^0$ are the aforementioned equivalent thermal conductivities (i.e., Equations (7.6) and (7.17), respectively), T_w is the wall temperature, T_{ap} is the extrapolation of the temperature profile within the bed to $x = 0$ (i.e.,

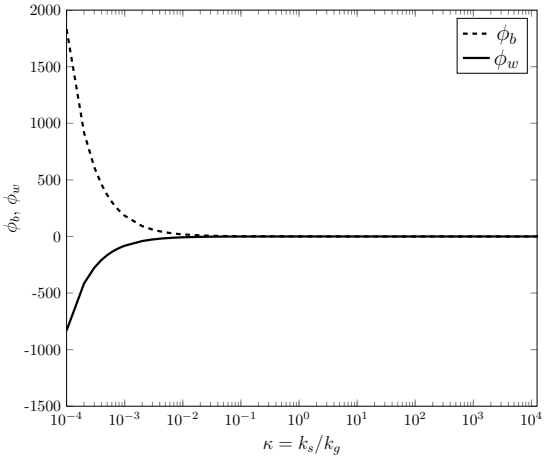

(a) Kunii & Smith (1960)

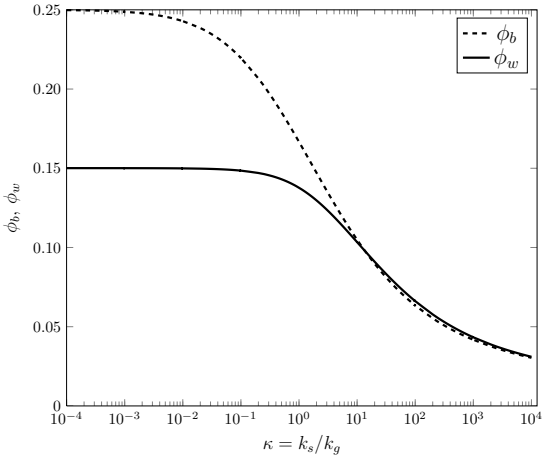

(b) Proposed model

Figure 7.5: Graphical representation of ϕ_b and ϕ_w for two models and different values of κ. The data for ϕ_b are calculated for $\varepsilon_b = 0.4$.

the apparent temperature), $\partial T/\partial x|_{x=0}$ represents the temperature slope in the region close to the surface ($x < d_p/2$) and $\partial T/\partial x|_b$ represents the variation of the temperature in the bed, far from the influence of the heat transfer surface.

From Figure 7.1, partial derivatives of Equation (7.25) can be computed as follows

$$k^0_{e,w}\,\frac{T_w - T_b}{d_p/2} = k^0_{e,b}\,\frac{T_{ap} - T_b}{d_p/2} = h^0_w\,(T_w - T_{ap})\,. \tag{7.26}$$

Solving the system, the expression obtained is

$$\frac{2}{\dfrac{d_p\,h^0_w}{k_g}} = \frac{1}{\dfrac{k^0_{e,w}}{k_g}} + \frac{1}{\dfrac{k^0_{e,b}}{k_g}}. \tag{7.27}$$

Equation (7.27) calculates h^0_w if the equivalent thermal conductivity in the bed $k^0_{e,b}$ and the equivalent thermal conductivity near the wall surface $k^0_{e,w}$ are known. The model can be used whether the granular material contains PCM or not.

7.2.2 Fluidized Bed

The classical concepts of two phases (i.e., emulsion and bubble) and packet renewal ((Mickley & Fairbanks, 1955)) are used in this model because the model is considered a bubbling gas-solid fluidized bed for type B particles (according to the Geldart classification system (Geldart, 1973)). In this way, the average heat transfer coefficient between an immersed surface and fluidized particles can be expressed as (Grace *et al.*, 2006)

$$h_w = \delta\,\bar{h}_g + (1-\delta)\,\bar{h}_s, \tag{7.28}$$

where δ is the bubble fraction at the wall location and $\bar{h}_g$ and $\bar{h}_s$ account for the convection for the period when the surface is bathed by bubbles and for the period when the surface is bathed by emulsion packets, respectively. Radiation contributions are neglected due to low temperatures.

The convective component $\bar{h}_g$ can be obtained from Baskakov *et al.* (1973)

$$\bar{h}_g = 0.009\frac{k_g}{d_p}Ar^{0.5}Pr^{0.33}, \tag{7.29}$$

where Ar is the Archimedes number. This correlation has been accepted by many researchers as a good estimation of the gas convective coefficient over a wide range of fluidizing conditions (Glicksman & Decker, 1980; Modrak, 1979).

When a group of particles touches a heated surface, a transient heat transfer occurs between the surface at T_s and the group of particles that are initially at the temperature of the bed T_b. The group of particles, following the model of heat transfer through packed beds presented earlier, can be studied as a two-region model. One region has a thickness $d_p/2$ and a voidage ε_w adjacent to the surface; a second region exists at a distance larger than $d_p/2$ from the surface and has a voidage ε_b. Therefore, to determine the heat transferred from the surface to the dense phase, a one-dimensional conduction problem through two regions with different properties has to be solved (see gray-profiles in Figure 7.1). The equation to solve is

$$\frac{\partial T}{\partial t} = \alpha \frac{\partial^2 T}{\partial x^2}, \tag{7.30}$$

where T is the temperature and α is the equivalent thermal diffusivity, which is equal to

$$\alpha_{x \leq d_p/2} = \frac{k^0_{e,w}}{(\rho\, c_p)_w}, \tag{7.31}$$

$$\alpha_{x > d_p/2} = \frac{k^0_{e,b}}{(\rho\, c_p)_b}. \tag{7.32}$$

Variables with the subscript w are evaluated with ε_w, and variables with the subscript b are evaluated with ε_b. Under typical fluidization conditions with air, the volumetric heat capacities of solids are several orders of magnitude larger than that of air, such that their expressions can be approximated as

$$(\rho\, c_p)_w \approx (1-\varepsilon_w)\ (\rho\, c_p)_s, \tag{7.33}$$

$$(\rho\, c_p)_b \approx (1-\varepsilon_b)\ (\rho\, c_p)_s. \tag{7.34}$$

Kubie & Broughton (1975) identified the equivalent thermal conductivity as the greatest source of error. Determining this parameter incorrectly causes the model to systematically over or under-predict experimental results for different flow conditions.

To solve Equation (7.30), it is convenient to introduce a change of variable

$$\eta = \frac{x}{2\sqrt{\alpha\, t}}, \tag{7.35}$$

which transforms the partial differential equation (7.30) into an ordinary differential equation

$$\frac{\mathrm{d}^2 T}{\mathrm{d}\eta^2} = -2\,\eta \frac{\mathrm{d}T}{\mathrm{d}\eta}. \tag{7.36}$$

The solution of this equation is in the form (Nellis & Klein, 2009)

$$T_{x\leq d_p/2} = C_1 \frac{\sqrt{\pi}}{2} \operatorname{erf}(\eta_w) + C_2, \tag{7.37}$$

$$T_{x>d_p/2} = C_3 \frac{\sqrt{\pi}}{2} \operatorname{erf}(\eta_b) + C_4, \tag{7.38}$$

where η_w and η_b are variables defined in Equation (7.35) evaluated near and far from the surface, respectively. Boundary conditions necessary to obtain constants $C_{i=1\ldots4}$ and their values are presented in Appendix A.

The instantaneous heat transfer coefficient on the surface when the solids are in contact can be determined as

$$-k_w \left.\frac{\partial T}{\partial x}\right|_{x=0} = h_s \left(T_w - T_\infty\right). \tag{7.39}$$

By introducing the derivative of the temperature profile in the above Equation (7.37), an expression for the instantaneous heat transfer coefficient is obtained

$$h_s = \frac{-A\, k_w}{\sqrt{\pi\, \alpha_w\, t}\left[\operatorname{erf}\left(\eta_{b_{x=d_p/2}}\right) - \operatorname{erf}\left(\eta_{w_{x=d_p/2}}\right) A - 1\right]}, \tag{7.40}$$

where erf is the error function and

$$A = \frac{k_b}{k_w}\sqrt{\frac{\alpha_w}{\alpha_b}} \exp\left(\operatorname{erf}\left(\eta_{b_{x=d_p/2}}\right) - \operatorname{erf}\left(\eta_{w_{x=d_p/2}}\right)\right) \tag{7.41}$$

is a function that varies with time. The average heat transfer coefficient during the time t_s that solids are in contact with the surface is expressed as

$$\bar{h}_s = \frac{1}{t_s}\int_0^{t_s} h_s(t)\, \mathrm{d}t, \tag{7.42}$$

which has to be computed numerically. The time t_s can be estimated as

$$t_s = \frac{1-\delta}{f_w}, \tag{7.43}$$

where f_w is the bubble frequency at the height of the surface. Small variations in the contact times strongly affect mean values of the heat transfer coefficient. Most correlations found in the literature for the contact time of a packet with a surface refer to vertical walls. The bubbling frequency inside the bed is larger than that in a vertical wall, so the time t_s is smaller. In this way, the correlation proposed by Lu *et al.* (1993) has been used to calculate contact times with 0.1 s subtracted from their expressions.

The numerical integration of Equation (7.42) is not easy to compute because h_s approaches infinity as the time approaches zero. An alternative approach to compute $\overline{h}_s$ is to define the instantaneous Nusselt number

$$Nu_s = \frac{h_s\sqrt{\pi\,\alpha_w\,t}}{k_w}, \tag{7.44}$$

where $\sqrt{\pi\,\alpha_w\,t}$ is the characteristic length of the problem. Hence, the average Nusselt number is

$$\overline{Nu}_s = \frac{\bar{h}_s\sqrt{\pi\,\alpha_w\,t_s}}{k_w}. \tag{7.45}$$

From Equation (7.42), the average Nusselt number can be expressed as

$$\overline{Nu}_s = \frac{1}{t_s}\int_0^{t_s}\frac{\sqrt{\pi\,\alpha_w\,t_s}}{k_w}h_s(t)\,\mathrm{d}t. \tag{7.46}$$

Introducing the change of variable

$$\beta = \sqrt{\pi\,\alpha_w\,t}, \tag{7.47}$$

the average Nusselt number can be computed as

$$\overline{Nu}_s = \frac{2}{\beta_s}\int_0^{\beta_s} Nu_s(t)\,\mathrm{d}\beta, \tag{7.48}$$

where the integral

$$\int_0^{\sqrt{\pi\,\alpha_w\,t_s}} Nu_s(t)\,\mathrm{d}\beta = \int_0^{\sqrt{\pi\,\alpha_w\,t_s}} \frac{-A}{\left[\mathrm{erf}\left(\eta_{b_{x=d_p/2}}\right) - \mathrm{erf}\left(\eta_{w_{x=d_p/2}}\right)A - 1\right]}\,\mathrm{d}\beta \tag{7.49}$$

is easier to compute numerically as Nu_s approaches one and $\overline{Nu}_s$ approaches two as time approaches zero. Once the average Nusselt number is obtained, the average heat transfer coefficient $\bar{h}_s$ can be obtained from Equation (7.45).

Figure 7.6(a) shows the instantaneous and mean heat transfer coefficients calculated using the theoretical model for the sand as a function of the flow rate. Figure 7.6(b) presents corresponding contact times for the same flow rates. The higher the flow rate, the greater the heat transfer coefficient and the quicker the contact time.

7.2.3 Fluidized bed with granular material with PCM

If the solid phase is filled with a PCM, the governing equation of the heat transfer process is

$$\frac{\partial i_s}{\partial t} = \frac{k}{\rho}\frac{\partial^2 T}{\partial x^2}, \tag{7.50}$$

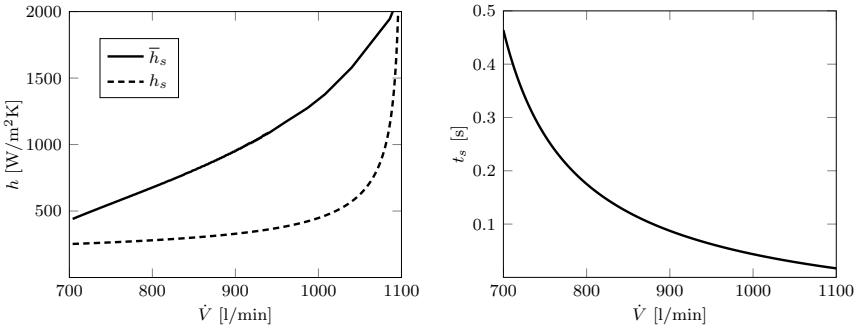

(a) (b)

Figure 7.6: (a) Evolution of the mean $\overline{h}_s$ and instantaneous h_s heat transfer coefficient for the sand as a function of the flow rate. (b) Corresponding contact times for the flow rate.

where $k = k^0_{e,w}$ and $\rho = \rho_w$ if $x \leq d_p/2$ and $k = k^0_{e,b}$ and $\rho = \rho_b$ if $x > d_p/2$. This equation has an analytical solution if the phase change process occurs at constant temperature. Solutions for different geometries can be found in Mehling & Cabeza (2008). If the phase change takes place over a range of temperatures, the equation should be solved numerically. Indeed, because the phase change occurs over a temperature range, the equation is numerically solved using an explicit finite difference scheme. A uniform spatial step of $\Delta x = 25$ μm and a time step of $\Delta t = 6.5 \cdot 10^{-5}$ s are used. Once the non-steady-state problem is solved, the heat transfer coefficient can be computed according to Equation (7.39), and the mean value over the time t_s can be found by Equation (7.42).

The heat transfer coefficients obtained through the model for the PCM as a function of the flow are depicted in Figure 7.7(a), and corresponding contact times for each flow are also shown in Figure 7.7(b).

7.3 Comparison of the model with experimental results

The experiments carried out by Izquierdo-Barrientos *et al.* (2014) and described in Chapter 6 for the commercial PCM GR50 Rubitherm® and the sand are used to validate the proposed model. The PCM is available in two particle sizes. A

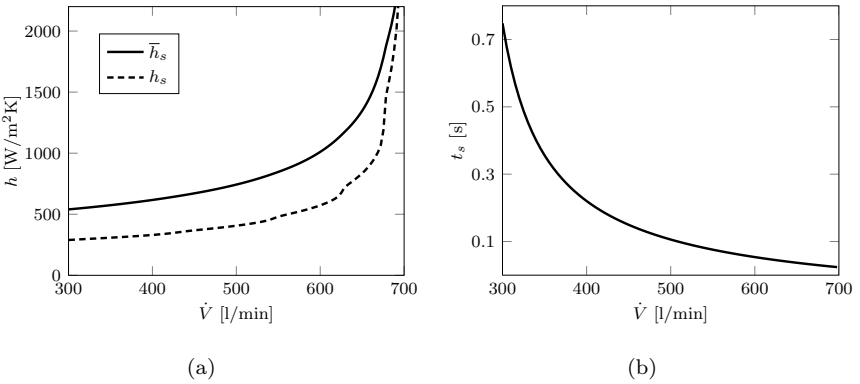

(a) (b)

Figure 7.7: (a) Evolution of the mean $\overline{h}_s$ and instantaneous h_s heat transfer coefficient for the PCM as a function of the flow rate. (b) Corresponding contact times for the flow rate.

coarser size is used in the fixed bed because its minimum fluidization is above the 1000 l/min flow rate; a finer size is used in the fluidized bed.

7.3.1 Fixed bed

Figure 7.8 displays the experimental results from Chapter 6 and the model results for the sand and the PCM in the packed bed. The experimental data for the heat transfer coefficient are plotted in the form of the Nusselt number, $Nu = (h_w \cdot d_p)/k_g$, as a function of the product between the Reynolds and Prandtl numbers, using Equation (7.24). The slope of the linear regression corresponds to the parameter a_w. For $a_w = 0.29$ for the sand and $a_w = 0.25$ for the PCM, the model reasonably predicts the value of Nusselt number and therefore, the heat transfer coefficient. The stagnant fluid model result for the Nusselt number, $Nu^0 = (h_w^0 \cdot d_p)/k_g$, obtained by Equation (7.27), yields 4.18 for the PCM and 4.20 for the sand, which agrees with the experimental results (see Figure 7.8). The wall surface used in experiments is a small-diameter cylindrical wall (see Figure 6.3). A larger voidage at the wall is expected due to the curved profile of the probe and the small ratio between the probe and particle diameter, D_t/d_p. Therefore, the voidage affected by the presence of the wall is $\varepsilon_w = 0.9$.

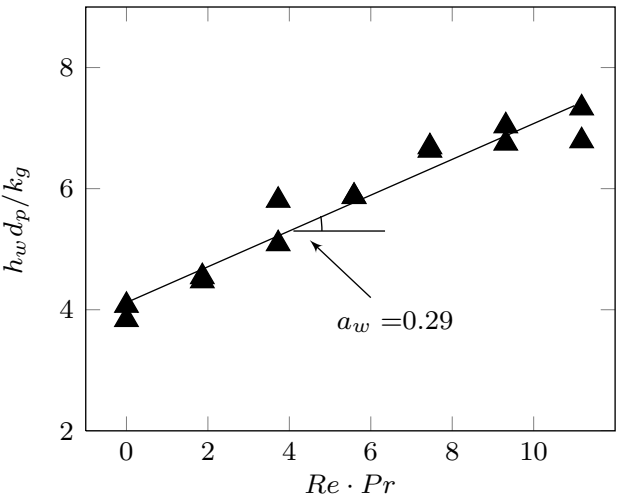

(a) Sand

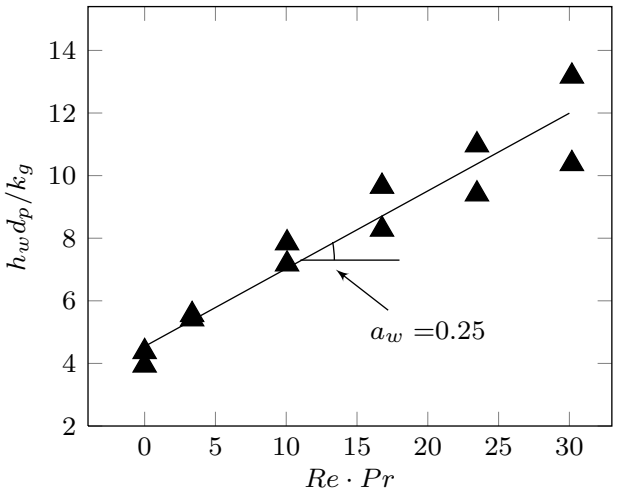

(b) PCM

Figure 7.8: Evolution of the Nusselt number for (a) the sand and (b) the PCM in the fixed bed as a function of the product between the Reynolds and Prandtl numbers. Continuous lines are the results for the theoretical model with $a_w = 0.29$ for the sand and $a_w = 0.25$ for the PCM. $\varepsilon_w = 0.9$

7.3.2 Fluidized bed

Figure 7.9(a) shows the total heat transfer coefficients obtained for the sand from the experiments detailed in Chapter 6 and from the model of a fluidized bed. The minimum fluidization velocity of the sand, U_{mf}, is 0.33 m/s, which corresponds to 622 l/min. Therefore, all selected flow rates are above this value. As observed for the fixed bed case, the heat transfer coefficient increases when the flow rate increases. The proposed model predicts trends similar to the results observed in the experiments, with approximately constant differences. These differences can be attributed to uncertainties in the value of the equivalent thermal conductivity (Kubie & Broughton, 1975). Kubie & Broughton (1975) observed similar differences in their experimental data.

Figure 7.9(b) displays the total heat transfer coefficients obtained from the experiments and from the model for the PCM. In the case of the PCM, the minimum fluidization velocity is $U_{mf} = 0.13$ m/s, which corresponds to a flow rate of 250 l/min. The selected flow rates for the PCM experiments are above 250 l/min. The model is observed to fit the experimental data for nearly all selected flow rates. At higher flow rates, the model does over-predict the transfer coefficients. At these higher rates, the smaller contact times do not allow the PCM to complete its phase change. For instance, for a flow rate of 500 l/min, the contact time for the granular PCM is approximately 0.1 s (see Figure 7.7(b)). The corresponding characteristic length for this contact times is $\sqrt{\pi\,\alpha_w\,t} \simeq d_p/2$ which means that the heat conduction do not penetrate the whole particle, thus, the granulate does not completely melt.

7.4 Conclusions

The proposed model for the heat transfer coefficient in packed beds was validated with experiments carried out with sand and a PCM. The potential benefit of the phase change of the PCM is limited because there is no observed change to the liquid PCM particles touching the heat transfer surface.

The model of the heat transfer coefficient in a fluidized bed properly predicts the trend of h_w when the sand and the PCM are fluidized. Only for very short contact times between the PCM and the wall surface does the model over-predict heat transfer coefficients. Small deviations of the model prediction for the sand may be due to uncertainties in parameters introduced in the model, such as the equivalent thermal conductivity (Kubie & Broughton, 1975).

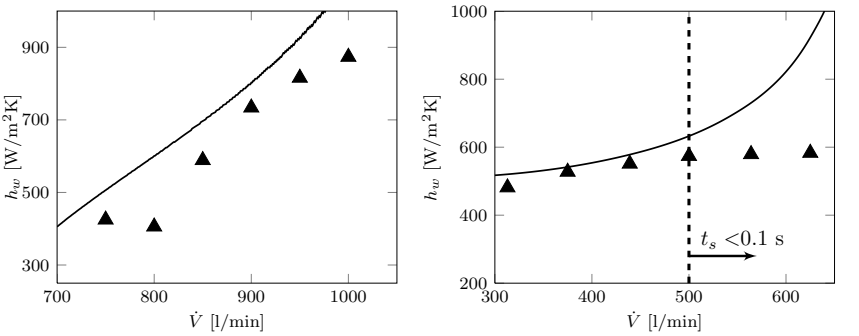

(a) Sand (b) PCM

Figure 7.9: Total heat transfer coefficient h_w calculated through the model (continuous line) and the experiments (isolated triangles) as a function of the flow for (a) the sand and (b) the PCM GR50.

When comparing heat transfer coefficients for fixed and fluidized beds, the heat transfer coefficient in the fluidized bed is nearly three times larger than that for the fixed bed.

Notation

A	heat transfer area [m^2]
Ar	Archimedes number [-]
a_w	parameter that depends on experimental conditions [-]
c_p	specific heat [J·kg^{-1}·K^{-1}]
D_t	heat transfer probe diameter [m]
d_p	particle diameter [m]
H	height of the bed [m]
$\overline{h}$	mean heat transfer coefficient [W·m^{-2}·K^{-1}]
h_w	convective heat transfer coefficient from the bed to the inner surface of the bed [W·m^{-2}·K^{-1}]
i	enthalpy [J]
k	thermal conductivity [W·m^{-1}·K^{-1}]
l_s	effective length of the solid particles [m]
l_v	effective length of the fluid film near the stagnation point of two neighboring particles [m]
m	mass [kg]

n	number of contact points between two neighboring particles [-]
f_w	bubble frequency at the height of the surface [s^{-1}]
Nu	Nusselt number [-]
Pr	Prandtl number [-]
$\dot{Q}$	heat flux [W]
$\dot{q}$	heat flux per area [$W \cdot m^{-2}$]
q	power of the resistance probe [W]
R	radius of the particle [m]
R_p	particle radius [m]
Re	Reynolds number [-]
R	equivalent resistance of the heat transferred [$m^3 \cdot K \cdot W^{-1}$]
T	temperature [°C]
t	time [s]
t_s	time the solids are in contact with the surface [s]
U_{mf}	minimum fluidization velocity [$m \cdot s^{-1}$]
$\dot{V}$	flow rate [$m^3 \cdot s^{-1}$]

Greek symbols

α	thermal diffusivity [$m^2 \cdot s^{-1}$]
β	ratio of the distance between the center of two adjacent particles to the particle diameter [m]
ρ	density [$kg \cdot m^{-3}$]
σ_{dp}	standard deviation of the mean particle diameter [m]
θ	angle [rad]
ξ	$R \sin \theta$
ε	voidage [-]
δ	bubble fraction at the wall location [-]
ΔT	temperature difference [K]
Δx	effective length between the center of two neighboring particles [m]
κ	$= k_s/k_g$
ϕ	$= l_v/d_p$
γ	$= l_s/d_p$
η	$= x/(2\sqrt{\alpha\, t})$

Subscripts

0	ambient/initial
ap	apparent
b	bed

c	contact point
e	effective/equivalent
exp	experiments
g	gas phase
pc	phase change
s	solid phase
w	wall
∞	far from the surface wall

Superscripts

0	motionless fluid

Appendix A

In this appendix, the boundary conditions necessary to obtain constants $C_{i=1\ldots4}$ in Equations (7.37) and (7.38) are explained. The boundary conditions consist of a fixed temperature at the wall surface and continuity in the temperature and its first derivative at the interface between both mediums. Additionally, at locations far away from the heat transfer surface, the temperature of the solid phase should be equal to the initial temperature. In this manner, the boundary conditions are:

- boundary condition at $x = 0$

$$T|_{x=0} = T_w \tag{7.51}$$

- first boundary condition at $x = d_p/2$

$$T|_{x=d_p/2^-} = T|_{x=d_p/2^+} \tag{7.52}$$

- second boundary condition at $x = d_p/2$

$$\dot{q}_{x=d_p/2} = -k_w \left.\frac{\partial T}{\partial x}\right|_{x=d_p/2^-} = -k_b \left.\frac{\partial T}{\partial x}\right|_{x=d_p/2^+} \tag{7.53}$$

- boundary condition at $x \to \infty$

$$\lim_{x\to\infty} T = T_\infty. \tag{7.54}$$

Introducing these boundary conditions into Equations (7.37) and (7.38), and after some manipulation, the constants are:

$$C_1 = \frac{2}{\sqrt{\pi}} A \frac{T_w - T_\infty}{\text{erf}\left(\eta_{mf_{x=d_p/2}}\right) - \text{erf}\left(\eta_{w_{x=d_p/2}}\right) A - 1} \tag{7.55}$$

$$C_2 = T_w \tag{7.56}$$

$$C_3 = \frac{2}{\sqrt{\pi}} \frac{T_w - T_\infty}{\text{erf}\left(\eta_{mf_{x=d_p/2}}\right) - \text{erf}\left(\eta_{w_{x=d_p/2}}\right) A - 1} \tag{7.57}$$

$$C_4 = T_\infty - \frac{T_w - T_\infty}{\text{erf}\left(\eta_{mf_{x=d_p/2}}\right) - \text{erf}\left(\eta_{w_{x=d_p/2}}\right) A - 1}. \tag{7.58}$$

References

Bartel, W.J. & Genetti, W.E. 1973 Heat transfer from a horizontal bundle of bare and finned tubes in an air fluidized bed. *Chemical engineering progress symposium series* 69, 85–93.

Baskakov, A.P. 1964 The mechanism of heat transfer between a fluidized bed and a surface. *International Chemical Engineering* 4, 320–324.

Baskakov, A.P., Berg, B.V., Vitt, O.K., Filippovsky, N.F., Hirakosyan, V.A., Goldobin, J.M. & Maskaev, V.K. 1973 Heat transfer to objects immersed in fluidized beds. *Powder Technology* 8, 273–282.

Benenati, R.F. & Brosilow, C.B. 1962 Void fraction distribution in beds of spheres. *American Institute of Chemical Engineers Journal* 8, 359–361.

Botterill, J.S.M. 1975 *Fluid-Bed Heat Transfer*. Academic Press, New York.

Botterill, J.S.M. & Desai, M. 1972 Limiting factor in gas-fluidized bed heat transfer. *Powder Technology* 6, 231–238.

Brown, R.C. & Overmann, S.P. 1998 The influence of particle thermal time constants on convection coefficients in bubbling fluidized beds. *Powder Technology* 98, 13–20.

Brown, R.C., Rasberry, J.D. & Overmann, S.P. 1998 Microencapsulated phase-change materials as heat transfer media in gas fluidized beds. *Powder Technology* 98, 217–222.

Chandran, R., Chen, J.C. & Staub, F.W. 1980 Local heat transfer coefficient around horizontal tubes in fluidized beds. *American Institute of Chemical Engineers Journal* 102, 152–157.

Chen, J.C. 1976 Heat transfer to tubes in fluidized bed. In *National Heat Transfer Conference*. St. Louis MO.

Chen, J.C. 2003 *Handbook of fluidization and fluid-particle systems*, chap. Heat Transfer. Taylor & Francis Group LLC.

Doherty, J.A., Verma, R.S., Shrivastava, S. & Saxena, S.C. 1986 Heat transfer from immersed horizontal tubes of different diameter in a gas fluidized bed. *Energy* 11, 773–783.

Elsari, M. & Hughes, R. 2002 Axial effective thermal conductivities of packed beds. *Applied Thermal Engineering* 22, 1969–1980.

Flamant, G. & Menigault 1987 Combined wall-to-fluidized bed heat transfer. bubble and emulsion contributions at high temperature. *International Journal Heat Mass Transfer* 30, 1803–1812.

Friedman, J, Koundakjian, P., Naylor, D. & Rosero, D. 2006 Heat transfer to small horizontal cylinders immersed in a fluidized bed. *Transactions of the ASME, Journal Heat Transfer* 128, 984–988.

Geldart, D. 1973 Types of gas fluidization. *Powder Technology* 7, 285–292.

Glicksman, L.R. & Decker, N.A. 1980 Design relationships for predicting heat transfer to tube bundles in fluidized bed combustion. In *Proceedings of the Sixth Annual International Conference on Fluidized Bed Combustors*, , vol. III, p. 152. Atlanta.

Gonzo, E.E. 2002 Estimating correlation for the effective thermal conductivity of granular materials. *Chemical Engineering Journal* 90, 299–302.

Grace, J.R., Leckner, B., Zhu, J. & Cheng, Y. 2006 *Mutiphase Flow Handbook*, chap. Fluidized beds, pp. 1–93. Taylor & Francis.

Grewal, N.S. & Saxena, S.C. 1977 Investigation of heat transfer from immersed tubes in a fluidized bed. In *Fourth National Heat Mass Transfer Conference*, pp. 53–58.

Grewal, N.S. & Saxena, S.C. 1979 Effect of surface roughness on heat transfer from horizontal immersed tubes in fludized bed. *Transactions of American Institute of Mechanical Engineers Journal Heat Transfer* 101, 397–403.

Grewal, N.S. & Saxena, S.C. 1980 Heat transfer between a horizontal tube and a gas-solid fluidized bed. *International Journal of Heat and Mass Transfer* 23, 1505–1519.

Grewal, N.S., Saxena, S.C., Dolidovich, A.F. & Zabrodsky, S.S. 1979 Effect of distributor design on heat transfer from an immersed horizontal tube in a fluidized bed. *Chemical Engineering Journal* 18, 197–201.

Hamidipour, M., Mostoufi, N., Sotudeh-Gharebagh, R. & Chaouki, J. 2005 Experimental investigation of particle contact time at the wall of gas fluidized beds. *Chemical Engineering Science* 60, 4349–4357.

Izquierdo-Barrientos, M.A., Sobrino, C. & Almendros-Ibáñez, J.A. 2014 Experimental heat transfer coefficient in fixed and fluidized beds with pcm. *Submitted to Applied Thermal Engineering* .

Karamavruc, A.I. & Clark, N.N. 1996 A correction factor for one-dimensional heat transfer coefficients around a horizontal tube in a fluidized bed. *Powder Technology* 86, 209–217.

Khan, T. & Turton, R. 1992 The measurements of instantaneous heat transfer coefficients around the circumference of a tube immersed in a high temperature fluidized bed. *International Journal of Heat and Mass Transfer* 35, 3397–3406.

Kim, S., Ahn, J., Kim, S.D. & Lee, D. 2003 Heat transfer and bubble characteristics in a fludized bed with immersed horizontal tube bundle. *International Journal of Heat and Mass Transfer* 46, 399–409.

Krupiezka, R. 1967 Analysis of thermal conductivity in granular materials. *International Chemical Engineering* 7, 122–144.

Kubie, J. & Broughton, J. 1975 A model of heat transfer in gas fluidized beds. *International Journal of Heat and Mass Transfer* 18, 289 – 299.

Kunii, D. & Levenspiel, O. 1991*a* *Fluidization Engineering*. Butterworth-Heinemann.

Kunii, D. & Levenspiel, O. 1991*b* A general equation for the heat transfer coefficient at wall surface of gas/solid contactors. *Industrial and Engineering Chemistry Research* 30, 136–141.

Kunii, D. & Smith, J.M. 1960 Heat transfer characteristics of porous rocks. *American Institute of Chemical Engineers Journal* 6, 71–78.

Kunii, D. & Suzuki, M. 1966 Heat transfer between wall surface and packed solids. In *International Heat Transfer Conference IV*, pp. 344–352.

Lese, H.K. & Kermode, R.I. 1972 Heat transfer from a horizontal tube to a fluidized bed in the presence of unheated tubes. *Canadian Journal of Chemical Engineering* 50, 44–48.

Li, H.S., Qian, R.Z., Huang, W.D. & Bi, K.J. 1993 An investigation on instantaneous local heat transfer coefficients in high temperature fluidized beds. i experimental results. *International Journal of Heat Mass and Transfer* 36, 4389–4395.

Lu, J.D., Flamant, G. & Snabre, P. 1993 Towards a general model for vertical wall to gas-solid fluidized beds heat transfer. i particle convection and gas convection. *Chemical Engineering Science* 48, 2479–2492.

Masoumifard, N., Mostoufi, N., Hamidi, A.A. & Sotudeh-Gharebagh, R. 2008 Investigation of heat transfer between a horizontal tube and gas-solid fluidized bed. *International Journal of Heat and Fluid Flow* 29, 1504–1511.

Mehling, H. & Cabeza, L.F. 2008 *Heat and cold storage with PCM*. Springer.

Mickley, H.S. & Fairbanks, D.F. 1955 Mechanism of heat transfer to fluidized beds. *American Institute of Chemical Engineers Journal* 2, 374–384.

Mickley, H.S. & Trilling, C.A. 1949 Heat transfer characteristics of fluidized beds. *Industrial and Engineering Chemistry* 41, 1135–1147.

Modrak, T. 1979 Fluidized bed combustion development facility and commercial utility afbc design assessment. *Tech. Rep.*. Quarterly technical progress report prepared for ERPI.

Molerus, O. 1992 Heat transfer in gas fluidized beds. part i. *Powder Technology* 70, 1–14.

Molerus, O., Burschka, A. & Dietz, S. 1995 Particle migration at solid surface and heat transfer in bubbling fluidized bed ii, prediction of heat transfer in bubbling fluidized beds. *Chemical Engineering Science* 50, 879–885.

Nallusamy, N., Sampath, S. & Velarj, R. 2006 Study on performance of a packed bed latent heat thermal energy storage unit integrated with solar water heating system. *Journal of Zhejiang University SCIENCE A* 8, 1422–1430.

Nellis, G. & Klein, S. 2009 *Heat Transfer*. Cambridge University Press.

Oró, Eduard, Castell, Albert, Chiu, Justin, Martin, Viktoria & Cabeza, Luisa F. 2013 Stratification analysis in packed bed thermal energy storage systems. *Applied Energy* 109, 476 – 487.

Ozkaynak, T.F. & Chen, J.C. 1980 Emulsion phase residence time and its use in heat transfer models in fluidized beds. *American Institute of Chemical Engineers Journal* 26, 544–550.

Patel, R.D. 1967 Surface-renewal model for heat transfer between wall and fluidized beds. ANL-7353 110. Research and Development Report.

Penny, C., Naylor, D. & Friedman, J. 2010 Heat transfer to small cylinders immersed in a packed bed. *International Journal of Heat and Mass Transfer* 53, 5183–5189.

Priebe, S.J. & Genetti, W.E. 1977 Heat transfer from a horizontal bundle of extended surface tubes to an air fluidized bed. *Chemical Engineering Progress Symposium Series* 73, 38–43.

Rady, M. 2009 Granular phase change materials for thermal energy storage: experiments and numerical simulations. *Applied Thermal Engineering* 29, 3149–3159.

Ranz, W.E. & Marshall, W.R. 1952 Evaporation from drops. part ii. *Chemical Engineering ProChemical Engineering Progress* 48, 173–179.

Regin, A.F., Solanki, S.C. & Saini, J.S 2009 An analysis of a packed bed latent heat thermal energy storage system using pcm capsules: Numerical investigation. *Renewable Energy* 34, 1765–1773.

Schwartz, C.E. & Smith, J.M. 1953 *Industrial and Engineering Chemistry*, pp. 45–1209.

Trp, A. 2005 An experimental and numerical investigation of heat transfer during technical grade paraffin melting and solidification in a shell-and-tube latent thermal energy storage unit. *Solar Energy* 79, 648 – 660.

Vortmeyer, D. & Adam, W. 1984 Steady-state measurements and analytical correlation of axial effective thermal conductivities in packed beds at low flow rates. *International Journal of Heat and Mass Transfer* 27, 1465–1472.

Vreedenberg, H.A. 1958 Heat transfer between a fluidized bed and a horizontal tube. *Chemical Engineering Science* 1, 52–60.

Wakao, N. & Kaguei, S. 1982 *Heat and Mass Transfer in Packed Beds.* Gordon and Braech. Science Publishers New York.

Wang, X.S. & Rhodes, M.J. 2003 Determination of particle residence time at the wall of gas fluidized beds by district element method simulation. *Chemical Engineering Science* 58, 387–397.

Wen, D. & Ding, Y. 2006 Heat transfer of gas flow through a packed bed. *Chemical Engineering Science* 61, 3532–3542.

Wood, R.T., Staub, F.W., Canada, G.S. & McLaughlin, M.H. 1978 Two-phase flow and heat transfer. *Tech. Rep.* 525-1. General Electric Co.

Yagi, S. & Kunii, D. 1957 Studies on effective thermal conductivities in packed beds. *American Institute of Chemical Engineers Journal* 3, 373–381.

Yagi, S. & Kunii, D. 1960 Studies on heat transfer near wall surface in packed beds. *American Institute of Chemical Engineers Journal* 6, 97–104.

Yagi, S. & Kunii, D. 1962 Studies on heat transfer in packed beds. *International Development in Heat Transfer.* Part IV, 750–759.

Yagi, S., Kunii, D. & Wakao, N. 1960 Studies on axial effective thermal conductivities in packed beds. *American Institute of Chemical Engineers Journal* 6, 373–381.

Zarghami, R., Mostoufi, N., Sotudeh-Gharebagh, R. & Chaouki, J. 2007 Analysis and modeling of particle-wall contact time in gas fluidized bed. *Chemical Engineering Science* 62, 4573–4578.

Zhang, R., H. Yang, J. Lu & Wu, Y. 2013 Theoretical and experimental analysis of bed-to-wall heat transfer in heat recovery processing. *Powder Technology* 249, 186–195.

Ziegler, E.N., Koppel, L.B. & Brazelton, W.T. 1964 Effects of solid thermal properties on heat transfer to gas fluidized beds. *Industrial and Engineering Chemistry Fundamentals* 3, 324–328.

CHAPTER

EIGHT

Conclusions

This PhD thesis presents an study about the thermal energy storage in fixed and fluidized beds with PCM and about the heat transfer between the bed and an immersed surface eventually used for removing (or adding) heat from the bed. This chapter summarizes the general conclusions obtained from this research.

The study of the performance of an air-fluidized bed of granular PCM shows that, under the experimental conditions tested in this work, greater efficiencies are obtained during the charging and recovery processes with PCM than with sand in fixed and fluidized beds. The influence of the bed height for the fluidized bed with PCM shows that higher efficiency can be achieved when more mass is used, however, it takes longer to reach a certain temperature. The analysis of the flow rate shows that for the charging process the set temperature is achieved sooner for higher flow rates. Nevertheless, similar efficiencies at the end of the charging period are obtained regardless of the flow rate selected. During the cycling the PCM suffers attrition, although no loss of PCM is observed during the test of 75 hours in continuous operation.

The model of the transient response during the charging process of a packed bed with granular PCM shows good agreement with the experimental results. The numerical model accounts for the progressive evolution of the enthalpy with temperature during the phase change. This temperature-dependent enthalpy is included in the model as an apparent specific heat that is dependent on temperature according to the measurements obtained by differential scanning calorimetry (DSC). The form of the energy conservation equation for the solid phase proposed is valid for any granular material whether it has PCM inside. This model also quantifies the energy stored in the wall which represents between 8 and 17% of the energy stored in the material.

A numerical model for the transient response of a fluidized bed with granular PCM material has been developed. The formulation of the non-dimensional

energy equation for the emulsion phase presented can be used with granular material containing PCM or not, as well as for the model proposed for the packed bed with PCM. The temperature of the feed gas differs from that of the gas that leaves the distributor plate and enters the bed. Consequently, the heat accumulated in the plate distributor and in the stainless steel vessel is included in the simulations. The comparison between the numerical and experimental data shows good agreement for the conventional granular material, sand. In order to have an accurate prediction of the temperature profile during the phase change, DSC measurements for the determination of the specific heat and heating experiments should have similar heating rates. Charging experiments at slow heating rates similar to those applied in DSC measurements ensuring thermal equilibrium in the sample, accurately fit the model proposed. As a consequence, to come up with a good agreement between the model and the experiments for the PCM in fluidized bed similar heating rate for the experiments and for the DSC measurements should be selected.

The heat transfer coefficient between a horizontal probe immersed in a fixed and fluidized bed and granular material (with or without PCM) is measured. For both fixed and fluidized bed, the heat transfer coefficient increases with increasing the flow rate. Due to the continuous renovation of particles touching the heat transfer probe higher heat transfer coefficients are obtained for the fluidized beds.

Similar heat transfer coefficients are obtained for the PCM and the sand in packed beds because they have similar conductivities and the phase change of the PCM only takes place for the particles surrounding the probe. Therefore, there is no enhancement of the heat transfer coefficient for the PCM due to the phase change. On the other hand, the heat transfer coefficient in the fluidized bed with granular PCM is notably increased because of the latent energy stored by the PCM when the bed is at a temperature below the transition temperature, doubling the coefficient when there is no phase change. The continuous phase change of particles in the fluidized bed configuration occurs because the particles heated up by the probe surface are continuously renovated.

These heat transfer coefficients between an immersed surface and a fixed or fluidized bed are also modeled. The proposed model for the heat transfer coefficient in packed beds is satisfactorily validated with the experiments carried out with sand and PCM. The model of the heat transfer coefficient in a fluidized bed predicts properly the trend of the measurements. Only for very short contact times between the PCM and the wall surface the model over-predicts

the heat transfer coefficients. Small deviations of the model prediction for the sand might be due to the uncertainties in the input parameters of the model, such as the equivalent thermal conductivity.

Future work will comprise experiments with a water cooling coil immersed in the bed of particles.

It has been observed that the models proposed for the transient response and the determination of the heat transfer coefficient of a fluidized bed with PCM are sensitive to input parameters such as enthalpy-temperature relation and effective thermal conductivity. In the literature only measurements of these properties for pure PCMs are found, but there are not effective mean properties in a bed, which can be used in numerical simulations. To have a more accurate value of the effective thermal conductivity additional experiments in a new set-up would be needed to measure this property in axial and radial directions. In addition, the determination of the enthalpy with a T-history method could be explored. This method allows bigger sample sizes, and hence, the samples will be more representative than the smaller used in the DSC analysis, which seems to be an advantage specially for granular materials.

Alphabetical list of references

Al-Busoul, M. & Abu-Ein, S. 2003 Local heat transfer coefficient around a horizontal heated tube immersed in a gas fluidized bed. *Heat and Mass Transfer* 39, 355–358.

Arkar, C. & Medved, S. 2005*a* Influence of accuracy of thermal property data of a phase change material on the result of a numerical model of a packed bed latent heat storage with spheres. *Thermochimica Acta* 438, 192–201.

Arkar, C. & Medved, S. 2005*b* Influence of accuracy of thermal property data of a phase change material on the result of a numerical model of a packed bed latent heat storage with spheres. *Thermochimica Acta* 438, 192–201.

ASTM 2006 Standard test method for determination of attrition and abrasion of powdered catalysts by air jets. *Tech. Rep.* D5757-00.

Baskakov, A.P. 1964 The mechanism of heat transfer between a fluidized bed and a surface. *International Chemical Engineering* 4, 320–324.

Baskakov, A.P., Berg, B.V., Vitt, O.K., Filippovsky, N.F., Hirakosyan, V.A., Goldobin, J.M. & Maskaev, V.K. 1973 Heat transfer to objects immersed in fluidized beds. *Powder Technology* 8, 273–282.

Beasley, D.E. & Clark, J.A. 1984 Transient response of a packed bed for thermal energy storage. *International Journal of Heat and Mass Transfer* 27, 1659–1669.

Benenati, R.F. & Brosilow, C.B. 1962 Void fraction distribution in beds of spheres. *American Institute of Chemical Engineers Journal* 8, 359–361.

Benmansour, A., Hamdan, M.A. & Bengeuddach, A. 2006 Experimental and numerical investigations of solid particles thermal energy storage unit. *Applied Thermal Engineering* 26, 513–518.

Botterill, J.S.M. 1975 *Fluid-Bed Heat Transfer*. Academic Press, New York.

Botterill, J.S.M. & Desai, M. 1972 Limiting factor in gas-fluidized bed heat transfer. *Powder Technology* 6, 231–238.

Brown, R.C. & Overmann, S.P. 1998 The influence of particle thermal time constants on convection coefficients in bubbling fluidized beds. *Powder Technology* 98, 13–20.

Brown, R.C., Rasberry, J.D. & Overmann, S.P. 1998 Microencapsulated phase-change materials as heat transfer media in gas fluidized beds. *Powder Technology* 98, 217–222.

Cabeza, L.F., Castell, A., Barreneche, C., de Gracia, A. & Fernández, A.I. 2011 Materials used as pcm in thermal energy storage in buildings: A review. *Renewable & Sustainable Energy Reviews* 15, 1675–1695.

Cao, Y. & Faghri, A. 1990 A numerical analysis of phase change problems including natural convection. *ASME Journal of Heat Transfer* 112, 812–816.

Chandran, R., Chen, J.C. & Staub, F.W. 1980 Local heat transfer coefficient around horizontal tubes in fluidized beds. *American Institute of Chemical Engineers Journal* 102, 152–157.

Chen, J.C. 1976 Heat transfer to tubes in fluidized bed. In *National Heat Transfer Conference*. St. Louis MO.

Chen, J.C. 2003 *Handbook of fluidization and fluid-particle systems*, chap. Heat Transfer. Taylor & Francis Group LLC.

Darton, R.C., LaNauze, R.D., Davidson, J.F. & Harrison, D. 1977 Bubble growth due to coalescence in fluidized beds. *Transactions of the Institution of Chemical Engineers* 55, 274–280.

Davidson, J.F. & Harrison, D. 1963 *Fluidised particles*. Cambridge University Press.

Delgado, M., Lázaro, A., Mazo, J. & Zalba, B. 2012 Review of phase change materials emulsions and microencapsulated phase change material slurries: materials, heat transfer studies and applications. *Renewable & Sustainable Energy Reviews* 16, 253–273.

Dhifaoui, B., Jabrallah, S. Ben, Belghith, A. & Corriou, J.P. 2007 Experimental study of dynamic behaviour of a porous medium submitted to a wall heat flux in view of thermal energy storage by sensible heat. *International Journal of Thermal Sciences* 46, 1056–1063.

Dincer, I. & Rosen, M. 2002 *Thermal energy storage*. John Wiley & Sons.

Doherty, J.A., Verma, R.S., Shrivastava, S. & Saxena, S.C. 1986 Heat transfer from immersed horizontal tubes of different diameter in a gas fluidized bed. *Energy* 11, 773–783.

Dutil, Y., Rousse, D.R., Salah, N. Ben, Lassue, Stéphane & Zalewski, Laurent 2011 A review on phase-change materials: Mathematical modeling and simulations. *Renewable and Sustainable Energy Reviews* 15, 112–130.

El-Halwagi, A.M., El-Rifai, M.A. & El-Halwagi, M.M. 1991 Maximization of thermal efficiency of fluidized-bed heat regenerators. *Heat Recovery Systems and CHP* 11, 141–148.

Elsari, M. & Hughes, R. 2002 Axial effective thermal conductivities of packed beds. *Applied Thermal Engineering* 22, 1969–1980.

Elsayed, M.M., Megahed, I.E. & El-Refaee 1988 Experimental testing of fluidized beds thermal storage. *Solar & Wind technology* 5, 15–25.

Faghri, A. & Zhang, Y. 2006 In *Transport Phenomena in Multiphase Systems* (ed. Amir Faghri & Yuwen Zhang), pp. 1–106. Boston: Academic Press.

Farid, M.M., Hamad, F.A. & Abu-Arabi, M. 1998 Melting and solidification in multi-dimensional geometry and presence of more than one interface. *Energy Conversion and Management* 39, 809–818.

Farid, M.M., Khudhair, A.M., Razack, S.A.K. & Al-Hallaj, S. 2004 A review on phase change energy storage: materials and applications. *Energy Conversion and Management* 45, 1597–1615.

Flamant, G. & Menigault 1987 Combined wall-to-fluidized bed heat transfer. bubble and emulsion contributions at high temperature. *International Journal Heat Mass Transfer* 30, 1803–1812.

Friedman, J, Koundakjian, P., Naylor, D. & Rosero, D. 2006 Heat transfer to small horizontal cylinders immersed in a fluidized bed. *Transactions of the ASME, Journal Heat Transfer* 128, 984–988.

Galloway, T.R. & Sage, B.H. 1970 A model of the mechanism of transport in packed, distended, and fluidized beds. *Chemical Engineering Science* 25, 495–516.

Geldart, D. 1973 Types of gas fluidization. *Powder Technology* 7, 285–292.

Geldart, D., Abdullah, E.C., Hassanpour, A., Nwoke, L.C. & Wouters, I. 2006 Characterization of powder flowability using measurement of angle of repose. *China Particuology* 4, 104–107.

Giro-Paloma, J., Oncins, G., Barreneche, C., Martínez, M., Fernández, I. & Cabeza, L.F. 2012 Physico-chemical and mechanical properties of microencapsulated phase change material. *Applied Energy* 109, 441–448.

Glicksman, L.R. & Decker, N.A. 1980 Design relationships for predicting heat transfer to tube bundles in fluidized bed combustion. In *Proceedings of the Sixth Annual International Conference on Fluidized Bed Combustors*, , vol. III, p. 152. Atlanta.

Gonzo, E.E. 2002 Estimating correlation for the effective thermal conductivity of granular materials. *Chemical Engineering Journal* 90, 299–302.

Grace, J.R., Leckner, B., Zhu, J. & Cheng, Y. 2006 *Mutiphase Flow Handbook*, chap. Fluidized beds, pp. 1–93. Taylor & Francis.

Grewal, N.S. & Saxena, S.C. 1977 Investigation of heat transfer from immersed tubes in a fluidized bed. In *Fourth National Heat Mass Transfer Conference*, pp. 53–58.

Grewal, N.S. & Saxena, S.C. 1979 Effect of surface roughness on heat transfer from horizontal immersed tubes in fludized bed. *Transactions of American Institute of Mechanical Engineers Journal Heat Transfer* 101, 397–403.

Grewal, N.S. & Saxena, S.C. 1980 Heat transfer between a horizontal tube and a gas-solid fluidized bed. *International Journal of Heat and Mass Transfer* 23, 1505–1519.

Grewal, N.S., Saxena, S.C., Dolidovich, A.F. & Zabrodsky, S.S. 1979 Effect of distributor design on heat transfer from an immersed horizontal tube in a fluidized bed. *Chemical Engineering Journal* 18, 197–201.

Hamidipour, M., Mostoufi, N., Sotudeh-Gharebagh, R. & Chaouki, J. 2005 Experimental investigation of particle contact time at the wall of gas fluidized beds. *Chemical Engineering Science* 60, 4349–4357.

Heertjes, P.M., de Boer, H.G.J. & de Haas van Dorsser, A.H. 1953 Temperature and humidity measurements in a drying fluidized bed. *Chemical Engineering Science* 2, 97–107.

Hänchen, M., Brückner, S. & Steinfeld, A. 2011 High temperature thermal storage using a packed bed of rocks. heat transfer analysis and experimental validation. *Applied Thermal Engineering* 31, 1798–1806.

Hoebink, J.H.B.J. & Rietema, K. 1980 Drying granular solids in fluidized beds i: Description on basis of mass and heat transfer coefficients. *Chemical Engineering Science* 35, 2135–2139.

Husnain, S.M. 1998 Review on sustainable thermal energy storage technologies, part i: heat storage materials and techniques. *Energy Conversion and Management* 39, 1127–38.

Izquierdo-Barrientos, M.A., Sobrino, C. & Almendros-Ibáñez, J.A. 2013*a* Thermal energy storage in a fluidized bed of pcm. *Chemical Engineering Journal* 230, 573–583.

Izquierdo-Barrientos, M.A., Sobrino, C. & Almendros-Ibáñez, J.A. 2014*a* Experimental heat transfer coefficient in fixed and fluidized beds with pcm. *Submitted to Applied Thermal Engineering* .

Izquierdo-Barrientos, M.A., Sobrino, C. & Almendros-Ibáñez, J.A. 2014*b* Modeling of the heat transfer coefficient in fixed and fluidized beds with pcm. In *Eurotherm Seminar 99: Advances in Thermal Energy Storage*. Lleida.

Izquierdo-Barrientos, M.A., Sobrino, C. & Almendros-Ibáñez, J.A. 2014*c* Modeling the heat transfer coefficient between a surface and fixed and fluidized beds with pcm. *Submitted to International Journal of Heat and Mass Transfer* .

Izquierdo-Barrientos, M.A., Sobrino, C., Almendros-Ibáñez, J.A., Ellis, N., Bi, X.T. & Epstein, N. 2013*b* Experimental studies of phase change materials in a bubbling fluidized bed. In *Fluidization XIV From fundamentals to products.*. Noordwijkerhout, Holland.

Karamavruc, A.I. & Clark, N.N. 1996 A correction factor for one-dimensional heat transfer coefficients around a horizontal tube in a fluidized bed. *Powder Technology* 86, 209–217.

Kathuria, D.G. & Saxena, S.C. 1987 A variable thickness two-dimensional bed for investigating gas-solid fluidized bed hydrodynamics. *Powder Technology* 53, 91–96.

Khan, T. & Turton, R. 1992 The measurements of instantaneous heat transfer coefficients around the circumference of a tube immersed in a high temperature fluidized bed. *International Journal of Heat and Mass Transfer* 35, 3397–3406.

Kim, S., Ahn, J., Kim, S.D. & Lee, D. 2003 Heat transfer and bubble characteristics in a fludized bed with immersed horizontal tube bundle. *International Journal of Heat and Mass Transfer* 46, 399–409.

Krupiezka, R. 1967 Analysis of thermal conductivity in granular materials. *International Chemical Engineering* 7, 122–144.

Kubie, J. & Broughton, J. 1975 A model of heat transfer in gas fluidized beds. *International Journal of Heat and Mass Transfer* 18, 289 – 299.

Kunii, D. & Levenspiel, O. 1968 Bubbling bed model for kinetic processes in fluidized plate. gas-solid mass and heat transfer and catalytic reactions. *Industrial and Engineering Chemistry Process Design and Development* 7, 481–492.

Kunii, D. & Levenspiel, O. 1991*a* *Fluidization Engineering*. Butterworth-Heinemann.

Kunii, D. & Levenspiel, O. 1991*b* A general equation for the heat transfer coefficient at wall surface of gas/solid contactors. *Industrial and Engineering Chemistry Research* 30, 136–141.

Kunii, D. & Smith, J.M. 1960 Heat transfer characteristics of porous rocks. *American Institute of Chemical Engineers Journal* 6, 71–78.

Kunii, D. & Suzuki, M. 1966 Heat transfer between wall surface and packed solids. In *International Heat Transfer Conference IV*, pp. 344–352.

Kuznik, F., David, D., Johannes, K. & Roux, J.J. 2011 A review on phase change materials integrated in building walls. *Renewable and Sustainable Energy Reviews* 15, 379–391.

Lane, G.A. 1980 Low temperature heat storage with phase change materials. *International Journal of Energy Research* 5, 155–160.

Lese, H.K. & Kermode, R.I. 1972 Heat transfer from a horizontal tube to a fluidized bed in the presence of unheated tubes. *Canadian Journal of Chemical Engineering* 50, 44–48.

Li, H.S., Qian, R.Z., Huang, W.D. & Bi, K.J. 1993 An investigation on instantaneous local heat transfer coefficients in high temperature fluidized beds. i experimental results. *International Journal of Heat Mass and Transfer* 36, 4389–4395.

Lin, C.L., Peng, T.H. & Wang, W.J. 2011 Effect of particle size distribution on agglomeration/defluidization during fluidized bed combustion. *Powder Technology* 207, 290–295.

Lu, J.D., Flamant, G. & Snabre, P. 1993 Towards a general model for vertical wall to gas-solid fluidized beds heat transfer. i particle convection and gas convection. *Chemical Engineering Science* 48, 2479–2492.

Masoumifard, N., Mostoufi, N., Hamidi, A.A. & Sotudeh-Gharebagh, R. 2008 Investigation of heat transfer between a horizontal tube and gas-solid fluidized bed. *International Journal of Heat and Fluid Flow* 29, 1504–1511.

Mehling, H. & Cabeza, L.F. 2008 *Heat and cold storage with PCM*. Springer.

Merry, N. & Rubinsky, B. 1989 Energy storage in a fluidized bed. *Transactions of the ASME. Journal of Heat Transfer* 111, 726–730.

Mickley, H.S. & Fairbanks, D.F. 1955 Mechanism of heat transfer to fluidized beds. *American Institute of Chemical Engineers Journal* 2, 374–384.

Mickley, H.S. & Trilling, C.A. 1949 Heat transfer characteristics of fluidized beds. *Industrial and Engineering Chemistry* 41, 1135–1147.

Modrak, T. 1979 Fluidized bed combustion development facility and commercial utility afbc design assessment. *Tech. Rep.*. Quarterly technical progress report prepared for ERPI.

Molerus, O. 1992 Heat transfer in gas fluidized beds. part i. *Powder Technology* 70, 1–14.

Molerus, O., Burschka, A. & Dietz, S. 1995 Particle migration at solid surface and heat transfer in bubbling fluidized bed ii, prediction of heat transfer in bubbling fluidized beds. *Chemical Engineering Science* 50, 879–885.

Nagano, K., Takeda, S., Mochida, T. & Shimakura, K. 2004 Thermal characteristics of a direct heat exchange system between granules with phase change material and air. *Applied Thermal Engineering* 24, 2131–2144.

Nallusamy, N., Sampath, S. & Velarj, R. 2006 Study on performance of a packed bed latent heat thermal energy storage unit integrated with solar water heating system. *Journal of Zhejiang University SCIENCE A* 8, 1422–1430.

Nellis, G. & Klein, S. 2009 *Heat Transfer*. Cambridge University Press.

Oró, E., Castell, A., Chiu, J., Martin, V. & Cabeza, L.F. 2013 Stratification analysis in packed bed thermal energy storage systems. *Applied Energy* 109, 476 – 487.

Ozkaynak, T.F. & Chen, J.C. 1980 Emulsion phase residence time and its use in heat transfer models in fluidized beds. *American Institute of Chemical Engineers Journal* 26, 544–550.

Patel, R.D. 1967 Surface-renewal model for heat transfer between wall and fluidized beds. ANL-7353 110. Research and Development Report.

Peng, H., Dong, H. & Ling, X. 2014 Thermal investigation of pcm-based high temperature thermal energy storage in packed bed. *Energy Conversion and Management* 81, 420–427.

Penny, C., Naylor, D. & Friedman, J. 2010 Heat transfer to small cylinders immersed in a packed bed. *International Journal of Heat and Mass Transfer* 53, 5183–5189.

Pis, J.J., Fuertes, A.B., Artos, V., Suárez, A. & Rubiera, F. 1991 Attrition of coal ash particles in a fluidized bed. *Powder Technology* 66, 41–46.

Priebe, S.J. & Genetti, W.E. 1977 Heat transfer from a horizontal bundle of extended surface tubes to an air fluidized bed. *Chemical Engineering Progress Symposium Series* 73, 38–43.

Rady, M. 2009*a* Granular phase change materials for thermal energy storage: experiments and numerical simulations. *Applied Thermal Engineering* 29, 3149–3159.

Rady, M. 2009*b* Study of phase changing characteristics of granular composites using differential scanning calorimetry. *Energy Conversion and Management* 50, 1210–1217.

Ranz, W.E. & Marshall, W.R. 1952 Evaporation from drops. part ii. *Chemical Engineering ProChemical Engineering Progress* 48, 173–179.

Ray, Y.C. & Jiang, T.S. 1987 Particle attrition phenomena in a fluidized bed. *Powder Technology* 49, 193–206.

Rees, A.C., Davidson, J.F, Dennis, J.S., Fennell, P.S., Gladden, L.F., Hayhurst, A.N., Mantle, M.D., Mu̇ller, C.R. & Sederman, A.J. 2006 The nature of the flow just above the perforated plate distributor of a gas-fluidised bed, as imaged using magnetic resonance. *Chemical Engineering Journal* 61, 6002–6015.

Regin, A.F., Solanki, S.C. & Saini, J.S. 2008 Heat transfer characteristics of thermal energy storage system using pcm capsules: A review. *Renewable and Sustainable Energy Reviews* 12, 2438–2458.

Regin, A.F., Solanki, S.C. & Saini, J.S 2009 An analysis of a packed bed latent heat thermal energy storage system using pcm capsules: Numerical investigation. *Renewable Energy* 34, 1765–1773.

Saxena, S.C., Grewal, N.S., Gabor, J.D., Zabrodsky, S.S. & Galershtein, D.M. 1979 Heat transfer between a gas fluidized bed and immersed tubes. *Advances in Heat Transfer*, vol. 14, pp. 149 – 247. Elsevier.

Schumann, T.E.W. 1929 Heat transfer: A liquid flowing through a porous prism. *Journal of the Franklin Institute* 208, 405–416.

Schwartz, C.E. & Smith, J.M. 1953 *Industrial and Engineering Chemistry*, pp. 45–1209.

Sozen, Z.Z., Grace, J.R. & Pinder, K.L. 1988 Thermal energy storage by agitated capsules of phase change material: pilot scale experiments. *Industrial and Engineering Chemistry Research* 27, 679–684.

Talmatsky, E. & Kribus, A. 2008 Pcm storage for solar dhw: An unfulfilled promise? *Solar Energy* 82, 861 – 869.

Thoméo, J.C., Rouiller, C.O. & Freire., J. 2004 Experimental analysis of heat transfer in packed beds with air flow. *Industrial and Engineering Chemistry Research* 43, 4140–4148.

Trp, A. 2005 An experimental and numerical investigation of heat transfer during technical grade paraffin melting and solidification in a shell-and-tube latent thermal energy storage unit. *Solar Energy* 79, 648 – 660.

Vortmeyer, D. & Adam, W. 1984 Steady-state measurements and analytical correlation of axial effective thermal conductivities in packed beds at low flow rates. *International Journal of Heat and Mass Transfer* 27, 1465–1472.

Vortmeyer, D. & Schaefer, R.J. 1974 Equivalence of one- and two-phase models for heat transfer processes in packed beds: one dimensional theory. *Chemical Engineering Science* 29, 485–491.

Vreedenberg, H.A. 1958 Heat transfer between a fluidized bed and a horizontal tube. *Chemical Engineering Science* 1, 52–60.

Wagialla, K.M., Fakeeha, A.H., Elnashaire, S.S.E.H. & Almaktary, A.Y. 1991 Modeling and simulation of energy storage in fluidized beds using the two-phase model. *Energy Sources* 13, 189–201.

Wakao, N. & Kaguei, S. 1982 *Heat and Mass Transfer in Packed Beds*. Gordon and Braech. Science Publishers New York.

Wang, X.S. & Rhodes, M.J. 2003 Determination of particle residence time at the wall of gas fluidized beds by district element method simulation. *Chemical Engineering Science* 58, 387–397.

Wen, D. & Ding, Y. 2006 Heat transfer of gas flow through a packed bed. *Chemical Engineering Science* 61, 3532–3542.

Werther, J. & Reppenhagen, J. 2003 *Handbook of fluidization and fluid-particle systems, chapter 8*. Marcel Dekker Inc., New York.

Wong, A. Chi-Ying 2002 Use of angle of repose and bulk densities for powder characterization and the prediction of minimum fluidization and minimum bubbling velocities. *Chemical Engineering Science* 57, 2635–2640.

Wood, R.T., Staub, F.W., Canada, G.S. & McLaughlin, M.H. 1978 Two-phase flow and heat transfer. *Tech. Rep.* 525-1. General Electric Co.

www.rubitherm.com 2014 Last access on. August.

Xavier, A.M. & Davidson, J.F 1985 *Fluidization*, chap. Heat transfer in fluidized beds. Academic Press, London.

Xia, L., Zhang, P. & Wang, R.Z. 2010 Numerical heat transfer analysis of the packed bed latent heat storage system based on an effective packed bed model. *Energy* 35, 2022–2032.

Yagi, S. & Kunii, D. 1957 Studies on effective thermal conductivities in packed beds. *American Institute of Chemical Engineers Journal* 3, 373–381.

Yagi, S. & Kunii, D. 1960 Studies on heat transfer near wall surface in packed beds. *American Institute of Chemical Engineers Journal* 6, 97–104.

Yagi, S. & Kunii, D. 1962 Studies on heat transfer in packed beds. *International Development in Heat Transfer* Part IV, 750–759.

Yagi, S., Kunii, D. & Wakao, N. 1960 Studies on axial effective thermal conductivities in packed beds. *American Institute of Chemical Engineers Journal* 6, 373–381.

Yang, R., Xu, R. H. & Zhang, Y. 2003 Preparation, physical property and thermal physical property of phase change microcapsule slurry and phase change emulsion. *Solar Energy Materials & Solar Cells* 80, 405–416.

Zalba, B., Marín, J.M., Cabeza, L.F. & Mehling, H. 2003 Review on thermal energy storage with phase change: materials, heat transfer analysis and applications. *Applied Thermal Engineering* 23, 251 – 283.

Zarghami, R., Mostoufi, N., Sotudeh-Gharebagh, R. & Chaouki, J. 2007 Analysis and modeling of particle-wall contact time in gas fluidized bed. *Chemical Engineering Science* 62, 4573–4578.

Zhang, R., H. Yang, J. Lu & Wu, Y. 2013 Theoretical and experimental analysis of bed-to-wall heat transfer in heat recovery processing. *Powder Technology* 249, 186–195.

Zhang, Y., Ding, J., Wang, X., Yang, R. & Lin, K. 2006 Influence of additives on thermal conductivity of shape-stabilized phase change material. *Solar Energy Materials & Solar Cells* 90, 1692–1702.

Ziegler, E.N., Koppel, L.B. & Brazelton, W.T. 1964 Effects of solid thermal properties on heat transfer to gas fluidized beds. *Industrial and Engineering Chemistry Fundamentals* 3, 324–328.

List of publications

The results of this PhD thesis have been published or submitted for publication:

- Izquierdo-Barrientos M.A., Sobrino C., Almendros-Ibáñez J.A. 2013 Thermal energy storage in a fluidized bed with PCM. *Chemical Engineering Journal* 230, 573 - 583.

- Izquierdo-Barrientos M.A., Sobrino C., Almendros-Ibáñez J.A. 2014 Modeling and experiments of energy storage in a packed bed with PCM. *Submitted for publication in Applied Thermal Engineering.*

- Izquierdo-Barrientos M.A., Sobrino C., Almendros-Ibáñez J.A. 2014 Energy storage with PCM in fluidized beds: modeling and experiments. *Submitted for publication in Chemical Engineering Journal.*

- Izquierdo-Barrientos M.A., Sobrino C., Almendros-Ibáñez J.A. 2014 Experimental heat transfer coefficients between a surface and fixed and fluidized beds with PCM *Submitted for publication in Applied Thermal Engineering.*

- Izquierdo-Barrientos M.A., Sobrino C., Almendros-Ibáñez J.A. 2014 Modeling the heat transfer coefficient between a surface and fixed and fluidized beds with PCM *Submitted for publication in International Journal of Heat and Mass Transfer.*

and presented in the following conference:

- Izquierdo-Barrientos M.A., Sobrino C., Almendros-Ibáñez J.A. 2014 Modeling of the heat transfer coefficient in fixed and fluidized beds with PCM. In *Eurotherm Seminar 99. Advances in Thermal Energy Storage.* Lleida, Spain. Oral presentation.

- Izquierdo-Barrientos M.A., Sobrino C., Almendros-Ibáñez J.A. 2014 Modeling and experiments of energy storage in a fluidized bed with PCM. In 7^{th} *World Congress on Particle Technology.* Beijing, China. Oral presentation.

- Izquierdo-Barrientos M.A., Sobrino C., Almendros-Ibáñez J.A. 2013 Estudio numérico y experimental de un lecho fijo con materiales de

cambio de fase como sistema de almacenamiento de energía. In *Congreso Nacional de Ingeniería Termodinámica.* Burgos, Spain. ISBN: 978-84-9268162-4. Oral presentation.

- Izquierdo-Barrientos M.A., Sobrino C., Almendros-Ibáñez J.A. 2013 Estudio del coeficiente convectivo en lecho fijo y fluidizado con material de cambio de fase (MCF). In *Congreso Nacional de Ingeniería Termodinámica.* Burgos, Spain. ISBN: 978-84-9268162-4. Oral presentation.

- Izquierdo-Barrientos M.A., Sobrino C., Almendros-Ibáñez J.A. Ellis N., Bi X.T., Epstein N., 2013 Experimental studies of phase change materials in a bubbling fluidized bed. In *Fluidization XIV From fundamentals to products.* Noordwijkerhout, Holland. Keynote: Oral presentation.

- Izquierdo-Barrientos M.A., Sobrino C., Almendros-Ibáñez J.A. 2013 Convective heat transfer coefficient in a bubbling fluidized bed with PCM. In *Fluidization XIV From fundamentals to products.* Noordwijkerhout, Holland. Poster presentation.

- Izquierdo-Barrientos M.A., Sobrino C., Almendros-Ibáñez J.A. 2012 Experimental study of thermal storage in fixed and fluidized beds with phase change materials (PCM). In *12^{th} International Conference on Energy Storage.* Lleida, Spain. ISBN: 978-84-938793-3-4. Poster presentation.

During this research period the following papers have been published. They are not included in this thesis since their content is out of scope of the present work.

- Izquierdo-Barrientos M.A., Belmonte J.F., Rodríguez-Sánchez D., Molina A.E., Almendros-Ibáñez J.A. 2012 A numerical study of external building walls containing phase change materials (PCM). In *Applied Thermal Engineering* 47, 73 - 85.

- Rodríguez-Sánchez D., Belmonte J.F., Izquierdo-Barrientos M.A., Molina A.E., Rosengarten G., Almendros-Ibáñez J.A. 2014 Solar energy captured by a curved collector designed for architectural integration. In *Applied Energy* 116, 66 - 75.

• Belmonte J.F., Izquierdo-Barrientos M.A., Eguía P., Molina A.E., Almendros-Ibáñez J.A. 2014 PCM in the heat rejection loops of absorption chillers. A feasibility study for the residential sector in Spain. In *Energy and Buildings* 80, 331 - 351.